Universidade de Aveiro
2019

Departamento de Química

Marco André Costa Sousa

Post-Combustion flue gas purification using Ionic Liquids

Purificação de correntes de Pós-Combustão usando Líquidos Iónicos

Universidade de Aveiro
2019

Departamento de Química

Marco André Costa Sousa

Post-Combustion flue gas purification using Ionic Liquids

Purificação de correntes de Pós-Combustão usando Líquidos Iónicos

Dissertação apresentada à Universidade de Aveiro para cumprimento dos requisitos necessários à obtenção do grau de Mestre em Engenharia Química, realizada sob a orientação científica do Doutor Pedro Jorge Marques de Carvalho, Equiparado a Investigador Auxiliar do Departamento de Química da Universidade de Aveiro.

Este trabalho é financiado pelo Portugal 2020 através do Fundo Europeu de Desenvolvimento Regional (FEDER), enquadrado no Programa Operacional Competitividade e Internacionalização (POCI), no âmbito do projeto Smart Green Homes - BOSCH - POCI-01-0247-FEDER-007678 e no âmbito do projeto CICECO- Instituto de Materiais de Aveiro, POCI-01-0145-FEDER-007679 (FCT Ref. UID/CTM/50011/2013), Laboratório Associado da Universidade de Aveiro, cofinanciado por fundos nacionais através da FCT/MEC

Dedico este trabalho ao meu pai, foi por ele que estou onde estou.

o júri

presidente

Professor Doutor Carlos Manuel Santos da Silva
Professor Associado, Universidade de Aveiro

Doutor Pablo Navarro Tejedor
Professor Assistente, Universidade Autónoma de Madrid

Doutor Pedro Jorge Marques de Carvalho
Equiparado a Investigador Auxiliar, Universidade de Aveiro

agradecimentos

I can only express gratitude to my supervisor Pedro Carvalho for his guidance during this thesis, his availability and his ease to talk to, that made a timid person like me capable of work freely and with great joy.

This thesis would be impossible without the contribution of various people, and so, I would also like to thank Cristian Moya, for without him the isochoric cell setup would be impossible and Liliana Silva for the synthesis of compounds to study. I would also like to thank them for their readiness and eagerness to help, which also made this thesis a pleasure to work on.

To my girlfriend, Sofia, for making me truly focus on this course, for supporting me and making me better every day.

To my friends, which helped trough rough times and made the stay in Aveiro easier and more welcoming. Thank you, Pedro, São, Sebii, Sónia, Margarida, Milene and all the others that escape me, for your support.

To my family, my mother, Graciela and my sister, Sofia, which never doubted me, supported me and sacrificed much along all these years. And my father, which unfortunately did not make it to see me finish this part of my life.

Thank you all.

palavras-chave absorção; amino-ácido; CO_2; líquidos iónicos; CCS; contator membrana

resumo

Devido à excessiva emissão de gases de efeito de estufa para a atmosfera o fenómeno conhecido como aquecimento global torna-se cada vez mais relevante e preocupante. A consciência do problema identificado incentivou muitos investigadores a encetar esforços focados no desenvolvimento de novos processos e metodologias capazes de mitigar o efeito de estufa recorrendo à captura e sequestro dos gases de efeito de estufa. Entre os solventes propostos como inovadores e com elevado potencial para a captura de gases, nomeadamente o CO_2, os líquidos iónicos têm-se distinguido entre os demais devido às suas propriedades excecionais. Contudo, sendo possível sintetizar aproximadamente um milhão de líquidos iónicos, a sua caracterização torna-se inviável. Procurando identificar as famílias de líquidos iónicos com maior potencial, ferramentas preditivas, como o COSMO-RS, e/ou modelos e correlações apresentam-se como ferramentas matemáticas úteis na identificação dos solventes com maior potencial. Nesta tese, líquidos iónicos baseados em amino ácidos são avaliados como solventes com absorção química para a captura de CO_2 a baixa pressão e pressões parciais de gás moderadas.

Para a caracterização do diagrama de fases dos sistemas de interesse, um equipamento de solubilidade a volume constante, célula isocórica, foi desenvolvido e validado permitindo posteriormente a caracterização do diagrama *pVT* na gama de temperaturas e pressões de 30 a 80 ºC e 0.5 a 5 bar.

Embora o potencial dos líquidos iónicos seja indiscutível a sua aplicação em processos unitários tradicionais, como colunas de enchimento, mostrou-se impraticável. Contudo outros mecanismos, como imobilização dos líquidos iónicos em partículas de sílica ou de carbono ou o uso de contactores de membranas gás-líquido têm vindo a ser propostos e avaliadas. Tendo como objetivo último a identificação do solvente ou mistura de solventes como maior potencial para a separação em causa e implementação num sistema de contactores gás-líquido, como unidade de separação, os solventes estudados foram ainda avaliados em relação à sua difusividade quando suportados em membranas comerciais usando o método de "*time-lag*".

keywords absorption; amino acid; CO_2; ionic liquids; CCS;membrane contactor

abstract

Due to the emissions of greenhouse gases to the atmosphere the phenomenon known as global warming has risen awareness and real concern. The knowledge of the problem has driven many researchers to pursuit work on the development of new methodologies and processes able to mitigate the greenhouse gas effect by the capture and sequestration of greenhouse gases.

Among the solvents proposed as innovative and feasible for the gas capture, namely CO_2, the ionic liquids have stand out as those with the highest potential due to their exceptional properties.

However, being possible to synthesize over one million different ionic liquids, their full characterization stands unrealistic. Aiming at identifying the families of ionic liquids with the highest potential, computational predictive tools, like COSMO-RS, and/or models and correlations have hampered the selection of the best solvents. In this thesis, ionic liquids based on amino-acids are evaluated as solvents with chemisorption for the capture of CO_2 at low pressures and moderate partial pressures of the gas. For the characterization of the *pVT* phase diagram of the selected solvents a constant volume setup, isochoric cell, was design, developed and validated allowing to further evaluate the studied ionic liquids at temperature and pressure ranges of 30 to 80 ºC and up to 5 bar, respectively.

Although, ionic liquids stand out as solvents with high potential their application on traditional separation units have been shown unfeasible. Nonetheless, other mechanisms and separation units, like the ionic liquid immobilization in silica or carbon particles or their use in gas-liquid membrane contactors, have been proposed as alternatives.

Having as ultimately goal the selection of a solvent or mixture of solvents with high potential for the intended separation and their implementation on a continuous gas-liquid membrane contactor separation unit, the studied solvents were further evaluated for the diffusivity when supported in commercial membranes using the "*time-lag*" method.

Contents

List of tables

List of figures

Nomenclature

Symbols

a	Peng-Robinson Equation of State term	
A	Peng-Robinson Equation of State term	
A_h	Area of one hole	(cm^2)
A_s	Surface area available for mass transfer	(cm^2)
b	Peng-Robinson Equation of State term	
B	Peng-Robinson Equation of State term	
$D_{C,IL}$	Diffusion coefficient of CO_2 in IL	($cm^2\ s^{-1}$)
Δn_i	Molar difference of compound *i*	(mol)
H	Henry's constant	(bar)
l	Membrane thickness	(cm)
m_i	Molality of the sorbed compound *i*	(mol kg^{-1})
M_w	Molecular weight	(g mol^{-1})
n_h	Number of holes	
n_{CO2}	Number of moles of CO_2	(mol)
n_{IL}	Number of moles of ionic liquid	(mol)
P	System pressure	(bar)
P_b	Permeate pressure	(bar)
P_c	Critical pressure	(bar)
$P_{C,IL}$	Permeability of CO_2 in the ionic liquid	(barrer)
P_t	Pressure of the feed manifold	(bar)
R	Ideal gas constant	(mL bar K^{-1} mol^{-1})
S_i	Solubility coefficient	($cm^3_{STP}\ cm^{-3}\ cmHg^{-1}$)
T_c	Critical temperature	(ºC)
t_l	Time-lag	(s)
T_i	Temperature at the place *i*	(ºC)
T_R	Relative temperature	
V	Total Volume	(mL)
V_b	Volume of the permeate manifold	(mL)
V_F	Free volume available to the gas	(mL)

V_M	Molar volume	($cm^3\ mol^{-1}$)
V_p	Total volume of the membrane	(cm^3)
x_i	Mole fraction of compound *i*	($mol\ mol^{-1}$)
Z	Compressibility factor	

Greek letters

α	Peng-Robinson Equation of State term	
ρ_i	Density of the compound i	(g/mL)
φ	Membrane porosity	
ω	Acentric factor	

List of Abbreviations

AAIL	Amino acid-based ionic liquids
AC	Alternate Current
CCS	Carbon Capture and Storage
CR	Carriage Return
CS	Checksum
DC	Direct Current
DSC	Datalogging and Supervisory Control
EN-IL	Encapsulated ionic liquids
EoS	Equation of state
FS	Full scale reading
GUI	Graphical user interface
LF	Line Feed
LRC	Longitudinal Redundancy Check
MOF	Metal organic framework
SILM	Supported Ionic Liquids Membrane
VISA	Virtual Instrument Software Architecture

List of Chemical Compounds

$[C_4C_1im][Ac]$	1-Buthyl-3-methylimidazolium acetate
$[C_4C_1im][DCA]$	1-Butyl-3-methylimidazolium dicyanamide
$[C_4C_1im][PF_6]$	1-Butyl-3-methylimidazolium hexafluorophosphate
$[C_4C_1im][BF_4]$	1-Butyl-3-methylimidazolium tetrafluoroborate

$[C_2C_1im][Ac]$	1-Ethyl-3-methylimidazolium acetate
DEA	Diethanolamine
[DEEA][Ac]	Diethylethanolamonium acetate
CO	Carbon Monoxide
CO_2	Carbon Dioxide
H_2	Hydrogen
$[N_{1112(OH)}][L\text{-}Phe]$	2-(Hydroxyethyl)trimethylammonium L-phenylalaninate
$[N_{1112(OH)}][L\text{-}Pro]$	2-(Hydroxyethyl)trimethylammonium L-prolinate
MEA	Methylethanol amine
N_2	Nitrogen
N_2O	Nitrous Oxide
O_2	Oxygen
$[P_{4444}][Ac]$	Tetrabutylphosphonium acetate
PES	Polyethersulfone
PVDF	Polyvinylidene fluoride
SO_2	Sulfur dioxide

1. Introduction

1.1. Greenhouse Gases

In recent years there has been an increase in energy demand due to a global economic growth. A large chunk of this demand has been met resorting to the burning of fossil fuels [1]. This means that the dependency on the combustion of fossil fuels to produce energy is still present and will likely persist since it is the most readily available technology and the most mature. Other sources such as renewable energies are still too immature, unreliable and expensive to subsidize the energy demand with its availability depending on geographical position [2]; nuclear fission energy is still too controversial due to the byproducts formed and questionable economic viability.

Even though the combustion of fossil fuels stands as the simplest process it has the inconvenience of producing byproducts that are hazardous to the environment and thus, need to be removed before the flue gas released if one aims to mitigate the impact of greenhouse gases on the environment. Greenhouse gases, like water vapor, carbon dioxide, methane, nitrous oxide and ozone, are capable of resonating with the infrared radiation emitted by the cooling of the planet and as such increase the vibration of these molecules, this energy is easily transferred to another molecules such as N_2 and O_2 and as a consequence the planet gets warmer [3].

Removing pollutants from the flue gas does not stand as the only way to reduce emissions but it is considered to be the most efficient way of achieving the goals of the European Union Horizon 2020 programme on climate policies and carbon emissions reduction. Other approaches, such as increasing energy efficiency and promoting energy conservation are also available however, alone are insufficient, counting with reductions of at most 20% of the energy consumption. Geoengineering tactics like afforestation and reforestation can also be used but, they require too much unavailable land area. Thus, carbon capture and sequestration (CCS) from anthropogenic sources stand as the most promising option to reduce emissions and avoid aggravating the effect of global warming [2].

Carbon dioxide stands as one of the primary contributors to the global warming effect. CCS can be applied to three principal carbon sources, namely pre-combustion, post-combustion and oxyfuel combustion.

In pre-combustion separation, coal is gasified into a synthetic gas (syngas) of CO/H_2 or natural gas is reformed with water to form the syngas and then the syngas goes through a water-shift reaction that forms more H_2 and CO_2 the fluid now has relative high CO_2 content and is separated. In oxyfuel combustion, the combustion occurs with oxygen instead of air, which reduces the N_2 in the exhaust and makes the CO_2 separation easier. Finally, in post-combustion there is no alteration to the combustion process and the CO_2 is separated from the flue gas.

Due to the alterations required to the process in pre-combustion and oxyfuel processes, the post combustion strategies are most easily retrofitted into existing systems and as such will be the prime focus of this work.

The separation of CO_2 from the rest of the fluid can be performed through numerous processes as briefly summarized in **Table 1**.

Absorption is a process in which a sorbent is removed using liquids solvents as basis, the sorbent is then removed from this solvent in a posterior process called solvent regeneration. The absorption processes can be divided in two types, depending on the type of bond formed between the sorbent and gas molecules, if the bond formed is a molecular one, then it is determined to be chemical absorption if the sorbent occupies the free space between the solvent molecules and is stabilized trough intermolecular forces, then it is referred to as physical absorption. The regeneration usually occurs with the increase of the solvent temperature, which promotes the gas desorption due to a lower solubility value.

The adsorption processes are also divided onto two categories, also related to the bonds formed during the sorption, physical adsorption and chemical adsorption. The difference resides in the separating agent, in these processes a solid separating agent is used and the sorption only occurs at the surface of the adsorbent, as such in this type of processes highly porous materials are used to separate CO_2 from the rest of the fluid, as such the most used compounds are zeolites, activated carbons, metal oxides, silica gel, and ion-exchange resins, when one bed is saturated or reaches the breaking point, the flow of gas to treat is redirected to a clean bed while the first one undergoes regeneration processes. This process of adsorption can be performed trough three different pathways, pressure swing adsorption (PSA) where the adsorption occurs at high pressures and after the bed's breaking point is reached it is regenerated with low pressure, temperature swing adsorption (TSA), where the adsorption occurs at a given viable temperature at during the

regeneration step the sorbent suffers an increase in temperature to favor the desorption, finally electric swing adsorption (ESA) can also be used, where after the adsorption a low voltage electric current is supplied to the sorbent to regenerate it.

Table 1-Summary, advantages and disadvantages of various gas separation processes [2].

	Advantages	**Disadvantages**	**Summary**
Absorption	High efficiency (>90%) Sorbents can be regenerated Most mature process for CO2 separation.	Efficiency depends on CO_2 concentration A lot of energy required for regeneration Sorbent degradation can be environmental threatening	Gas is absorbed in a liquid solvent and then regenerated
Adsorption	Reversible and the absorbent can be recycled. High efficiency achievable (>85%).	Require high temperature adsorbent High energy required for CO2 desorption.	Gas is adsorbed in a solid that is then regenerated
Cryogenic Separation	Mature technology Adopted for many years in industry for CO2 recovery.	High CO2 concentration (>90% v/v) Should be conducted at very low temperature Very energy intensive	Low temperature process in which distillation of CO_2 can occur
Membrane Separation	Process has been adopted for separation of other gases High separation efficiency achievable (>80%).	Operational problems include low fluxes and fouling.	Membranes allow CO_2 to pass through but no other compounds

Cryogenic separation is a process in which CO_2, along with the rest of the feed, is liquified, due to the low temperature and is then separated from the rest of the feed through evaporation condensation steps as is the case in a traditional column distillation, this method is used when the CO_2 is relatively high due to its huge energy requirements, it is

however usually applied when used in tantum with oxyfuel combustion due to its higher CO_2 content in the flue gas.

Membranes could also be used in the separation of CO_2, in this process a stream is fed to a chamber with a selective membrane to the compound in question (CO_2) this allows the formation of an almost pure CO_2 stream and a mostly CO_2 free stream, being the other compounds retained by the membrane. These processes, however, usually have low flows and can be victims of fouling if the stream is not pretreated correctly but do achieve a great separation as they can be highly selective.

1.2. Solvents for CCS

The most used method of CO_2 separation is absorption, with alkane-amines-based solvents, like methylethanol amine (MEA) and diethanolamine (DEA), being the most used for the chemical absorption processes. Furthermore, MEA, is the most efficient solvent (>90% efficiency) and also the most used [2]. Nonetheless, these solvents are volatile, leading to losses to the gas stream or to the environment, and can corrode process materials, which causes environmental problems [2]. Physical absorption solvents like dimethyl ether of polyethylene glycol (Selexol™), *n*-methyl-2-pyrrolidone (Purisol®) and chilled methanol (Rectisol®) are preferred, since the regeneration of these compounds are much easier due to the lower bonding energy between the compounds. Physical absorption process, however, is only economically viable when the partial pressure of the compound, to be removed, is high compensating thus, their lower sorption capabilities when compared to chemically bonding solvents [4].

Ionic liquids, which are salts that are liquid at low to moderate temperatures, are composed by asymmetric ions with low lattice energy; characteristics that impose to the compounds interesting properties, like low melting points, negligible vapor pressure and high thermal stability, making these compounds highly interesting as replacement of common organic compounds in many processes. Although, ILs were coined as green solvents, mainly due to their negligible volatility, they are not always “green”. In fact, most are significantly toxic and are hardly biodegradable and most of their synthesis is also far from green. Ionic liquids are, however, a class of solvents with a big repertoire of compounds due to the easy combination of different anions and cations, which leads to 10^6 different ILs possible to be synthesized – featuring ILs as designer solvents. Nonetheless,

even not being green solvents, they still stand as solvents greener than those they intend to replace.

Ionic liquids have been reported to be potential candidates for CO_2 capture [5]. As many solvents, ILs can either present physical or chemical absorption depending on their structure. On a perspective of post-combustion, ILs presenting physisorption also have lower solubilities, require lower energy demands on regeneration but large separation units; on the other hand, ILs with chemical absorption present high solubility of CO_2 at low CO_2 partial pressure (<15%) but the compounds formed upon mixing tend to present very high viscosity. Nonetheless, despite these drawbacks ILs with chemisorption still stand as the best promise for the intended separation.

Regarding chemical absorption, few ionic liquids have been studied but, those that were have shown promising results. Among those reported as most interesting are dialkylimidazolium acetates [6], [7] and amino acids families of ionic liquids [8], that although do show promise, are still understudied for its use as a sorption solvent alternative.

Amino acid-based ionic liquids (AAIL) are even more interesting due to their biodegradability, positioning them as the greener option. However, due to their large chains size and amino functional groups these ILs present very high viscosities, higher than those reported for conventional ionic liquids, which makes hard to use, manipulate but mostly impose mass transfer limitations hard to overcome on an envisioned process. These compounds, however, do possess high solubilities as it is capable of chemically bonding with CO_2, reason that made researchers focus on these compounds as an option for the CO_2 separation. A few studies have tackled the problems of high viscosity of AAIL, for example in the work of Santiago et al. [9], the encapsulation (better described later) of these compounds greatly enhanced their kinetics of sorption and desorption and made the AAIL use more reliable.

In order to enhance the properties of ionic liquids, the use of ionic liquids mixed solvents started to appear, this means that the ionic liquid is mixed with another solvent, like water, alkanolamines or other organic solvents. This technique is sometimes used to take advantage of novel solvents, like ionic liquids, while using traditional solvents to enhance its properties. This increases the potential for absorption of the solvents and systems, like the studied by Ma et al. [10] where a mixture of MEA, 1-butyl-3-

methylimidazolium tetrafluoroborate ([C_4C_1im][BF_4]) and 1-butyl-3-methylimidazolium hexafluorophosphate ([C_4C_1im][PF_6]) is reported to have an energy consumption significantly lower than MEA based systems, but still possesses the same drawbacks as RTILs and the traditional solvents, like high viscosity, which can harm pumping systems, form precipitates and the carbamate formed can promote the corrosion during the regeneration process. Another way of using this types of mixtures is the mixture of low viscosity fluids with promising ionic liquids, in the hopes of reducing the viscosity of the solvent, and as such the diffusional resistances, for example, in the work of Gómez-Coma et al. [11], the addition of water showed an increase in the efficiency of the absorption process using [C_2C_1im][Ac].

Deep Eutectic Solvents (DES) are another example of a new class of "greener" solvents. DES have raised a large deal of interest mainly because their similarity to ionic liquids, both in terms of the used compounds (many DES formulation include at least one IL) but mostly on their properties similarity to those of the ILs, in particular the thermal and chemical stability and negligible vapor pressure. DES are formed by a hydrogen bond donor and a hydrogen bond acceptor, the hydrogen bounds established and the interactions results in a delocalization between the acceptor and the donor, which drastically reduces the freezing point of the resulting mixture [12]. Few works are available reporting CO_2 capture with DES but those available report excellent results, making these compounds as potential substitutes of alkanolamines in the absorption processes for CO_2 removal.

Although ILs and DES show great promise in the use as solvents for separation units, these compounds do possess major drawbacks regarding its use, as explained by Leclaire and Heldebrandt [13], a novel separation unit of CO_2 with new solvents has some associated challenges regarding the engineering and implementation standpoint, separating this problem into five categories, the energy costs required for the process, the infrastructure needed, the life cycle of the solvent and its environmental analysis, transportation or storage and its utilization. As such the development of novel separation based on IL has not been an exception, since their high viscosity imposes great mass transfer resistances that makes them unfeasible for an industrial process. Most studied ionic liquids, as simulated in the work of Mota-Martinez et al.[6] do not appear to be capable of being used in the separation technologies commonly used with other solvents, giving rise to absorption columns that require units as high as highest operational industrial

absorption column and the highest building in the world. As such, these solvents (IL, DES, AAIL) do show promise as sorption solvents but, due to their limitations, if they are to be considered viable alternatives to current solvents, new techniques needed to be developed.

With this, this work will focus on room temperature ionic liquids and the amino acid-based ionic liquids as solvents for carbon dioxide capture trough chemical sorption.

1.3. New Separation Techniques

As previously mentioned, the use of ionic liquids to separate CO_2 is still far from being viable, and, as such new techniques with the purpose of increasing its kinetics and therefore, its reliability have been developed. The techniques here described are the use of membranes, the encapsulation of ionic liquids, the use of membrane contactors, or its immobilization in a membrane and a few adsorbents with high potential.

1.3.1. Ionic liquid encapsulation

The encapsulated ionic liquids (ENIL's) are ionic liquids trapped within activated carbon spheres just a few micrometers in diameter. This method of increasing the reliability of ionic liquids is recent and its development attributed to Palomar et al. [14], this method dramatically increases the contact surface area for mass transfer, thanks to the highly porous solid, and reducing thus, the known high diffusion limiting factor without altering the system equilibrium, but greatly enhancing the kinetics of the systems both at the adsorption and the desorption stages [15], [16]. ENIL's can substitute other adsorbents and due to their usually high mass fraction of ionic liquids to carbon ratio.

1.3.2. Membranes

One of previously mentioned separation techniques, membranes, has also been the focus of studies due to their high selective and relatively cheap cost, being even proposed as one of the most promising ways to mitigate the emission of unwanted gases to the atmosphere. New polymeric membranes [17] which achieve better separation and are more resistant and membranes based on zeolites, metal organic frameworks, with a supported solvent and carbon molecular sieves, are examples of the studies performed in this branch of gas separation with promising results [18], [19].

1.3.3. Supported Ionic Liquid Membrane

Supported ionic liquids membranes (SILM's), are a type of a supported liquid membranes in which are membranes that are impregnated with a solvent; these membranes work based on a combination of three unit stages, the absorption of the feed phase, the diffusion trough the membrane and the desorption of the molecules into the permeate side. These membranes present however some limitations, like the loss of the impregnated solvent either by evaporation or as leaching. As such, the impregnation of ionic liquids in this type of membranes became an interesting alternative mainly due to their negligible vapor pressure, which would reduce the loss of solvent dramatically [20]. Nonetheless, this process still possesses the same drawbacks as traditional membranes, like low flows of gas and fouling, with an added disadvantage of being able to operate only at low pressure differentials in order to avoid the solvent displacement and consequently, the loss of performance and separation.

1.3.4. Zeolites

Zeolites are a class of microporous aluminosilicate materials with a high chemical and thermal stability which can be used as adsorbents for gas separation. In the case of CO_2, several zeolites have been reported as physical sorbents for its separation, with a focus on highly crystalline structures and high surface area [21]. The manipulation of the Si/Al ratio seems to have a significant impact on the adsorption of CO_2 and the addition of extra framework cations in the structure seems to increase the selectivity of CO_2 due to the negative charge within the framework. Those cations can be used as well to fine tune the size of the pores as well as some adsorption characteristics and due to their defined crystalline structure of these materials can also be used as molecular sieves [22]. These compounds have shown great promising results for separation of CO_2 [23].

1.3.5. Metal Organic Frameworks (MOF)

Metal organic frameworks are a relative new class of materials and are composed by coordinated organic ligand molecules and metal ions, since they also possess high surface area. These compounds have the ability to vary the organic linkers within, which translates to tunable pore sizes and its shape as well as the chemical potential of the adsorbing surface (selectivity, kinetics and capacity) [22]. Because these properties they

have become extensively studied positioning the CO_2 separation capabilities of these compounds as one of systems that show promising results [21].

1.3.6. Gas-liquid Membrane Contactors

Membrane contactors tackle the mass transfer problem in a similar way as encapsulation; the prime objective is the increase of surface area for mass transfer per unit of volume. This type of separation unit shows great promise since they merge the benefits of both liquid absorption (high selectivity) and membrane separation (modularity, compactness and easily scaled-up) [24]. Furthermore, the contact area is constant and does not depend of the solvent rate and its temperature, like in conventional columns [25].

In a gas-liquid membrane contactor module, numerous hollow fibers are collected and coated with an epoxy to fixate the fibers between themselves and fixating them to the shell side of the module, in this type of module the solvent usually passes through the lumen side of the fibers while the feed passes through the shell side, a shell side feed design, but the feed of the fluid to treat trough the inside of the fibers, the bore-side feed design is also possible. This simple configuration allows an easy manipulation with the flow of both streams able to be controlled independently and thus, optimized envisioning an economic and technical viable unit. In order to maximize the surface area, the internal diameter of these fibers is really small, around 50 mm, but due to the expectance of high hydrostatic pressures it has thick walls, with an outer diameter of 100 to 200 mm.

The fibers of these membranes are a polymeric compound that is not selective to the compounds involved, instead it acts as a physical barrier of both sides, which does impose a another mass transfer resistance to the system, but this is usually not a problem, being the solvent used the deciding factor of the module sorption capabilities [26]. This makes membrane contactors a technique with high potential, compared to conventional/classical separation units, with separation units 70% smaller and requiring less solvent. To regenerate the solvent a second membrane contactor can be used, with either a constant flow of an inert gas, usually N_2, or under vacuum, which due to the low partial pressure of the compound in the shell side, promotes the desorption of the compound. The possibility of using an integrated sorption desorption unit allows the use the solvent on a close-cycle with no lost solvent and thus, no makeup or replacement expected, mitigating the environment impact and reduce the cost inherent to the operation. This possibility has already been studied with a few chemical absorption ionic liquid

solvents, like the previously referred study done by Gómez-Goma et al. [11] using a aqueous mixture of $[C_2C_1im][Ac]$ as a separation agent and pathway for the exploitation of ionic liquids great potential for CO_2 sorption.

1.4. Scope and Objectives

This thesis will focus on CO_2 solubility and permeation measurements of different acetate anion ionic liquids, namely diethylethanolamonium acetate ([DEEA][Ac]) and tetrabutylphosphonium acetate ($[P_{4444}][Ac]$), and amino acid-based ionic liquids, like 2-(hydroxyethyl)trimethylammonium L-phenylalaninate ($[N_{1112(OH)}]$[L-Phe]) and 2-(hydroxyethyl)trimethylammonium L-prolinate ($[N_{1112(OH)}]$[L-Pro]), aiming at evaluating their potential as solvents to be used in a gas-liquid membrane contactor continuous separation unit designed for CO_2 capture from post-combustion sources. To this end an isochoric solubility setup, constant volume setup, able to operate in the 30 ºC to 80 ºC temperature range and pressures up to 5 bar, was designed, developed, built and validated. This solubility equipment, developed based on the isochoric method, is described in **Chapter 2-Experimental setup**.

To further study the selected solvents the gas diffusion through the solvents supported in a polymeric membrane was conducted using the "time-lag" method using an equipment available in the laboratory and described in **Chapter 3-Gas Permeation in Supported Ionic Liquids** .

A gas-liquid membrane contactor separation unit was also designed, built and used to evaluate the studied solvents on the CO_2 capture on a continuous process; the setup is described in **Chapter 4-Gas-Liquid Membrane Contactor – A Continuous Separation Process**.

Finally in **Chapter 5-Final Remarks and Future work,** general conclusion are drawn and final remarks on future work presented.

2. Experimental setups

2.1. Isochoric Cell

Ionic liquids are known for their high, in mole fractions, gas sorption [5]. One can even identify ILs based on amino acids as ILs with high potential as solvents for post-combustion. However, despite their potential, not only a small number of amino acid-based ILs (AAIL) have been evaluated [8], [9] but evaluated at a single temperature or small range of temperatures. Aiming at full characterization of the phase behavior of these AAIL and CO_2 or other gases relevant to post-combustion capture, like N_2O, N_2 and SO_2, an equipment capable of evaluate the gas solubility at low to moderate pressures is highly relevant and indispensable. Probably, the most common commercial setup for gas sorption determination is the gravimetric sorption analyzer (being the most known model the ISOSORP GAS LP-flow from Rubotherm). However, commercial versions of this setup are very expensive, difficult to setup and operate.

Solubility cells based on the isochoric method are known for their high accuracy and simplicity [5], [27]. Here, a setup based on the isochoric method was developed, implemented, calibrated and validated. An isochoric cell is based on a setup with a known and fixed volume, allowing thus to determine the gas phase concentration with time – by knowing also the volume of the solvent. Knowing the change of the number of moles of the gas with time, at the gas phase, one can determine the number of moles absorbed into the liquid phase. The solubility or change of the number of moles of the gas at the gas phase can be determined by following the system pressure decay over time, at a constant temperature. The cell volume is calibrated and the available volume for the gas phase determined by subtracting the volume of solvent, whose mass is measured analytically using a high precision analytical balance. Knowing the change of the number of moles at the gas phase, from the beginning to the end of the experiment (upon reaching pressure and temperature equilibrium), the solubility of the gas in the solvent can thus be determined.

2.2. Equipment Description

The stainless steel isochoric cell developed here, and depicted in **Figure 1**, can be divided in two parts; a gas-manipulation section (delimited by the L-shaped blue region in **Figure 1**) and a solvent-containing section (rectangular orange region). The gas-manipulation section, composed by a cylinder with a large volume connected to the pressure sensor, a gas line feed and a vacuum line. This section, whose volume was

calibrated following the procedure described below, allows the operator to add gas to the setup (knowing the number of moles of the gas in the section) avoiding its contact with the solvent and allow the setup to reach temperature equilibrium prior to the solubility measurements. The second section, also with a known volume and isolated from the first section by **VALVE 0**, allows the addition of the solvent, its manipulation and temperature stabilization, by means of a type K thermocouple, prior to the measurements. Both sections are connected with a quick-fit from *Swagelock* allowing for an easy manipulation of the setup in terms of cleaning the system and replace the solvent.

Gas solubility measurements are known to be time-consuming with experiments taking several days for highly viscous systems, as shown in **Appendix D**. Thus, aiming at decreasing the experiment time, an agitation mechanism was implemented and placed below the cell containing the solvent. At first this was accomplished by modifying a 5 V Direct Current (DC) PC fan in which the blades were replaced by a lever, with the same width of that of the inner diameter of the measuring cell, fixed to the rotor axis, containing, two magnets at each extremity. However, the heat generated by the rotor, and its placement close to the cell, lead to an increase of the measuring cell temperature of 3 ºC. Furthermore, operating limitations of the apparatus did not allow to control the rotation speed that in turn translated often on excess mixing of the solvent, impacting negatively on the solubility determination, or in extreme cases to the complete detachment of the lever from the rotor axis, making the setup not safe for use.

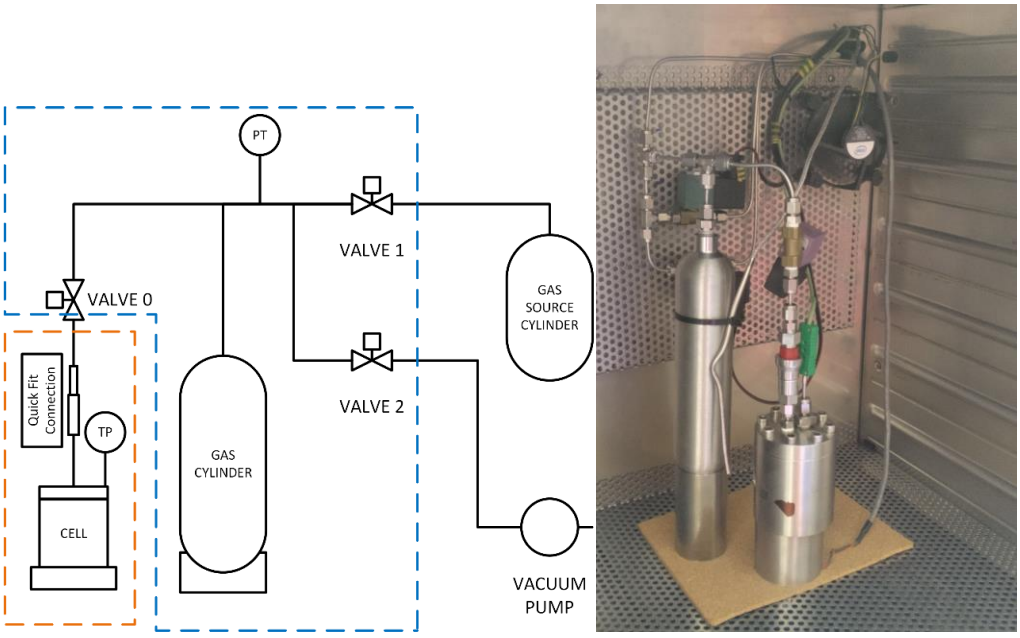

Figure 1-Schematic diagram (left) and photo (right) of the isochoric setup.

Recognizing that a proper agitation is fundamental for a fast an accurate measurement, a new stirring mechanism was developed. Thus, a stepper motor controlled by a 30A ESC brushless motor controller and a potentiometer connected to an Arduino, in order to be able to remotely control the agitation, was mounted. The source code of the magnetic agitator is provided in **Appendix D**.

The isochoric setup was developed, calibrated and validated to operate at pressures up to 5 bar. Since the gases of interest are supplied at higher pressures, a pressure reducing valve, coupled with a pressure gauge, was placed between the gas source cylinder and **VALVE 1** to ensure that the gas fed to the setup and its pressure could be controlled and managed to reach the intended initial pressure for the measurements. Note that, on opening **VALVE 0**, allowing the gas to contact with the solvent, the system pressure drops due to the increase of the setup volume.

With the purpose of fully automatize the equipment, electric solenoid valves were used for the connections to the gas cylinder, vacuum pump and between sections; it is noteworthy that these valves are normally closed, assuring that in case of a power outage not only the experiment would not be interrupted but most importantly, to ensure the safety of the equipment and laboratory staff – avoid the release of potentially dangerous gases to the laboratory environment or to other equipment attached to the setup.

The pressure of the system was monitored using a pressure transducer model PAA-11 from *Keller* able to measure the pressure from 0 to 5 bar with an uncertainty between 0.5 mbar and 5 mbar, depending on the temperature range of the pressure transducer operating conditions (with an output nominal signal of 175 mV).

In order to obtain solubility values at different temperatures and ensure a stable value of the temperature, the apparatus was placed inside an oven capable to operate within the envisioned temperatures. A PID temperature controller from Lae electronics, model AC1-5, was used to control the temperature within 0.1 ºC, this controller had a PT100 temperature sensor connected, which is capable of much higher precision than the controller, however, this precision is not accessible through this controller. Furthermore, the temperature controller has a communication board allowing monitoring and controlling the oven temperature set-point remotely.

Although the pressure transducer provides temperature compensation, the range of temperatures expected for the envisioned measurements (30 ºC to 80 ºC) would impose a

high noise on the transducer signal that would translate on pressure uncertainties higher than the temperature impact on the gas solubility. Thus, we opted to place the pressure transducer outside of the oven, minimizing nonetheless the volume of the gas line and any temperature change impact by insulating the gas line with cotton fibber and foam. The pressure transducer was calibrated against other pressure transducer calibrated and certified by an independent laboratory with IPAC accreditation, following the EN 837-1 standard and with accuracy better than 0.2%, as reported in **Appendix A**. The pressure transducer electrical current signal was registered for pressures ranging from 0 to 5 bar at room temperature and as expected, the pressure transducer signal follows a linear behavior within the pressure range evaluated, as reported in **Appendix A**.

It is noteworthy to mention that following the pressure transducer schematics a 24 VDC power adapter was used. Although the pressure transducer seemed to operate normally, for long periods of time (typically 12 hours) its signal would begin to degrade and shift the pressure values in around 0.2 bar compromising thus, the measurements. For example, in a closed system without solvent and at constant temperature and pressure, the pressure measured by the equipment changed over time increasing and decreasing in fixed intervals of time without any external perturbation occurring. After a deep analysis of the technical specifications, the problem appeared to be due to an overload of electric circuit. Following the initially overlooked manufacturer suggestion of using a current limited between 1 mA and 4 mA, the electric current supplied to the equipment was manipulated to provide only 1 mA. This current manipulation was achieved by using a 22 kOhm potentiometer regulated to supply the specified current intensity, as depicted in **Figure 2**.

This change in electrical current implied a new calibration of the pressure transducer, since the pressure transducer output signal is directly dependent to the input intensity. Once again, the abovementioned proceeding was used to recalibrate the pressure transducer at this new condition. This point forward the pressure transducer behavior remained consistent independently of the measuring time used (within 0.5 mbar in a closed system at constant temperature).

In order to follow and manipulate the system signals a series of RS-485 input/output modules from *Advantech* were used as interface between the experimental setup components and the computer. The *Advantech* modules use the RS-485 standard for serial communication between the modules and thus, to be able to communicate, acquire

and manipulate the signals registered using a computer, the module ADAM-4561 (RS-232/422/485 to USB converter) was used as RS-485 bridge interface between the I/O modules and the standard USB computer serial communication and consequently the acquisition software. For the temperature measurements the *Advantech*'s ADAM-4019 (universal analog input module) was used to read the temperature from the type K thermocouple and the electric current of the pressure transducer. On the other hand, the ADAM-4055 (Isolated Digital I/O Module) was used to actuate on the valves and check its state. The module information and control were done using the ASCII command serial communication protocol, in which every module has an address that allows identifying the module within the network and a function that determines the response of the equipment. This protocol is better described in **Appendix C**.

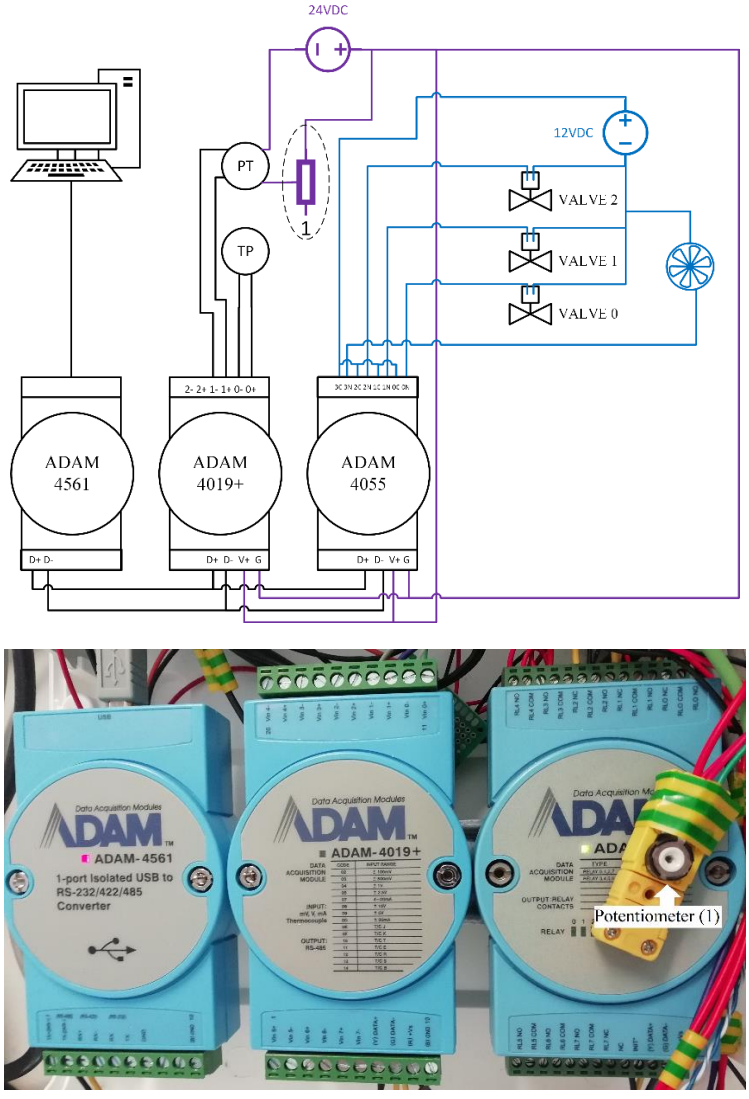

Figure 2-Eletrical diagram with the pressure transducer potentiometer (1) (up), ADAM's and the potentiometer (down).

The original oven temperature controller was damaged and therefore replaced by a LAE Electronic AC1-5 PID temperature controller, as previously stated. This temperature controller has a communication interface board that allows the equipment to be coupled to a RS-485 network. Although, one could place the controller to the existent ADAM RS-485 network, the communication protocol used by the temperature controller was different than that used by the ADAM modules and thus it stood easier, at an initial configuration setup and test run, to connect the temperature controller to other communication port on the PC using a stand-alone RS-232/RS-485 bundle. After this initial test, verification and communication algorithms defined, this controller was then added to the already existing ADAM's RS-485 network. The communication of this apparatus was done using a modified Modbus ASCII protocol variant in which only the temperature read and write functions were used. This communication protocol is explained in **Appendix C**.

Although the electrical valves were initially manipulated using the ADAM-4055 digital output module, this module was projected to operate with a maximum load of 200 mA (all channels combined) and a maximum allowed voltage of 3 V. Since the voltage required to operate the valves was higher than the module limitations the module short-circuited and burnt. To overcome the problem a different module, ADAM-4068 (8 channel relay output module with modbus), able to operate as a relay, was used; nonetheless to avoid future occurrences external relays were additionally used, and a much weaker electric circuit was supplied to the ADAM module. The final electrical diagram is depicted in **Figure 3**. In this diagram a 5 V circuit is controlled by the ADAM-4068 module, whenever a 5 V circuit is completed a relay is triggered and the corresponding 12 V circuit is completed and, as consequence, the corresponding valve is open.

A computer fan was also placed inside the oven to assure a faster temperature equilibration and homogenization. The placement of a new fan inside the oven lead to an un-optimized temperature controller behavior that presented a significant temperature overshoot, considerable temperature off-sets and longtime equilibration periods to reach the steady state condition. Thus, using the auto-tuning feature of the temperature controller the PID parameters were optimized for the new setup configuration allowing achieving moderate temperature offset, no permanent temperature off-set and fast steady state condition.

Although the use of solenoid valves in the long run would prove to be useful, allowing the automation of the process, in the beginning this type of valves appeared to be unreliable because they would easily overheat and close on its own. This malfunction lead to valves being closed mid-cycle impacting on the solubility measurements and compromising the experiments. Later it was discovered that the valves acquired were not the ones requested; the required valves were expected to operate at a 12 VDC while those acquired were manufactured to operate at 12 VAC (Alternate Current). Although, theoretically they still work under a DC voltage as long as it draws the same amount of current when operating in AC, the voltage that should be supplied would need to be only about 3.5 VDC (this value was determined experimentally as the lowest value capable of making the solenoid work as intended), which would explain the overheating problem. To solve this, the valve that connects the cell to the immovable part was replaced, since it is the only valve that received continuously voltage during the long measurement periods and thus, more susceptible to over-heat. There was no need to change the other valves as they only need to open for brief moments in time and as such represent no major problem in its use.

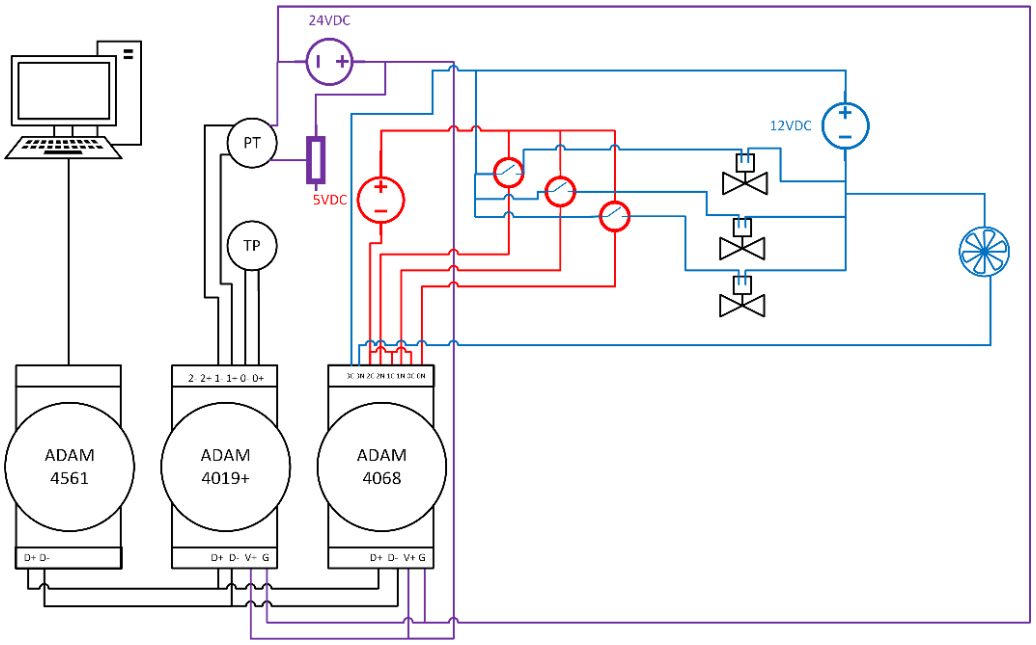

Figure 3-Final electrical circuit diagram of the data acquisition for the setup temperature, pressure and valves control.

To use the isochoric method, the volume of the system not only has to be fixed but it must also be known, and as such a volume calibration of the system was performed. First the whole system was subjected to vacuum and put at a constant temperature. Secondly the

gas contained in an ultra-light weight composite cylinder was put on top of a high precision/high weight analytical balance, with an accuracy of 1 mg (Sartorius LA2000P), and the amount of gas added to the cell to reach a desire pressure registered. Then, knowing the exact amount of gas added to the system and the system pressure it was possible to calculate the volume of the system through a rearrangement of the modified ideal gas law in which the *Z* parameter was calculated using the Peng-Robinson equation of state (EoS), as described in **Appendix A**. This procedure was applied to both section of the setup.

The procedure and methodology of using the isochoric cell is relatively simple. Before starting, the ionic liquid is subjected to a purification process comprised of high vacuum (10^{-3} mbar), continuous stirring and moderate temperature (30 ºC) for a period never smaller than 48 h with the purpose of removing any dissolved gases and volatile compounds that might be present from the synthesis and/or absorbed during the sample manipulation.

After the purification procedure, the ionic liquid is transferred to the measuring cell using a syringe. The exact mass of compound added to the measuring cell is determined using an analytical balance with an uncertainty of 0.001 g. The compound mass added to the measuring cell is determined by weighting a syringe containing the solvent before and after introducing the liquid in the cell. The cell is then closed (screwed on top) and connected to the remaining apparatus though the quick-fit connection. With all the system connected, **VALVE 0** is opened and vacuum (10^{-3} mbar) is applied to the system by opening **VALVE 2**; this procedure allows to remove any gases that could be absorbed during the sample manipulation. With the system under vacuum the oven temperature is set to the highest measuring temperature planned for the measurements and the system allowed to reach temperature equilibrium. The setup and the measuring vessel are then isolated, by closing **VALVE 0** and **VALVE 2,** and the gas is added to the apparatus top part (gas section) opening **VALVE 1** that connects setup to the gas line. The gas pressure is fixed by manipulating the abovementioned pressure regulator valve placed between **VALVE 1** and the gas cylinder. Once the gas reaches temperature and pressure equilibrium, **VALVE 1** is closed. This step is necessary, as the gas, due to pressure differentials is not at thermal equilibrium with the rest of the apparatus and, as such, needs

time to reach this equilibrium, as evidenced by the small decline in pressure in the first moments in **Figure 4**.

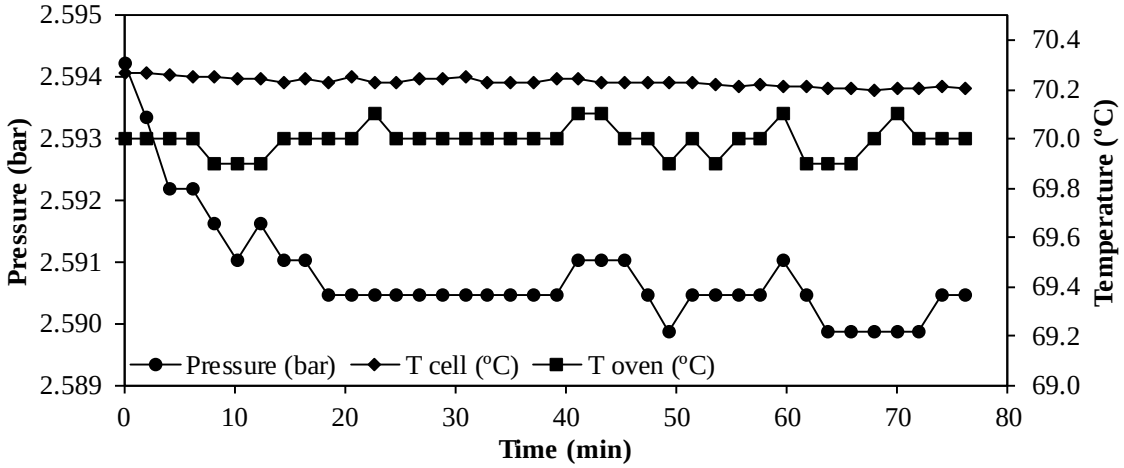

Figure 4-Pressure, cell and oven temperature monitoring as function of the measurement time upon adding CO_2 to the system.

In the first tests the exact mass of gas supplied to the cell was weighted aiming at increasing the level of confidence to the volume calibration done; this procedure allowed to conclude that the previous volume calibration was correct and the need to measure the exact mass of gas added at each measurement is not required on future measurements, simplifying the methodology adopted. This procedure allowed also to conclude that, knowing the density of the solvent and thus, knowing the solvent volume with temperature, the gas phase volume is adequately determined.

The choice of starting the measurement from the highest temperature and then consecutively reduce the temperature after reaching pressure equilibrium was due to two factors: first, an high temperature would allow to regenerate better the solvent upon manipulation and secondly, since the gas solubility increase with the temperature decrease, starting the measurements at a higher temperature allows to measure all the isotherms on a single run without the need to replace or regenerate the solvent at each temperature – at each new lower temperature an additional number of moles of CO_2 would absorb into the solvent.

The pressure is then monitored along the experiment and the equilibrium is considered reached when the pressure stabilizes within 0.3 mbar for a period of 60 minutes. These equilibrium conditions were established during the setup validation and found to be adequate to evaluate the equilibrium condition.

For each temperature the set-point of the oven is changed, to a lower temperature, and the pressure is again monitored until reaching new equilibrium. This procedure is repeated for all the temperatures envisioned for the system under study.

Once measuring the lowest defined temperature two outcomes are foreseeable: either the cell is depressurized to atmospheric pressure allowing the manipulation of the setup and the removal of the solvent, preparing the system for the next measurement, or the solvent undergoes a regeneration procedure that comprises the increase of temperature, normally to 70 ºC to start promoting the gas desorption, followed by applying vacuum (10^{-3} mbar) for a few hours. After the regeneration procedure the setup is closed from vacuum (closing **VALVE 2**) and the pressure monitored. In the case that the setup is not able to remain under vacuum (10^{-3} mbar), denoting that the solvent regeneration was not complete, the vacuum is reapplied for a longer period – the procedure is repeated until the regeneration if considered complete. After the regeneration procedure the solvent solubility is again measured at a different initial pressure allowing to fully characterize the system diagram within all the feasible pressure range.

It is noteworthy that an initial regeneration using only the effect of temperature is recommended to avoid the compound displacement due to violent bubbling resulting from the fast gas desorption, which ultimately would displace the solvent to parts of the setup, like the gas cylinder, that would become difficult to clean and would lead to measurements, on the following systems, influenced by unaccounted solvent mass and thus, erroneous.

2.3. Data acquisition and Software development

Using LabView with a few modules extra installed, namely the Virtual Instrument Software Architecture (VISA) and the Datalogging and Supervisory Control (DSC) module, a program with a graphical user interface (GUI) was developed so that the operator could follow the setup signals with time, save the monitored variables and define a measuring protocol.

This software went through numerous changes, not only during the apparatus development, due to changes on the used equipment, but also during its optimization cycle, by optimizing existent or adding new features. An initial version, envisioned to only monitor and register temperature and pressure and control the valves states, was

continuously changed to new optimized versions culminating in the latest version in which a measuring protocol feature was added allowing the user to pre-define a measuring protocol transforming the program to be more dynamic and user/solvent independent. This measuring protocol feature allows the user to define working temperatures at different intervals of time and thus, allowing room for posterior automation of this process. Furthermore, this protocol allows the use to pre-determine equilibria criteria and specify the moment that a new temperature set-point is adequate to be changed by evaluating the system equilibrium conditions. Besides monitoring the temperature, this equilibrium protocols use the Peng-Robinson equation of state to calculate the quantity of gas in the gas phase by monitoring the system pressure change – pressure standard deviation and pressure/time slope – within a defined period. The final version of the program is depicted in **Figures 5** and **6**.

The software allows an easy control and monitoring of the valves; in the GUI, the valves in the diagram are switches that open and close the physical valves and the circular indicators indicate the actual valve status. By measuring the actual status of the valves avoids situations where the user is erroneously led to believe that a valve is open while it is still closed due to electrical problems or malfunction of the program. The molecular weight and density of the compound under study are also inserted into the program and allow the use of the Peng-Robinson EoS and the correct gas phase volume available. The gas properties, required for the use of the EoS, are recorded in a separate text file and can be easily accessed with an external program and manipulated when needed.

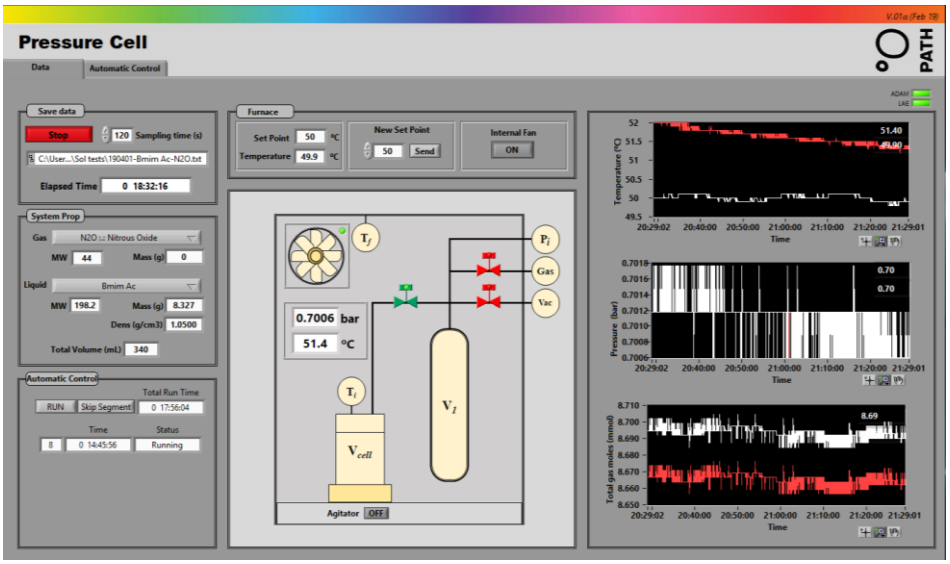

Figure 5-Graphical User Interface, principal screen.

The graphs in the GUI, depicted in **Figure 5**, represent, in descending order, the temperatures of the oven and the cell, the pressure of the system and the number of moles of the gas in the gas phase (it always assumes that the system is connected to the cell). By representing graphically, the system variables, the evolution of the system is easily visualized and conclusions about the system equilibria can be better drawn. It is important to note that these graphics are only capable of showing the last hour of experiments, as such if the system presents a slower kinetics, the evaluation of the system equilibrium must be made using another software to plot all data recorded. In the GUI top left, the path to a file, in which the data will be recorded, is indicated together with the sampling time of the data. Both fields can be changed to avoid an exorbitant amount of points that could crash the program used to manipulate the data. In the bottom left corner there is information about the current segment of the measuring protocol is running and its corresponding time and total time of the program. And finally, above the diagram this section allows the manual change of the oven set-point and its current temperature value (monitored continuously); the oven fan can also be turned off/on to avoid injuries in the manipulation of the system when needed.

2.4. Equipment Automation & measuring protocol

Due to the large time scale of the experiments, an automation tool was deemed necessary to optimize the experiments avoiding thus, “wasting” unnecessary time measuring the system variables within equilibrium conditions, but mostly avoid stopping the measurements mid-cycle or impose perturbations to the system when the equilibrium was not yet reached. As such, the program was changed so that the experiment could operate based on time scales and temperature and pressure equilibrium evaluation.

The latest program version allows the user to specify the minimum period that an experiment must run, at a given temperature, and evaluate if the pressure and temperature equilibrium conditions are met, by using an equilibrium verification algorithm, prior to change the system temperature to the next isotherm. Based on the user protocol and equilibrium evaluation algorithm the oven set point can be then changed automatically, as the equilibrium criteria is met, and the complete characterization of the system performed without user interaction. The equilibrium assessment, in this time-controlled segment, is done by evaluating the pressure and temperature standard deviations within the last 60

minutes of monitoring. It was found that 0.0003 bar for the standard deviation and 0.0015 bar for the pressure decay of the last 30 minutes was adequate for a correct decision. For the oven temperature, the equilibria criteria were defined as a maximum offset of 0.5 ºC, a standard deviation of 0.1 ºC and a temperature change of 0.5 ºC during the last 30 minutes of operation. The cell temperature equilibrium criterion was determined to be the same as that of the oven for the standard deviation and increase/decrease rate, but with a temperature offset of 2 ºC compared to the oven temperature. It is important to note that this values were adequate for the first solvents studied, for solvents with higher viscosity, studied later, the sorption kinetics were drastically slower requiring longer periods of equilibrium - For these highly viscous systems it was found that 60 min was necessary to correctly determine the pressure equilibrium.

Aiming at adding the possibility of performing sorption/desorption fully automated cycles the program algorithm was changed to include the possibility of changing the state of the valves in function of the measuring protocol defined by the user – note that in order for this protocol to work completely autonomous after the protocol is provided, the vacuum pump must be continuously on and the gas line must be always available and pressurized at the desired pressure (the option to automatically change the initial pressure of the experiments does not exist, as such the pressure regulator must also be changed between experiments if the objective is a full characterization of the system in study).

Due to the long periods of measurement and the large amount of raw data collected the computer tends to run out of resources leading, in the most extreme cases, to a system crash. Thus, to avoid the overload of the program, or the operating system crash, the software was changed to add an option to create a new output file and change the sampling time on periods far from the equilibrium, for example in the beginning of the measurements a larger number of points are recorded (typically each 2 seconds, the minimum the program can acquire data) but become more spread in time as the system reaches equilibrium. This initial fast recording allows the evaluation of the sorption kinetics while the longer registering at the end allows a better decision on the equilibrium state of the system.

In summary the segments able to be used in this program version are, in order of development:

- Temperature segment, with or without equilibria checks;

- Changing a valve position (only solenoid valves);
- Start a new output text file;
- Change the sampling time of the recorded data.

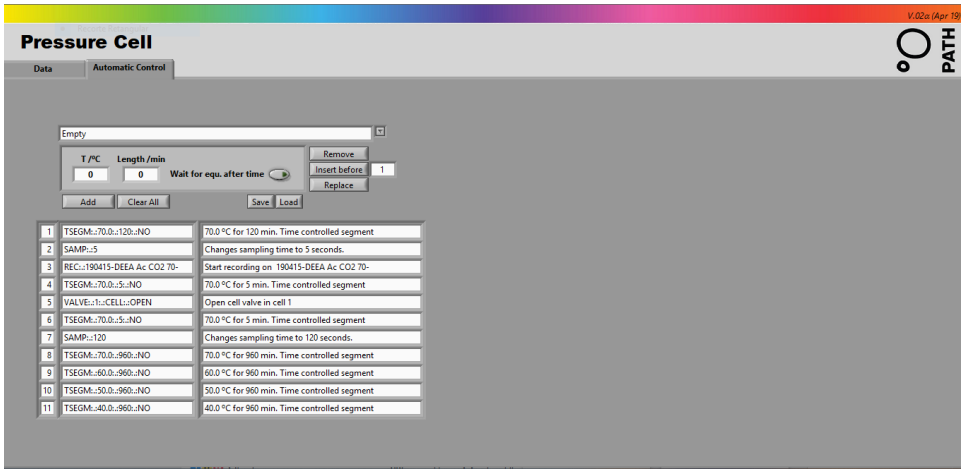

Figure 6-Screenshot of the "Automatic Control" feature user interface.

In **Figure 6** the GUI that allows the user to establish the measuring protocol is depicted; in the example given a temperature segment is used to make the system wait until the gas reaches an equilibrium state, then the sampling time is changed to 5 seconds and a new data output file is created, then, after 5 minutes, **Valve 1** is opened starting the experiment; after 5 minutes the sampling time is changed to 2 minutes and segments of 16 hours are added for each temperature.

2.5. Equipment uncertainty

The pressure transducer used, Keller PAA-11, has an error of 0.1%FS (full scale reading) or 0.01%FS depending on the temperature range, according to the manufacturer, which means that the pressure uncertainty is 0.1% or 0.01% of the full scale reading. At the maximum pressure allowed (5 bar) the uncertainty on the pressure is 5 mbar, when the temperature range is considerable, or 0.5 mbar when the pressure transducer temperature is constant (independent on the system temperature). Since the pressure transducer was placed outside of the oven it is not subject to temperature changes and so the standard uncertainty becomes 0.5 mbar.

The temperature probe placed in the gas phase is a PT100 with an uncertainty of 0.01 ºC. This uncertainty value is, however, not achievable on the current setup due to the normal operation of the oven temperature controller that imposes an expanded uncertainty

of 0.5 ºC to the temperature. The same uncertainty was found for the type K thermocouple placed in the solvent cell.

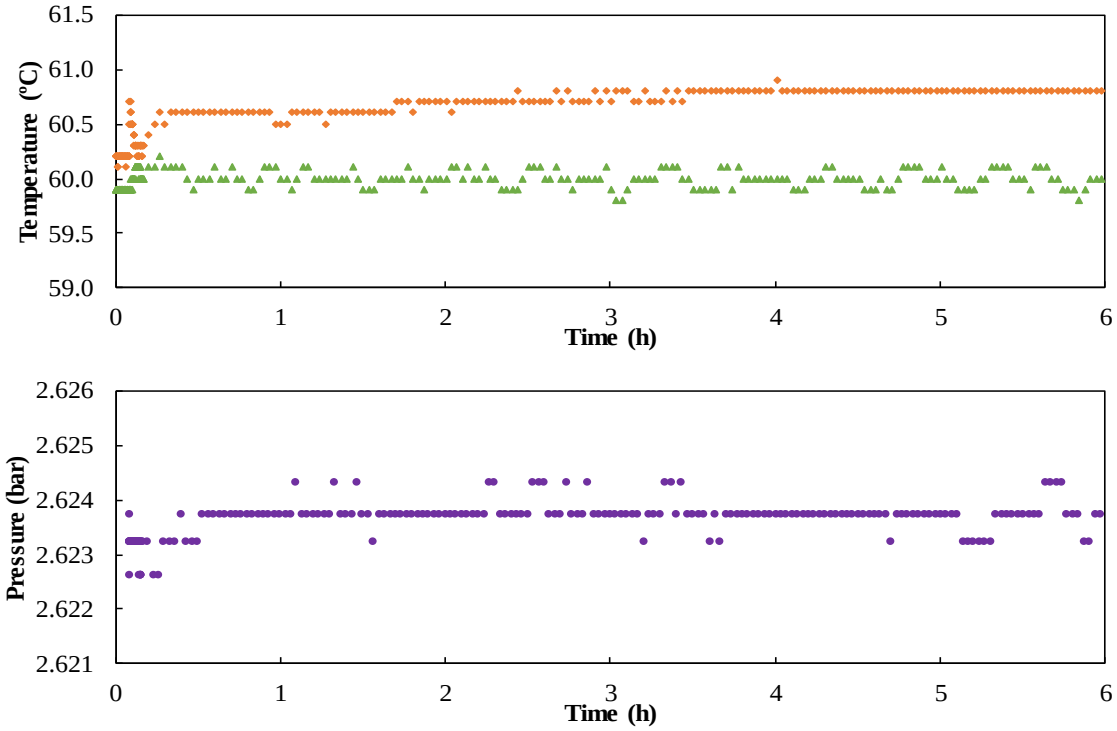

Figure 7-Temperature (top) and pressure (bottom) as function of time for the $[C_2C_1im][Ac]+N_2$ system at equilibrium conditions.

The pressure transducer expanded uncertainty, considering the power supply and the temperature variations due to the temperature controller, was found to be 0.4 mbar. As depicted in **Figure 7**, the system temperatures and pressure signals present the expected noise with small variations that impose an uncertainty of 0.07 ºC and 0.05 ºC for the temperature of the cell and the oven respectively. These expanded uncertainties impose an expanded uncertainty on the number of moles of the gas of 0.0050 mmol, which stands on a relative error of 0.016%, which makes this uncertainty completely irrelevant when compared with the sensor uncertainty, as such the equipment uncertainty is better defined by the pressure transducer and temperature controller uncertainties.

2.6. Equipment and Methodology Validation

With the purpose of validate the isochoric cell, a well characterized system, namely 1-butyl-3-methylimidazolium dicyanamide ($[C_4C_1im][DCA]$) + CO_2, was selected as a reference [28], [29]. On top of the full characterization of the system *pVT* phase diagram, this system, being governed by physical absorption, presents low solubilities on the

pressure range of this study allowing inferring on the sensibility and accuracy of the equipment. The Henry constants determined in this work, those reported in the literature and the deviation obtained are shown in **Table 2**.

Knowing the quantity of the gas at the gas phase between the beginning and end of each equilibrium step (at each temperature) one can determine the amount of gas absorbed in the solvent. To better determine the number of moles of the gas during the experiments the Peng-Robinson equation of state was used to determine the compressibility factor (*Z*), as explained in **Appendix A**. The compressibility factor is then used to calculate to correct the non-ideality of the gas phase on **Equation 1**.

$$n = \frac{P \cdot V}{Z \cdot R \cdot T} \tag{1}$$

The solubility is then calculated dividing the number of moles of the gas absorbed (Δn_{CO2}) by the total of moles of the species on the liquid phase, to better study the compounds further studied their molality (m_{CO2}) was also calculated.

$$\Delta n_{CO_2} = n_{CO_2}(initial) - n_{CO_2}(equilibrium) \tag{2}$$

$$x_{CO_2} = \frac{\Delta n_{CO_2}}{\Delta n_{CO_2} + n_{IL}} \tag{3}$$

$$m_{CO_2} = \frac{\Delta n_{CO_2}}{m_{IL}} \tag{4}$$

The solubility data obtained for this system is represented in **Figure 8** and the raw data is available in **Appendix D**.

Table 2-Henry Constants as function of temperature for the [C_4C_1im][DCA] + CO_2 system and its percentage relative deviation (%RD) from the work of Sanchez [28] and Carvalho et al. [29].

T (ºC)	*H* ± σ* (bar)	*H* ± σ* [28] (bar)	%RD	*H* ± σ* [29](bar)	%RD
70	135.5±3.6	111.4±4.8	21.6	121.4	11.6
60	106.5±4.0	94.4±3.5	12.8	104.8	1.6
50	88.5±2.1	------	----	89.2	0.7
40	75.1±2.6	------	----	74.9	0.4
30	67.4±1.9	60.3±1.2	6.7	61.9	4.0

* standard deviation

Through the evaluation of **Figure 8** it is possible to verify that the experimental data is within the acceptable range of the values reported in the literature. It is important, however, to point out that the values from the work of Carvalho et al. [29] were obtained by extrapolating high pressure data to the Henry's law pressure range.

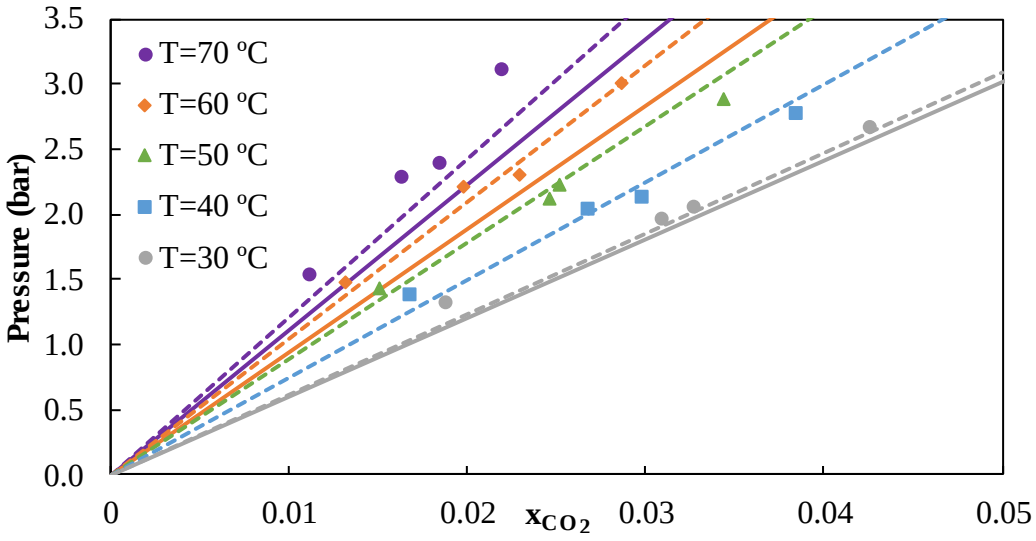

Figure 8-*pVT* phase diagram for the system of [C_4C_1im][DCA] + CO_2. The solid symbols represent the experimental data, the solid lines represent the work of Sanchez [28] and the dashed ones Carvalho et al.[29].

2.7. Solubility Measurements

Now with the equipment and methodology validated new ionic liquids were evaluated for their CO_2 solubility. According to literature, the acetate anion with an imidazolium cation is capable of chemically bonding with CO_2 [30]–[32], so different ionic liquids based on acetate anion were studied aiming to obtain a chemisorption solvent with low viscosity. Another type of solvents considered, which showed great promise were the amino acid-based ILs (AAIL) which due to their amine functionalization seem capable of chemisorption, as such ionic liquids based of l-phenylalanine (L-Phe) and l-proline (L-Pro) were also synthesized and studied.

2.7.1. Materials

With the purpose of determining the CO_2 in ionic liquids presenting chemisorption there was the need to synthesize new compounds. The acetate-based compounds chosen to this study were the aprotic tetrabutylphosphonium acetate ([P_{4444}][Ac]) and the protic diethylethanolamonium acetate ([DEEA][Ac]), while the amino acid based ionic liquid chosen were 2-(hydroxyethyl)trimethylammonium L-phenylalaninate ([$N_{1112(OH)}$][L-Phe])

and 2-(hydroxyethyl)trimethylammonium L-prolinate ([$N_{1112(OH)}$][L-Pro]). The precursors used for these syntheses are reported in **Table 3**.

Table 3-Compound name, supplier, CAS number and purity.

Compound	CAS	Supplier	Purity
Choline Bicarbonate	78-73-9	Sigma	80%(+water)
N,N-Diethylethanolamine	100-37-8	Acros Organics	99%
Tetrabutylammonium hydroxide	2052-49-5	Acros Organics	40%(+water)
L-proline	147-85-3	TCI	99%
L-phenylalanine	63-91-2	Alfa Aesar	99%
Acetic Acid	64-19-7	Honeywell	≥99.99%
L-Valine	72-18-4	Fisher Bioreagents	≥98.5%

The synthesis of the [DEEA][Ac] was done using a Brønsted acid-base neutralization method as indicated by Sharma et al.[33], in which, the diethylethanolamine is added drop wise to an equimolar quantity of acetic acid. The synthesis was done at low temperature 0°C. After the amine addition the mixture was mixed during 24 hours in a nitrogen atmosphere at room temperature in N_2 atmosphere. Afterwards the obtained reaction mixture was distilled under high vacuum (10^{-3} bar) The reaction mixture was dried under high vacuum (10^{-3} mbar) for 48 h at room temperature and was kept under nitrogen atmosphere to avoid the moisture.

The AAILs chosen to be studied in this work were also synthesized, this time following the procedure proposed by Sintra [34]; the l-phenylalanine and l-proline amino acids where chosen as basis to synthesize [$N_{1112(OH)}$][L-Phe] and [$N_{1112(OH)}$][L-Pro]. Briefly, a quantity of [$N_{1112(OH)}$]OH in a 45 w/w% methanol solution was added dropwise to an aqueous solution of the amino acid, with a molar excess of 10%, at room temperature. This reactional mixture was stirred for 2 hours protected from light. After this period, the water formed by the reaction was removed by applying vacuum (10^{-3} mbar). Afterwards, a mixture of acetonitrile/methanol in a volumetric ratio of 9 to 1 was added while vigorous stirring the mixture in order to precipitate the excess of amino acid. This mixture was then left stirring for 1 hour and the excess of amino acid was then filtered. In a final stage, the acetonitrile and methanol were evaporated by reduced pressure (10^{-3} mbar

using a rotor evaporator) and the desired compound was dried under high vacuum (10^{-3} mbar) for at least 48 hours.

The water mass fraction of the ionic liquids was determined by coulometric Karl Fischer titration (Metrohm, model 831) and it was verified to be less than 0.05% in mass. The structure of all compounds synthesized was confirmed by ^{1}H and ^{13}C NMR spectroscopy, showing a high purity level of all the ionic structures after their synthesis.

2.7.2. Ionic Liquid CO_2 Solubility

The first compound evaluated was the [DEEA][Ac]. However, during the purification procedure described before and on applying vacuum at 10^{-3} mbar the IL evaporated. The unusual high vapor pressure of the IL does not allow to measure the gas solubility in the isochoric cell if the measurement procedure is followed. A new strategy was thus needed for this solvent. One of the envisioned procedures is to apply vacuum to the setup containing the protic IL only for a very short period of time and pressurize the system short after. Nonetheless, it was not possible in the time frame of this thesis to evaluate if this procedure would lead to accurate results, since important concerns rise from the pressure and temperature equilibration short time and its impact on the equilibrium pressures. In fact, such procedure must be validated in other well characterized protic IL that similarly presents non-negligible volatility.

The next solvent tested was the [P_{4444}][Ac]. Contrary to the [DEEA][Ac] this IL could be used following the first mentioned procedure, not evaporating under low pressure conditions, and thus, the solubility was measured and is depicted in **Figure 9**.

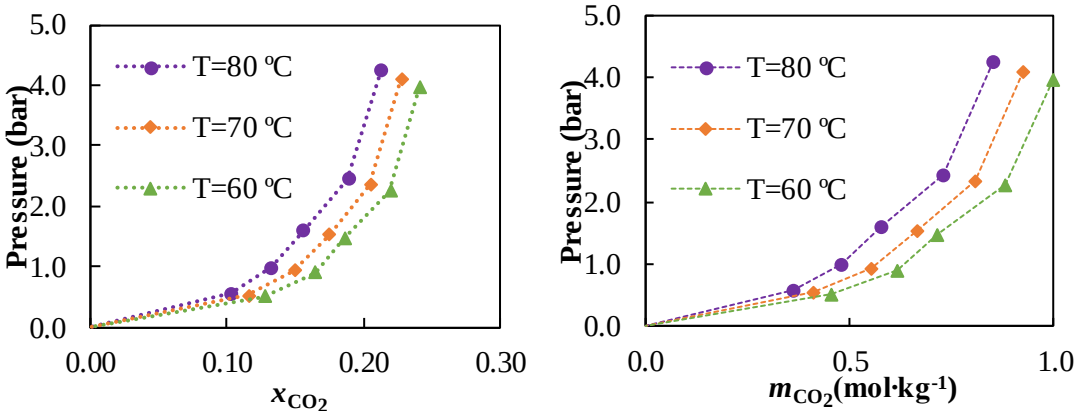

Figure 9-*pxT*(left) and *pmT*(right) phase diagram of the [P_{4444}][Ac] + CO2 system. The dashed lines are guides for the eyes.

The range of temperatures evaluated for this system were set to change between 60ºC to 80ºC, since the compound melting temperature appeared to be below 60ºC. The compound melting point was not possible to be determined using conventional techniques due to its high hygroscopicity, whose moisture absorption, even during manipulation times, would lead to its state change. The compound melting temperature is, though, planned to be determined by DSC.

2.7.3. Amino Acid based Ionic Liquid CO_2 Solubility

Amino acid-based ionic liquids stand as the most promising family of solvents for chemisorption due to the possibility of fine-tuning their structure to specifically interact with the CO_2. Amine and amino acid-based solvents that go through chemisorption are known to form highly viscous compounds upon reaction and the $[N_{1112(OH)}][L\text{-Phe}]$ was no exception. Although expected, the highly viscous reaction specie(s) formed at the gas-liquid interface limited the gas molecules diffusion through the bulk culminating in a extremely long measurement windows, as depicted in **Figure 10**.

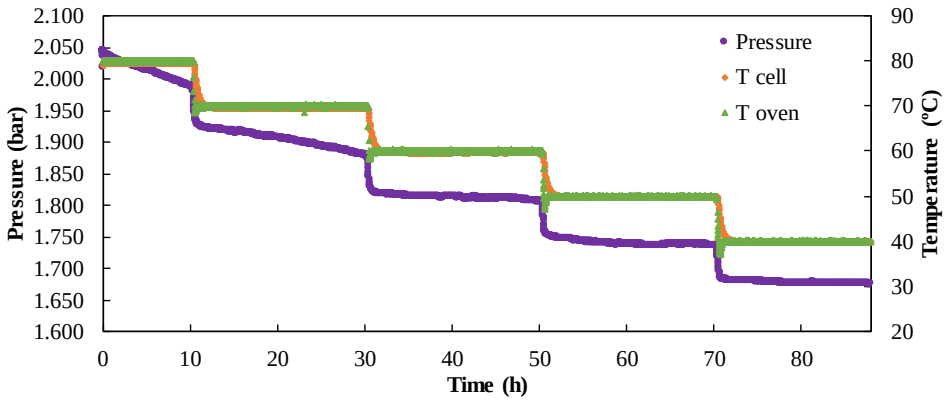

Figure 10- Pressure and Temperature as function of time of $[N_{1112(OH)}][L\text{-Pro}] + CO_2$.

As depicted, the slow kinetics lead to the first two measured temperature ending far from the equilibrium, as shown by the continuous decrease of the system pressure – no pressure plateau – up to the change on the temperature setpoint. The next three temperatures although seemed to have reached equilibrium a more thorough analysis (after opening the cell), although, allowed to infer that the system was still not at equilibrium. After inspecting the solvent, it was clear that only the top layer of the solvent has reacted with the CO_2 leading to the formation of a protective layer that prevented the CO_2 to continue to solubilize into the IL. These observations, thick highly viscous top layer and a day-long measurement, allowed to conclude that a new strategy/methodology was deemed

necessary. To circumvent this problem one of the methods envisioned was the IL encapsulation in submicro-capsules of carbon.

To encapsulate the IL, a pre-made set of carbon microspheres, whose synthesis is reported in other works [14], [35], were dowsed in a mixture of the ionic liquid with a volatile solvent. Methanol was chosen due to its miscibility with the IL and the low contact angle with the carbon spheres; allowing the mixture to easily impregnate and diffuse into the spheres' pores and interior. Then, the volatile solvent was evaporated by applying vacuum (10^{-3} mbar), allowing the IL to fill the carbon spheres. The spheres were weighted before and after the impregnation procedure and the mass of the ionic liquid on the spheres determined with an analytical balance with an uncertainty of 1 mg. Although the amount of IL impregnated in the carbon spheres could be determined gravimetrically an additional elemental analysis was performed. This elemental is done using a linear regression determined on literature work [36], [37], where the weight percentage of IL and the percentage of elemental N_2 supplied trough elemental analysis was show to be directly related. The values for the IL encapsulated in the $[N_{1112(OH)}][L\text{-Phe}]$ was 70 w/w% and 70 w/w% for the $[N_{1112(OH)}][L\text{-Pro}]$.

The encapsulation is known to improve the absorption kinetics considerably as depicted in **Figure 11**. For the studied ILs not only the sorption kinetics was drastically improved but mostly it allowed to determine the gas solubilities overcoming the limitations observed for the neat measurements. The $[N_{1112}(OH)][L\text{-Phe}]$ IL, when encapsulated, reaches equilibrium within one hour, becoming the temperature equilibration time the limiting set on the experiment.

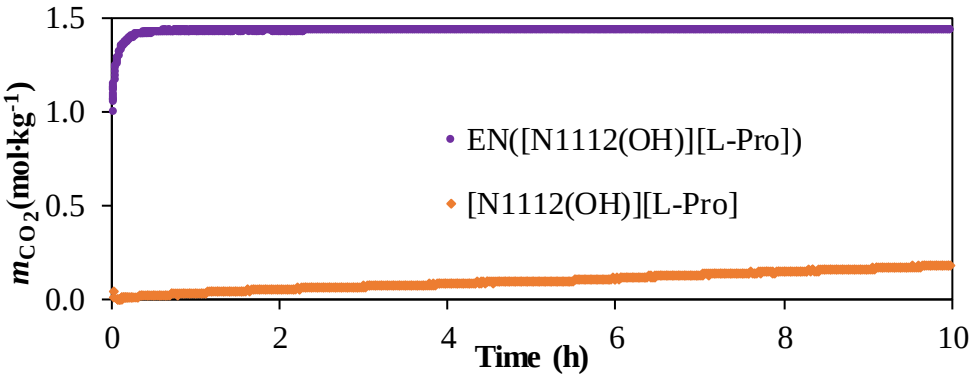

Figure 11- CO_2 molality as function of time for the EN($[N_{1112(OH)}][L\text{-Pro}]$) + CO_2 and $[N_{1112(OH)}][L\text{-Pro}]$ + CO_2 systems, at 70ºC for the first 10 hours.

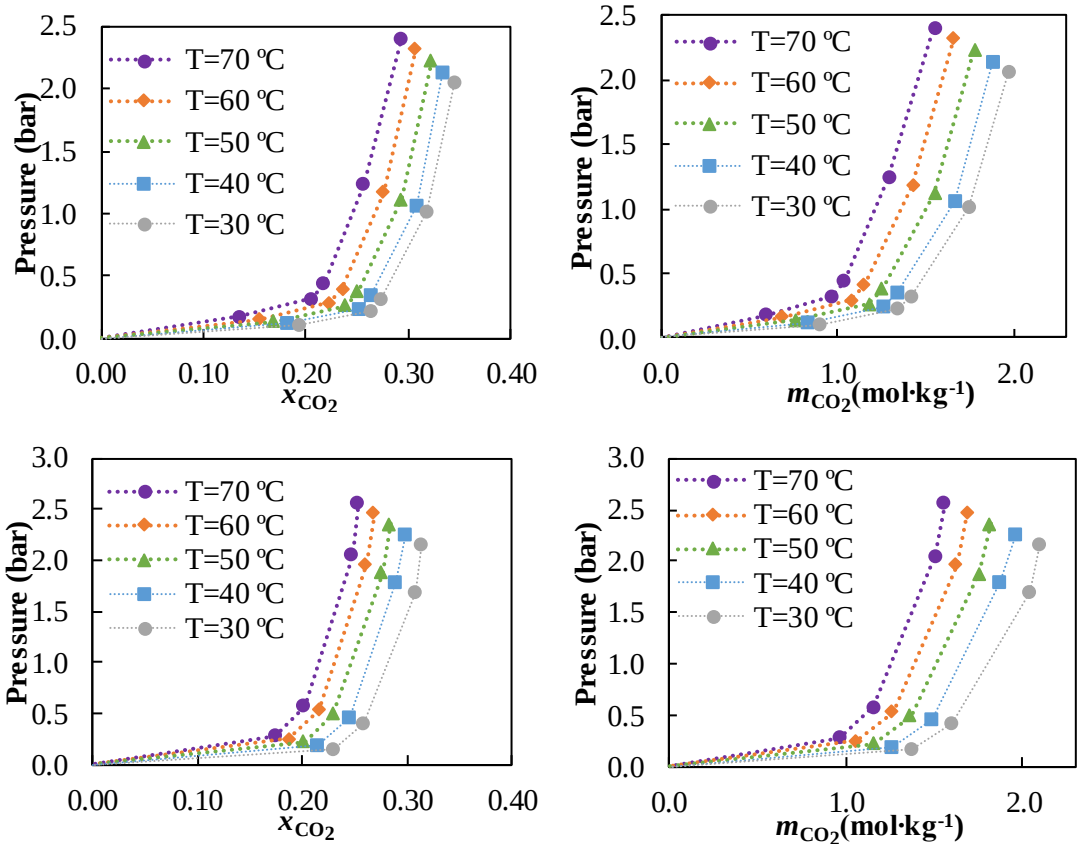

Figure 12-*pTx* (left) and *pTm* (right) phase diagram of the Encapsulated [$N_{1112(OH)}$][L-Phe] (up) and [$N_{1112(OH)}$][L-Pro] (down) +CO_2 phase diagrams. The dashed lines are guides for the eyes.

As depicted, the studied ILs presents chemical sorption, identified by the small change of pressure with CO_2 mole fractions up to 0.18 followed by an exponential increase of the equilibrium pressure upon full solvation. The high solubilities observed translate in a reaction of 1:2 (CO_2:IL).

To better study these IL the molality values were also calculated (also represented in **Figure 12**) and as seen in the solubility values, there is no discernable difference between these two AAIL used, both being capable to absorb a maximum quantity of 2 mol/kg at 30ºC at 2 bar. Which reaffirms the potential of these compounds as means of separation of CO_2, at it is even more than the acetate studied in this work.

3. Gas Permeation in Supported Ionic Liquids

3.1. Supported Ionic Liquid Membrane

The diffusion data and permeability of ionic liquids is important to study the compatibility of ionic liquid with the polymeric membrane. The system used to determine these values is represented in **Figure 13** and was already available at the laboratory. The chosen membranes present no resistance to the gas flow and as such the values obtained from this method will be the values of permeation and diffusion of the gas through the supported liquid. The chosen membranes were the hydrophilic polyvinylidene fluoride (PVDF), made by Millipore Durapore, and a hydrophilic polyethersulfone (PES) membrane made by Pall, Supor.

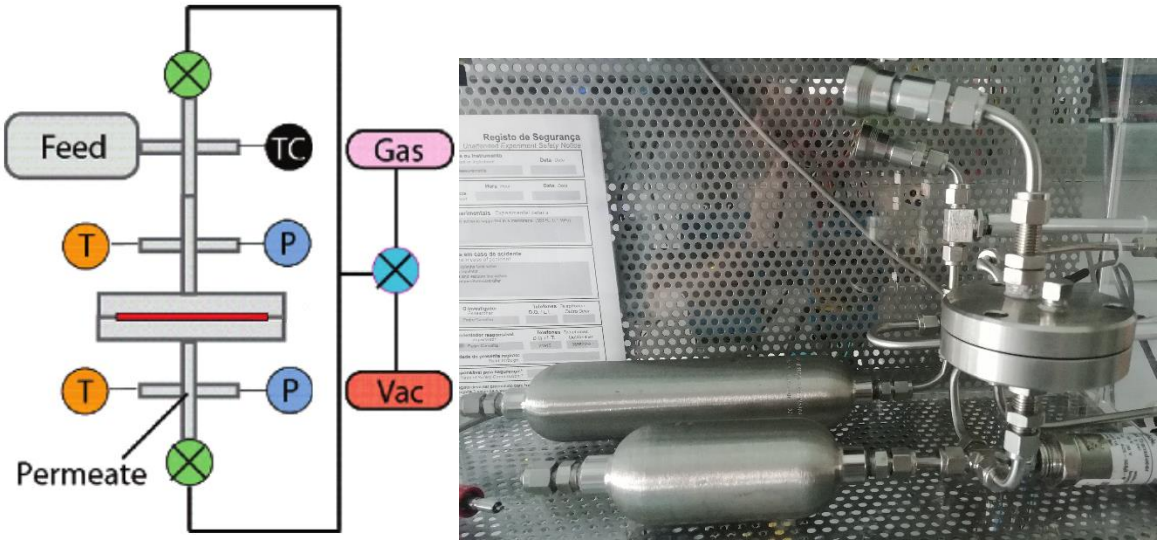

Figure 13-Diffusion and Permeation experiment schematic (left) and the equipment photo (right).

In order to prepare the supported ionic liquid, firstly the ionic liquid go through a purification procedure described before. Then the membrane is weighted and placed under vacuum (10^{-3} mbar) for 1 hour to remove the gas that are present in their pores. After this step, the membrane is wetted with the ionic liquid and the system placed under vacuum for a few hours to allow the ionic liquid to fill the membrane pores. After this step, the excess ionic liquid is removed using a chemical free tissue paper and the impregnated membrane weighted to determine the amount of ionic liquid impregnated.

The membrane is then placed in the equipment and the whole system is placed under vacuum (10^{-3} mbar). This step is done first in the permeate side to prevent the membrane to burst due to the lack of mechanical support on the feed side, and then to the rest of the system. The system is kept under vacuum for a period of few minutes

monitoring the pressures of the system to make sure it is without any sorbed gas. Then the permeation cell is isolated from the gas feed side by closing its respective valve and the gas added to the gas feed chamber at a pressure of 1 bar. The system is allowed to reach temperature and pressure equilibrium and then, the connection between the feed manifold and the membrane is opened.

The time that takes the gas to pass through the membrane, period that no pressure change is observed in the permeate side, is called time-lag and is an important variable to determine the diffusion of the gas across the liquid.

To avoid fluctuations in the pressure due to the temperature the whole equipment is encased in an acrylic box with an opening that regulates its temperature using a Peltier cell capable of maintain the temperature in the box within 30ºC and un uncertainty of 0.1ºC.

3.2. Diffusion and Permeability Determination

The determination of the diffusion coefficient of the gas through the membrane and the permeability of the supported ionic liquid was made based on the theoretical work done by Morgan et al.[38], in which these properties are calculated using the time-lag method. In this method the diffusion is calculated knowing the thickness of the membrane (l) and the time-lag (t_l), as described by **Equation 5**.

$$D_{C,IL} = \frac{l^2}{6 \cdot t_l} \tag{5}$$

The relation for the permeate pressure (P_b) with time (t) is given by Equation 6, in which it correlates to the porosity (φ), diffusion coefficient ($D_{C,IL}$), the solubility coefficient of the compound (S_i), the surface area available (A_s), the feed pressure (P_t), the membrane thickness (l), the permeate chamber volume (V_b) and the ideal gas constant (R).

$$P_b = \frac{\phi \cdot D_{C,IL} \cdot S_i \cdot A_s \cdot R \cdot T \cdot P_t}{V_b \cdot l} \cdot t - \frac{\phi \cdot D_{C,IL} \cdot S_i \cdot A_s \cdot R \cdot T \cdot P_t}{V_b \cdot l} \cdot t_l \tag{6}$$

This relation, **Equation 6**, only describes the linear region of the permeate pressure growth and while the feed pressure is the same, without any major variations. Knowing that the permeability is a multiplication of the diffusion coefficient and solubility coefficient (**Equation 7**), from a linear fit it is returned the slope $\left(m = \frac{\phi \cdot P_{C,IL} \cdot A_s \cdot R \cdot T \cdot P_t}{l \cdot V_b}\right)$ and the intercept$\left(b = -\frac{\phi \cdot P_{C,IL} \cdot A_s \cdot R \cdot T \cdot P_t}{V_b \cdot l} \cdot t_l\right)$.

$$P_{C,IL} = D_{C,IL} \cdot S_i \tag{7}$$

Then, the time lag can be calculated by a simple division of the additive inverse of the intercept by the slope, **Equation 8**. Being then the Diffusion coefficient easily calculated via **Equation 5**.

$$t_l = -\frac{b}{m} \tag{8}$$

To better determine the time-lag of the system, the permeate pressure is normalized so that its value is set to 0 before the feed and permeate sides are connected(due to the low pressure, vacuum, on the permeate side the pressure value can take values negative values, which can introduce variations on the determination of the permeability).

The value of permeability is then calculated by a rearrangement of the slope definition, **Equation 9**.

$$P_{C,IL} = \frac{l \cdot V_b \cdot m}{\phi \cdot A_s \cdot R \cdot T \cdot P_t} \tag{9}$$

3.3. Constants determination

The area available for mass transfer (A_s) cannot be used directly since not all the membrane area is available for mass transfer due not only to the perforated metallic plate support used to hold the polymeric membrane but also to the membrane porosity. Thus, the area available for diffusion imposed by the metallic support needs to be determined.

The metal supported is pictured in **Figure 14** and as depicted a simple determination using simple rulers would make the area determination unreliable. Thus, a picture of the plate was taken, and using an image manipulation software, ImageJ FIJI, a black and white version of the photo was created and the percentage of black, representing the membrane perforations, determined. The area available for mass transfer was determined by the area of the plate (A_p) multiplied by this porosity (φ_p) using **Equation 10**.

$$A_s = A_p \cdot \phi_p \tag{10}$$

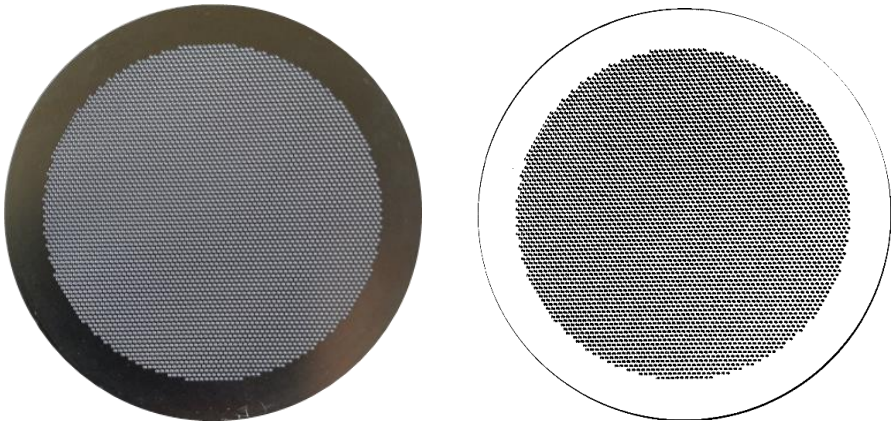

Figure 14-Metallic support for the membrane (left) and the manipulated image used in ImageJ software to determine the porosity (right).

The porosity of this plate was determined to be 0.3217 and the area available for mass transfer 5.58 cm^2.

The volume of the bottom cell was determined using the same calibration method as the isochoric volume calibration method; keeping up the whole system at a constant temperature a known mass of CO_2 was fed to each section (feed and permeate) of the apparatus, measuring the system pressure and, using the modified ideal gas law (**Equation 1**) in which the compressibility factor is determined using Peng-Robinson EoS, the volume of the apparatus calculated.

$$n = \frac{P \cdot V}{Z \cdot R \cdot T} \tag{1}$$

The membrane thickness was provided by the manufacturer and since the ionic liquid occupies the membrane pores and the excess is removed from the surface, this value is not expected to change after impregnation unless fouling is observed, which is not intended nor observed.

3.4. Diffusion and Permeability Determination

The permeability of $[C_4C_1im][DCA]$ in the two different membranes was determined determination and are reported in **Table 4**.

Table 4- Permeation, time-lag and diffusion of CO_2 in $[C_4C_1im][DCA]$ in PVDF or PES membrane, at 25ºC.

	PES	**PVDF**
Permeability (barrer)	713.0	875.4
Time Lag (s)	1.58	5.2
Diffusion (cm^2/s)	$2.21x10^{-5}$	$4.97x10^{-6}$

The CO_2 permeability in $[C_4C_1im][DCA]$ supported in the PVDF membrane were compared against the values reported in the literature. Although, some discrepancies are observed within the literature data, with values ranging from 145 [39] to 200 [40] barrer, the values obtained here present greater deviation. However, evaluating the value reported for the $[C_2C_1im][DCA]$ supported in a PES membrane (610 ± 20 barrer) [41] the value obtained here does not seem to be unreliable since the increase of the permeation with the increase of the imidazolium alkyl chain size is known to occur.[42] The value of the Diffusion coefficient obtained changes considerably depending on the data used to calculate the property since the system time-lag is considerably low (only a few seconds) and a small time variation lead to important changes on the diffusion coefficient. This problem, however, does not seem to impose great variation within the permeability calculation, with a variation of 15 barrrer in extreme cases (where the feed pressure is clearly no longer at the steady state regime).

When trying to determine the diffusional coefficient for [DEEA][Ac] its volatility became again a problem. During the IL impregnation on applying vacuum the IL evaporated. To overcome this phenomenon, the time the vacuum was applied was significantly decreased to 20 min, avoiding thus, the IL evaporation but assuring nonetheless the membrane impregnation.

Another problem surfaced upon placing the impregnated membrane in the apparatus and applying vacuum to both feed and permeate sides. On performing such procedure to remove any air sorbed during the manipulation, the IL would again evaporate. A new procedure was adopted: Upon placing the impregnated membrane in the apparatus, vacuum was applied only for a short period of time and the system, both feed and permeate sides, pressurized to 1 bar. Then the feed section was isolated from the membrane holder and the permeate side and more gas added to the apparatus up to achieving 2 bar. This new procedure allowed to achieve good results, reported in **Table 5** for the protic IL.

The permeation experiment was also conducted for the $[C_2C_1im][Ac]$. During the impregnation procedure the IL chemically interacted with the Millipore membrane leading to a membrane with a brown color (the natural color of the membrane is white and the IL yellow). Testing the permeation in this new membrane the feed seemed to rupture the membrane, which indicates that it was fragilized after the addition of the IL. The results for Pall membrane produced the results also presented in **Table 5**

The membranes impregnated in acetate based ionic liquids do possess much higher time lag, and, as such lower diffusion coefficients The $[C_2C_1im][Ac]$ permeability value is a few magnitudes lower than the values obtained by Santos et al. [43] for this compound of 878.8 barrer, as such, this variation is significant and can be a signal of incompatibility of this compound with this type of membranes (PES). The protic IL also has lower values of permeability than those obtained through the $[C_4C_1im][DCA]$ and can be a sign of incompatibility but without a reference value it is hard to draw comparisons.

Table 5- Permeation, time-lag and diffusion of CO_2 in $[C_2C_1im][Ac]$ IL and [DEEA][Ac] supported in PVDF and PES membranes, at 30ºC.

	PVDF ([DEEA][AC])	PES ($[C_2C_1im][Ac]$)
Permeability (barrer)	169.636	4.15
Time Lag (s)	114.3	9880
Diffusion (cm^2/s)	$2.10x10^{-7}$	$2.43x10^{-9}$

Within the studied ILs, permeation, diffusion and time-lag was not possible to be determined for the $[P_{4444}][Ac]$, since this compound is solid up to 50 ºC and the equipment is able to operate only at around room temperature. Due to the viscosity of the amino acid based ionic liquids, it was impracticable to impregnate the membranes with these compounds and as shown before the use of chemical absorption capable solvents does not yield satisfactory results.

4. Gas-Liquid Membrane Contactor – A Continuous Separation Process

4.1. Equipment Description

Has previously mentioned, one of the approaches to make use of the ionic liquids as solvents in gas extraction/separation relies on their use in gas-liquid membrane contactors. In this chapter a continuous separation unit using two membrane units, one to absorb the gas and the other to regenerate the solvent, as a mechanism to capture CO_2.

The 1-buthyl-3-methylimidazolium acetate ($[C_4C_1im][Ac]$) IL was chosen due to the well characterized chemical absorption reported on a previous work.[44] Furthermore, it was shown that adding water on a molar ration of 5:1 or 2:1 (IL:H_2O) the CO_2 capture, in molality, increases while reducing drastically the viscosity of the mixture. Moreover, according to the study performed by Gómez-Coma et al.[11], using the same IL + H_2O mixture in a gas-liquid membrane contactor, the best-case scenario to increase the capture efficiency was found by using a aqueous mixture of 70 v/v% of IL. And so, as a basis for this separation unit, a 70 v/v% of IL was used as solvent.

This equipment is composed by two membrane contactors, manufactured by *3M*, the Liqui-Cell mini-module 1.7x5.5, which will be used in the sorption unit, and a Liqui-Cell X50 2.5x8 module, also from *3M*, for the desorption unit, both containing polypropylene hollow-fibers capable of maximum liquid flow of 2500 mL/min. In an initial part of this project the second module was replaced by an heated temporary container, this was done so as to firstly test the compatibility of the polymer with the ionic liquid and avoid unnecessary damage to both membrane contactors, this regeneration was not ideal as the water in the solvent would start to evaporate, which was evidenced when the water condensed on the walls of the heated compartment. After substituting this type of regeneration for a pressure driven one, the module at reduced pressure, the loss of water would be null as the fibers are hydrophobic and initially designed to work with water as a solvent.

To evaluate the absorption capabilities of the equipment a pressure transducer, *Keller* PAA-11 (same model as the used in isochoric setup) with a standard deviation of 0.5 mbar was connected to monitor the pressure of the feed manifold (component responsible for the storage of gas to be treated), the results were interpreted using an *Agilent* 34970A data acquisition equipment that connects to the PC via a serial RS232 port that had to be converted to an USB type connection via an adaptor.

The solvent was supplied to the sorption module, from a temporary storage tank, using a flow meter, namely the *Bronkhorst*'s low flow Coriolis mass flow meter, model Mini Cori-Flow M14, this is composed by two components one that determines the fluid flow and density using the Coriolis measuring principle and its temperature and a second component (pump) that is controlled by this first component. The flow meter also came with its own RS 232 serial port connection that also was converted to an USB connection to be properly used to control the equipment via a software program developed in *Labview 2018*.

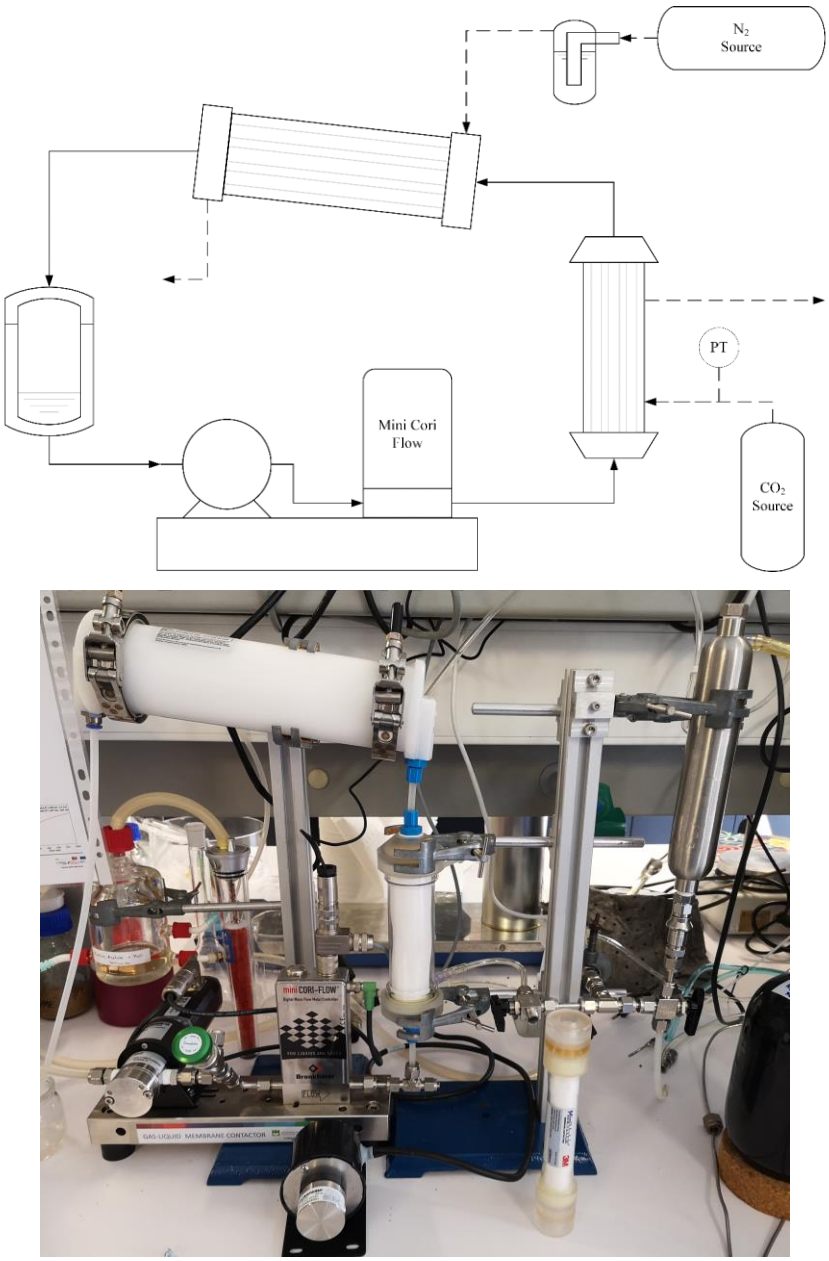

Figure 15-Membrane contactor with low partial pressure regeneration schematic (up) and photo (down).

The equipment is represented in **Figure 15** in which the process is as follows: the ionic liquid present in the jacketed reservoir is fed to the absorption membrane contactor by the flow meter according to a value supplied to it. This sorption module is also connected to the gas source to be treated, to see the evolution of the system the piezoresistive pressure is also connected to this feed tube.

After leaving the sorption area, the solvent is directed to the regeneration unit where, trough pressure differential, the solubilized gas desorbs, another alternative would be the use of a flow of N_2 or other inert gas as a carrier gas. In this study both vacuum and a feed of N_2 were used. In the absence of a flowmeter, when using N_2 as carrier gas the flow of the gas was controlled visually by making the N_2 to pass through a one-way valve, using a nonvolatile thermal oil.

This setup yielded some promising results as evidenced by **Figure 16** for the aqueous $[C_2C_1im][Ac]$ (70v/v%) + CO_2 system, where it shows a decrease of pressure of the feed gas when the setup is running, the top plot represents the gas pressure fed to the sorption unit, in real time, and the bottom graph the pressure but with a bigger sampling time as to avoid pressure noise. The apparatus was placed on the laboratory bench and each manipulation and/or temperature change led to some noise on the pressure measurement, as seen by the small jumps on the signal. This reaffirms that membrane contactors can be used for sorption of gases.

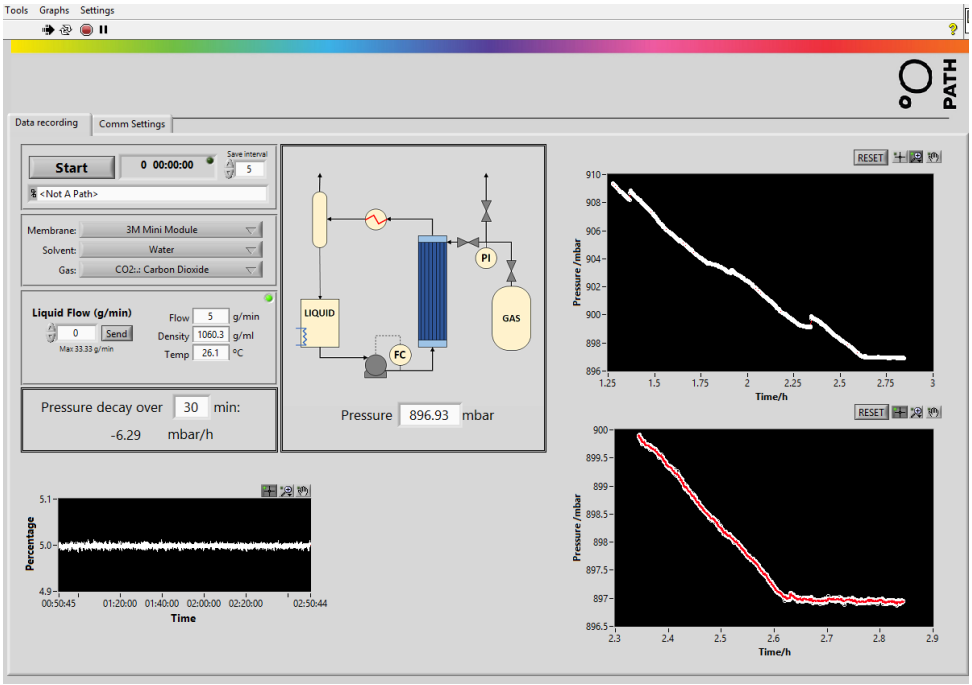

Figure 16-Screenshot of the Graphical User Interface for the Membrane Contactor.

This reaffirms that a chemical absorption ionic liquid could be a reliable way to remove CO_2 trough a Membrane contactor in a continuous way, unfortunately the other compounds studied in this work do not meet the criteria to be used in this type of equipment, the amino acids based ionic liquids are too viscous to be possible its pumping in a reliable way, unless used in an aqueous solution (as used in the initial step) which, if it is capable of reducing its viscosity could be an interesting fluid to study under this equipment. $[P_{4444}][Ac]$ is not liquid at the temperatures that this equipment works.

5. Final Remarks and Future work

An isochoric cell was built and validated allowing to determine the CO_2 solubility in acetate- and amino acid-based ionic liquids, namely $[P_{4444}][Ac]$, $[N_{1112(OH)}][L\text{-}Phe]$ and $[N_{1112(OH)}][L\text{-}Pro]$. Furthermore, a measurement methodology was developed in order to be able to determine the gas solubility in these families of ILs.

The solvents studied present high solubility values typical of chemical absorption; the compound based on acetate ($[P_{4444}][Ac]$) for example has x_{CO2}=0.24 at 4.0 bar and 50ºC as well as high molalities (m_{CO2}=1 at 4.0 bar and 50ºC), being the melting point of this compound however, the biggest drawback of this compound.

The amino acid-based ionic liquids, $[N_{1112(OH)}][L\text{-}Phe]$ and $[N_{1112(OH)}][L\text{-}Pro]$, however, without any modification (encapsulation or dilution) does not appear to be reliable because of its viscosity, which was predictable, but the limitations were much higher than expected, during experimentation the reaction with the CO_2 lead to the formation of a jellified top layer which then acted as a protective layer for further diffusion of the gas to the bulk of the IL. As such, the encapsulation of these compounds was deemed essential and did improve considerably its kinetics, like expected, and made these compounds solubility capable to be studied.

The sorption capability of the acetate compound is, higher than that of the AAIL studied, with higher solubilities (x_{CO2}=0.33 at 2.5 bar and 30ºC) as well as higher molalities (m_{CO2}=2 mol·kg^{-1}(IL) at 2.0 bar and 30ºC), at lower pressure points, having the same behavior as other chemical absorption solvents, with a linear growth until a solubility value (x_{CO2}=0.18) after which represents an exponential growth and after reaching the value of x_{CO2}=0.33, seems to have no dependence of the pressure value. So these compounds do chemically bond with CO_2 in a ratio of 2:1 (IL:CO_2). But there seems to be no difference in the anion used in the AA-ILL, whether it be on the solubility values or its molality. As future work, a study of other cations with these AAIL seems appropriate as the cation seems to not influence the value of solubility and molality.

The study of other greenhouse gases with ILs is still a need, as the only one studied in this thesis was CO_2

The study of the membrane contactor separation unit does reinforce it as a reliable way to use IL to remove CO_2, but this equipment needs to be better tested with mixture of gases and on a more realistic enviroment than the use of pure gas.

All in all, the use of AAIL for the use of CO_2 does seem reliable for its use in separation of this compound due to its high solubilities but does represent significant drawbacks in its use, and with the use of techniques like encapsulation does it seem reasonable its use.

The use of AAIL in the membrane contactor also doesn´t seem viable as a neat compound. But the same strategy as the one used with $[C_2C_1im][Ac]$ could be used to reduce its viscosity and make the separation (and mass transfer limitations) feasible.

Bibliography

[1] International Energy Agency, "Global energy demand rose by 2.3% in 2018, its fastest pace in the last decade," *2019-03-26*, 2019. [Online]. Available: https://bit.ly/2FmWjyY. [Accessed: 28-Mar-2019].

[2] D. Y. C. Leung, G. Caramanna, and M. M. Maroto-Valer, "An overview of current status of carbon dioxide capture and storage technologies," *Renew. Sustain. Energy Rev.*, vol. 39, pp. 426–443, 2014.

[3] T. M. Letcher, *Managing Global Warming : an Interface of Technology and Human Issues*. Academic Press, 2018.

[4] B. Burr and L. Lyddon, *A Comparison of Physical Solvents for Acid Gas Removal*, vol. 1. 2008.

[5] E. Torralba-Calleja, J. Skinner, and D. Gutiérrez-Tauste, "CO_2 Capture in Ionic Liquids: A Review of Solubilities and Experimental Methods," *J. Chem.*, vol. 2013, pp. 1–16, 2013.

[6] M. T. Mota-Martinez, P. Brandl, J. P. Hallett, and N. Mac Dowell, "Challenges and opportunities for the utilisation of ionic liquids as solvents for CO_2 capture," *Mol. Syst. Des. Eng.*, vol. 3, no. 3, pp. 560–571, 2018.

[7] A. Yokozeki, M. B. Shiflett, C. P. Junk, L. M. Grieco, and T. Foo, "Physical and Chemical Absorptions of Carbon Dioxide in Room-Temperature Ionic Liquids," *J. Phys. Chem. B*, vol. 112, no. 51, pp. 16654–16663, 2008.

[8] B. F. Goodrich *et al.*, "Effect of Water and Temperature on Absorption of CO_2 by Amine-Functionalized Anion-Tethered Ionic Liquids," *J. Phys. Chem. B*, vol. 115, no. 29, pp. 9140–9150, 2011.

[9] R. Santiago, J. Lemus, C. Moya, D. Moreno, N. Alonso-Morales, and J. Palomar, "Encapsulated Ionic Liquids to Enable the Practical Application of Amino Acid-Based Ionic Liquids in CO 2 Capture," *ACS Sustain. Chem. Eng.*, vol. 6, no. 11, pp. 14178–14187, 2018.

[10] T. Ma *et al.*, "A process simulation study of CO_2 capture by ionic liquids," *Int. J. Greenh. Gas Control*, vol. 58, pp. 223–231, 2017.

[11] L. Gómez-Coma, A. Garea, and Á. Irabien, "Hybrid Solvent ([emim][Ac]+water) To Improve the CO_2 Capture Efficiency in a PVDF Hollow Fiber Contactor," *ACS Sustain. Chem. Eng.*, vol. 5, no. 1, pp. 734–743, 2017.

[12] S. Sarmad, Y. Xie, J. P. Mikkola, and X. Ji, "Screening of deep eutectic solvents (DESs) as green CO_2sorbents: from solubility to viscosity," *New J. Chem.*, vol. 41, pp. 290–301, 2017.

[13] J. Leclaire and D. J. Heldebrant, "A call to (green) arms: a rallying cry for green chemistry and engineering for CO_2 capture, utilisation and storage," *Green Chem.*, vol. 20, no. 22, pp. 5058–5081, 2018.

[14] J. Palomar, J. Lemus, N. Alonso-Morales, J. Bedia, M. A. Gilarranz, and J. J. Rodriguez,

"Encapsulated ionic liquids (ENILs): from continuous to discrete liquid phase," *Chem. Commun.*, vol. 48, no. 80, p. 10046, 2012.

[15] R. Santiago, J. Lemus, C. Moya, D. Moreno, N. Alonso-Morales, and J. Palomar, "Encapsulated Ionic Liquids to Enable the Practical Application of Amino Acid-Based Ionic Liquids in CO2 Capture," *ACS Sustain. Chem. Eng.*, vol. 6, pp. 14178–14187, 2018.

[16] C. Moya, N. Alonso-Morales, J. De Riva, O. Morales-Collazo, J. F. Brennecke, and J. Palomar, "Encapsulation of Ionic Liquids with an Aprotic Heterocyclic Anion (AHA-IL) for CO2Capture: Preserving the Favorable Thermodynamics and Enhancing the Kinetics of Absorption," *J. Phys. Chem. B*, vol. 122, pp. 2616–2626, 2018.

[17] Y. Han and W. S. W. Ho, "Recent advances in polymeric membranes for CO_2 capture," *Chinese J. Chem. Eng.*, vol. 26, no. 11, pp. 2238–2254, 2018.

[18] S. Basu, A. Cano-Odena, and I. F. J. Vankelecom, "MOF-containing mixed-matrix membranes for CO_2/CH_4 and CO_2/N_2 binary gas mixture separations," *Sep. Purif. Technol.*, vol. 81, no. 1, pp. 31–40, 2011.

[19] S. R. Venna and M. A. Carreon, "Highly Permeable Zeolite Imidazolate Framework-8 Membranes for CO_2 /CH_4 Separation," *J. Am. Chem. Soc.*, vol. 132, no. 1, pp. 76–78, 2010.

[20] L. J. Lozano, C. Godínez, A. P. de los Ríos, F. J. Hernández-Fernández, S. Sánchez-Segado, and F. J. Alguacil, "Recent advances in supported ionic liquid membrane technology," *J. Memb. Sci.*, vol. 376, no. 1–2, pp. 1–14, 2011.

[21] C. H. Yu, C. H. Huang, and C. S. Tan, "A review of CO_2 capture by absorption and adsorption," *Aerosol Air Qual. Res.*, vol. 12, no. 5, pp. 745–769, 2012.

[22] A. Samanta, A. Zhao, G. K. H. Shimizu, P. Sarkar, and R. Gupta, "Post-Combustion CO_2 Capture Using Solid Sorbents: A Review," *Ind. Eng. Chem. Res.*, vol. 51, no. 4, pp. 1438–1463, 2012.

[23] * Ranjani V. Siriwardane, and Ming-Shing Shen, and E. P. Fisher, "Adsorption of CO_2, N_2, and O_2 on Natural Zeolites," 2003.

[24] S. Zhao *et al.*, "Status and progress of membrane contactors in post-combustion carbon capture: A state-of-the-art review of new developments," *J. Memb. Sci.*, vol. 511, pp. 180–206, 2016.

[25] J. L. Li and B. H. Chen, "Review of CO_2 absorption using chemical solvents in hollow fiber membrane contactors," *Sep. Purif. Technol.*, vol. 41, pp. 109–122, 2005.

[26] A. Gabelman and S.-T. Hwang, "Hollow fiber membrane contactors," *J. Memb. Sci.*, vol. 159, no. 1–2, pp. 61–106, 1999.

[27] Å. Wahlström and L. Vamling, "The solubility of HCFC22, CFC114 and HFC152A in n - hexadecane," *Can. J. Chem. Eng.*, vol. 74, no. 3, pp. 426–428, 1996.

[28] L. M. Galan Sanchez, "Functionalized ionic liquids : absorption solvents for carbon dioxide and olefin separation," Ph.D Thesis, Technische Universiteit Eindhoven, Eindhoven, 2008.

[29] P. J. Carvalho, V. H. Álvarez, I. M. Marrucho, M. Aznar, and J. A. P. Coutinho, "High pressure phase behavior of carbon dioxide in 1-butyl-3-methylimidazolium bis(trifluoromethylsulfonyl)imide and 1-butyl-3-methylimidazolium dicyanamide ionic liquids," *J. Supercrit. Fluids*, vol. 50, no. 2, pp. 105–111, 2009.

[30] M. I. Cabaço, M. Besnard, Y. Danten, and J. A. P. Coutinho, "Carbon Dioxide in 1-Butyl-3-methylimidazolium Acetate. I. Unusual Solubility Investigated by Raman Spectroscopy and DFT Calculations," *J. Phys. Chem. A*, vol. 116, no. 6, pp. 1605–1620, 2012.

[31] G. Gurau, H. Rodríguez, S. P. Kelley, P. Janiczek, R. S. Kalb, and R. D. Rogers, "Demonstration of Chemisorption of Carbon Dioxide in 1,3-Dialkylimidazolium Acetate Ionic Liquids," *Angew. Chemie Int. Ed.*, vol. 50, no. 50, pp. 12024–12026, 2011.

[32] J. Blath, N. Deubler, T. Hirth, and T. Schiestel, "Chemisorption of carbon dioxide in imidazolium based ionic liquids with carboxylic anions," *Chem. Eng. J.*, vol. 181–182, pp. 152–158, 2012.

[33] G. Sharma, D. Singh, S. Rajamani, and R. L. Gardas, "Influence of Alkyl Substituent on Optical Properties of Carboxylate-Based Protic Ionic Liquids," *ChemistrySelect*, vol. 2, no. 31, pp. 10091–10096, 2017.

[34] T. E. Sintra, "Synthesis of More Benign Ionic Liquids for Specific Applications," Ph.D Thesis, Department of Chemistry, University of Aveiro, 2018.

[35] S. B. Yoon, K. Sohn, J. Y. Kim, C.-H. Shin, J.-S. Yu, and T. Hyeon, "Fabrication of Carbon Capsules with Hollow Macroporous Core/Mesoporous Shell Structures," *Adv. Mater.*, vol. 14, no. 1, pp. 19–21, 2002.

[36] J. Lemus, J. Palomar, M. A. Gilarranz, and J. J. Rodriguez, "Characterization of Supported Ionic Liquid Phase (SILP) materials prepared from different supports," *Adsorption*, vol. 17, no. 3, pp. 561–571, 2011.

[37] J. Lemus, F. A. Da Silva F., J. Palomar, P. J. Carvalho, and J. A. P. Coutinho, "Solubility of carbon dioxide in encapsulated ionic liquids," *Sep. Purif. Technol.*, vol. 196, pp. 41–46, 2018.

[38] David Morgan, and Lee Ferguson, and P. Scovazzo*, "Diffusivities of Gases in Room-Temperature Ionic Liquids: Data and Correlations Obtained Using a Lag-Time Technique," 2005.

[39] R. Couto, L. Neves, P. Simões, and I. Coelhoso, "Supported Ionic Liquid Membranes and Ion-Jelly® Membranes with [BMIM][DCA]: Comparison of Its Performance for CO_2 Separation," *Membranes (Basel).*, vol. 5, no. 1, pp. 13–21, 2015.

[40] P. Jindaratsamee, Y. Shimoyama, H. Morizaki, and A. Ito, "Effects of temperature and anion species on CO_2 permeability and CO_2/N_2 separation coefficient through ionic liquid membranes," *J. Chem. Thermodyn.*, vol. 43, no. 3, pp. 311–314, 2011.

[41] P. Scovazzo, J. Kieft, D. A. Finan, C. Koval, D. DuBois, and R. Noble, "Gas separations using non-hexafluorophosphate [PF6]− anion supported ionic liquid membranes," *J. Memb. Sci.*, vol. 238, no. 1–2, pp. 57–63, 2004.

[42] L. A. Neves, J. G. Crespo, and I. M. Coelhoso, "Gas permeation studies in supported ionic liquid membranes," *J. Memb. Sci.*, vol. 357, no. 1–2, pp. 160–170, 2010.

[43] E. Santos, J. Albo, and A. Irabien, "Acetate based Supported Ionic Liquid Membranes (SILMs) for CO_2 separation: Influence of the temperature," *J. Memb. Sci.*, vol. 452, pp. 277–283, 2014.

[44] P. Navarro, J. García, F. Rodríguez, P. J. Carvalho, and J. A. P. Coutinho, "Impact of water on the $[C_4C_1im][Ac]$ ability for the CO_2/CH_4 separation," *J. CO_2 Util.*, vol. 31, pp. 115–123, 2019.

Appendix A

A.1. Volume Calibration and Sensibility

The isochoric volume calibration as previously explained was done knowing the mass, temperature and pressure of the system, as such, rearranging the modified ideal gas law the Equation A.1. is obtained.

$$V = \frac{Z \cdot R \cdot m}{P \cdot M_w} \tag{A.1}$$

Knowing that the mass differential in the source was of 1.308 g, that the temperature was of 39.9 ºC and that the pressure without the cell was of 2.5706 bar and with the cell was of 2.2785 bar, the calculated volume is of 297 mL without the cell and of 336 mL with the cell connected. This value however does not have to be to rigorous as shown before.

A.2. Pressure Transducer Calibration

Like previously mentioned the pressure had to be calibrated, the raw data for the first calibration can be found in **Table A.1**-First calibration data points and the regression in **Figure A.1**, the second calibration can be found in **Table A.2** and **Figure A.2**.

Table A.1-First calibration data points.

Electric Tension (V)	P(bar)
0.227	1.029
-0.003	0
0.117	0.53
0.18	0.815
0.324	1.464
0.44	1.985
0.552	2.488
0.682	3.071
0.783	3.528
0.851	3.832

These regressions were accomplished using the *Excel*'s linest function that determines the best fit using the least squares method.

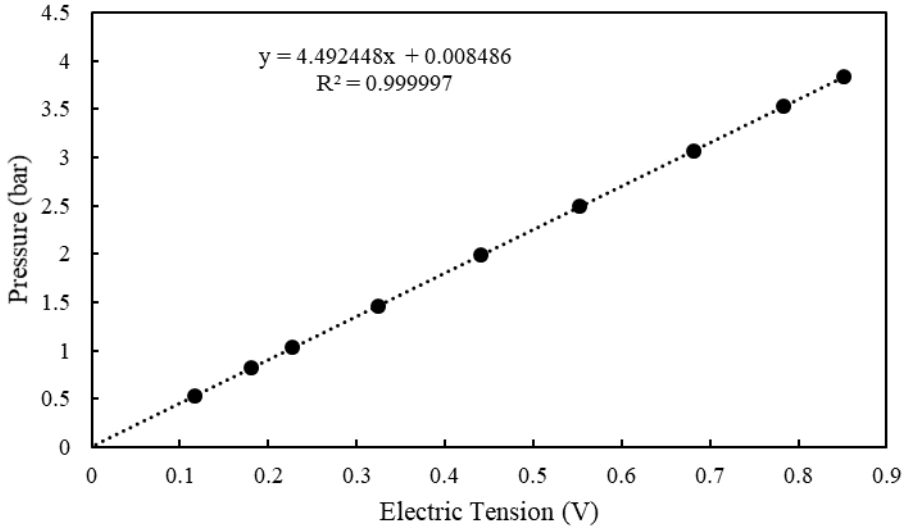

Figure A.1-Pressure transducer first calibration.

Table A.2-Data for pressure transducer calibration.

Electric Tension (mV)	Pressure (bar)
44.22	1.29
65.21	1.904
85.45	2.49
74.24	2.16
98.17	2.855

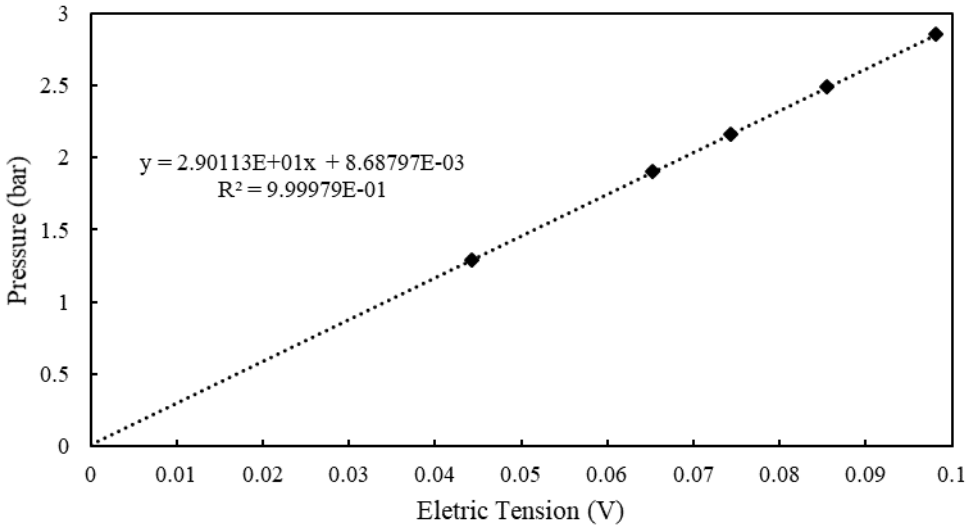

Figure A.2 - Linear regression of the pressure transducer calibration.

A.3. Peng-Robinson Equation of State

The Peng Robinson (EoS) was used to calculate the quantity of gas present in the system, this was done by resolving the polynomial function that determines the compressibility factor (*Z*), used in the altered ideal gas law, Equation A.2.

$$n = \frac{P \cdot V}{Z \cdot R \cdot T} \qquad (A.2.)$$

The Z factor is determined by the roots of the cubic function described in Equation A.3.

$$Z^3 - (1 - B) \cdot Z^2 + (A - 2 \cdot B - 3 \cdot B^2) \cdot Z - (A \cdot B - B^2 - B^3) = 0 \qquad (A.3.)$$

If the function returns more than one real solution, this means the compounds is in the two-phase region, the highest solution is the one that describes the vapor phase and the lowest the liquid phase.

The A factor and B factor are determined by the Equations A.4. and A.5. respectively.

$$A = \frac{a \cdot \alpha \cdot P}{R^2 \cdot T^2} \qquad (A.4.)$$

$$B = \frac{b \cdot P}{R \cdot T} \qquad (A.5.)$$

The a, b and α factors are, however determined by the Equations A.6., A.7. and A.8. respectively.

$$a = \frac{0.45724 \cdot R^2 \cdot T_c^2}{P_c} \qquad (A.6.)$$

$$b = \frac{0.07780 \cdot R \cdot T_c}{P_c} \qquad (A.7.)$$

$$\alpha = \left(1 + (0.37464 + 1.54226 \cdot \omega - 0.26992 \cdot \omega^2) \cdot (1 - T_r^{0.5})\right)^2 \qquad (A.8.)$$

In which the relative temperature (T_r) is the ratio of the system temperature and the critical temperature, Equation (A.9.).

$$T_r = \frac{T}{T_c} \qquad (A.9.)$$

Appendix B

B.1. Isochoric Method Labview Diagram

The full diagram is represented in **Figure B.1**, however this is too big and as such, the diagram will be subdivided in numbered regions to be more easily explained.

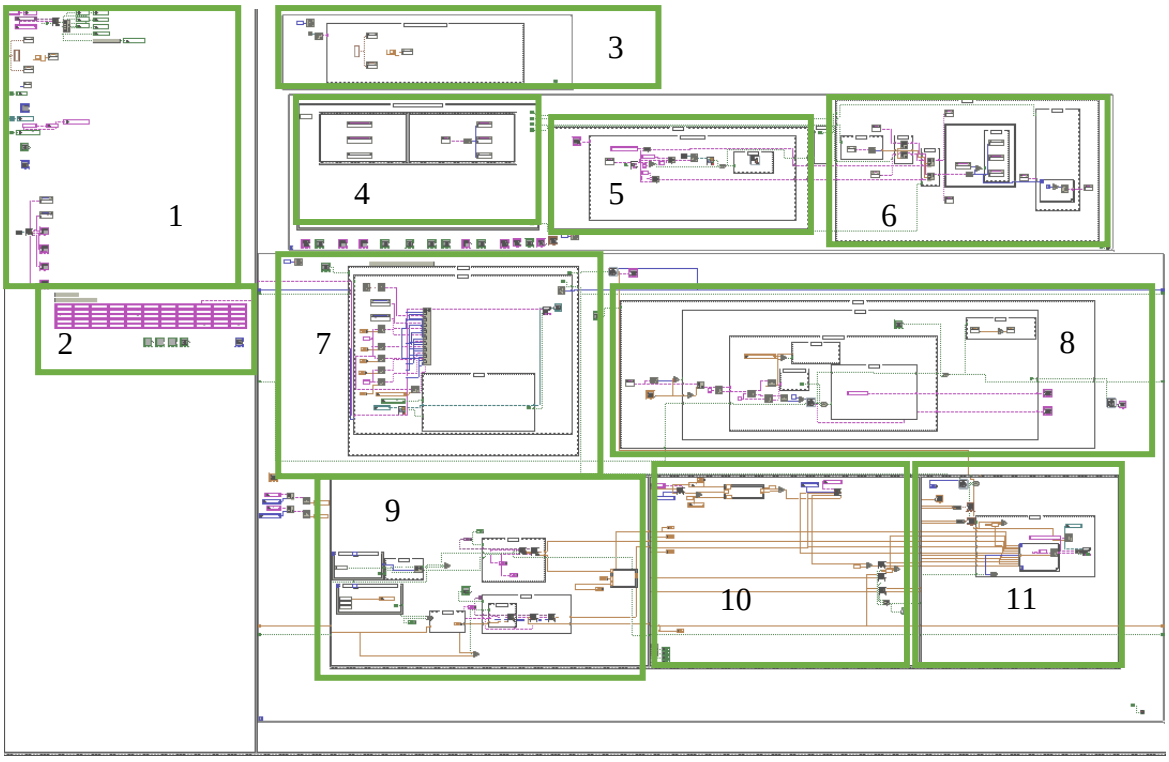

Figure B.1-Complete *Labview* diagram for the isochoric method cell.

Before starting the program, zone 1, all indicators are reset to their normal values, the valve position is checked, and the gas and liquids properties are loaded from their respective .txt files, Figure B.2 and Figure B.3.

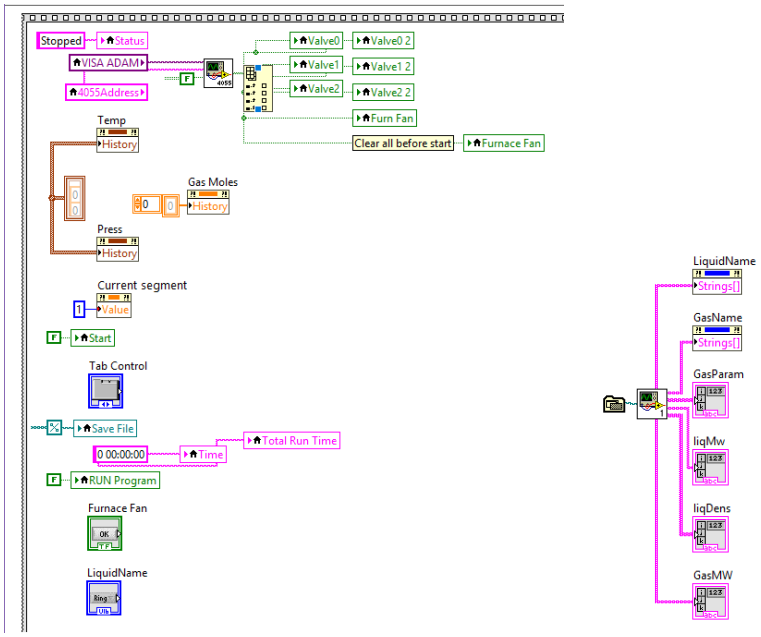

Figure B.2-Zone 1 of the diagram.

The diagram for the sub-VI used for loading the compounds properties is represented in Figure B.3

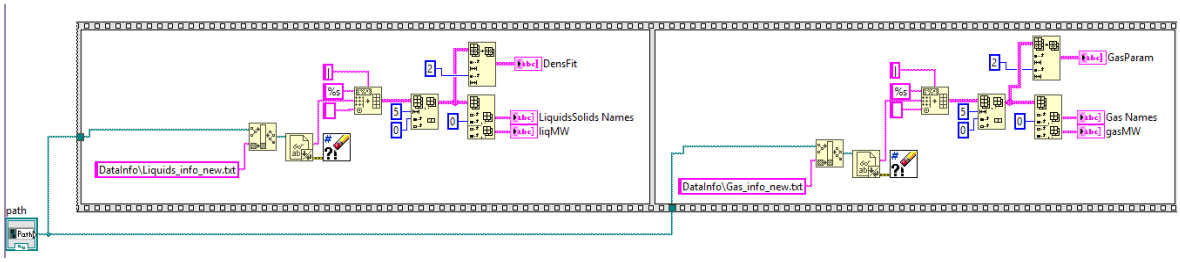

Figure B.3-Compound sub-VI loader.

In zone 3 the run time menu is defined, functions that alter the visibility the stabilization sub-VI, that alter the compounds properties, definitions regarding USB connection, change the calibration settings for the pressure transducer and an option to clear the graphs are found here Figure B.4.

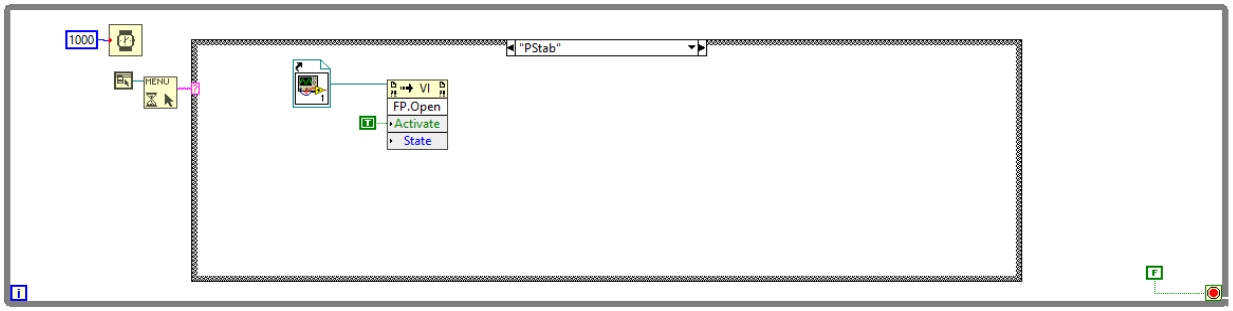

Figure B.4-Zone 3.

In zones 2 and 7 the save file header is constructed with important information regarding the compounds used in the experiment, such as both compounds name, molecular weight, the solvent mas and its density, **Figure B.5** and **Figure B.6**.

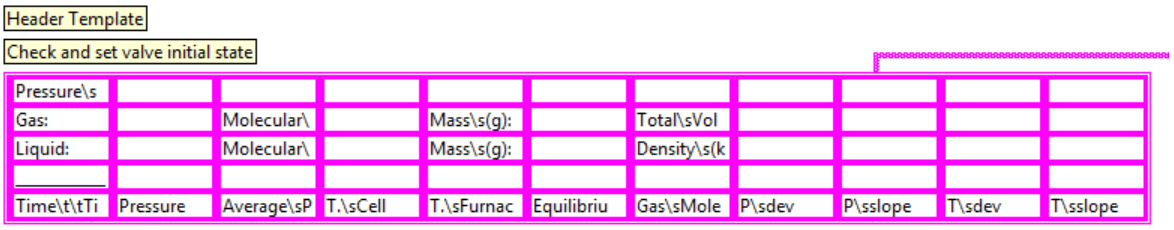

Figure B.5-Zone 2.

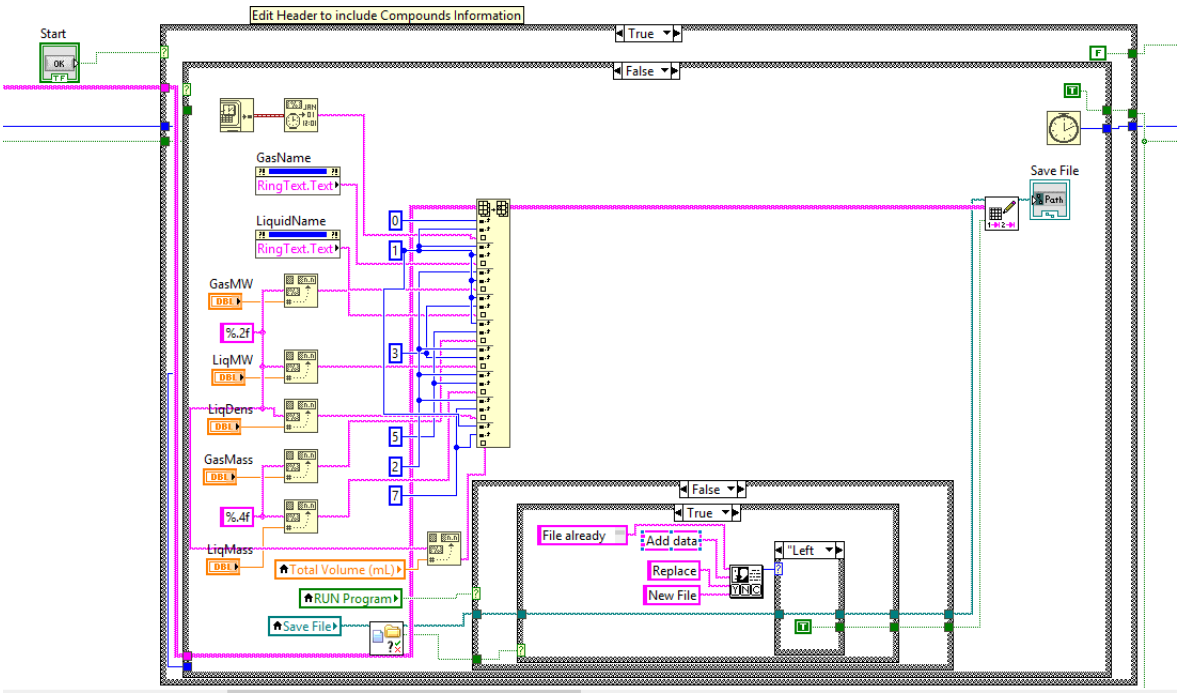

Figure B.6-Zone 7.

In zone 4 the initialization of the segment control is started, in this zone exists the function to save the programs made, Figure B.7, load a .txt file with a program made, Figure B.8, clear all segments, change the display of options depending on the type of segment chosen, for example hiding the setpoint changing option when a valve action is chosen, as it is not needed, Figure B.9, and the Booleans values that determine what actions to take when a segment is added in the end, or put before other segment or when it is done to substitute a preexisting segment or simply erase all segments, Figure B.10.

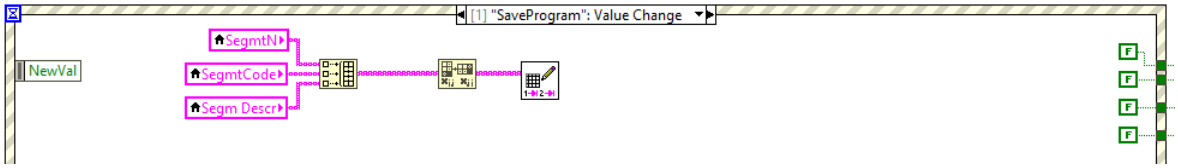

Figure B.7-Zone 4, Save Program option.

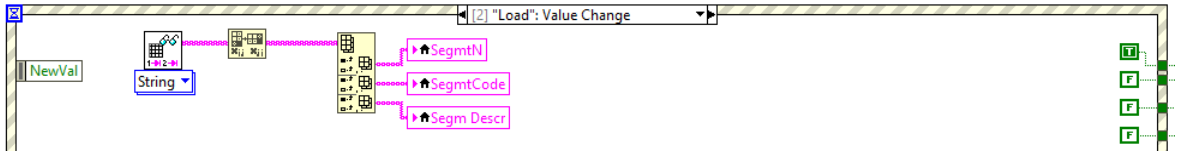

Figure B.8-Zone 4, Load Program option.

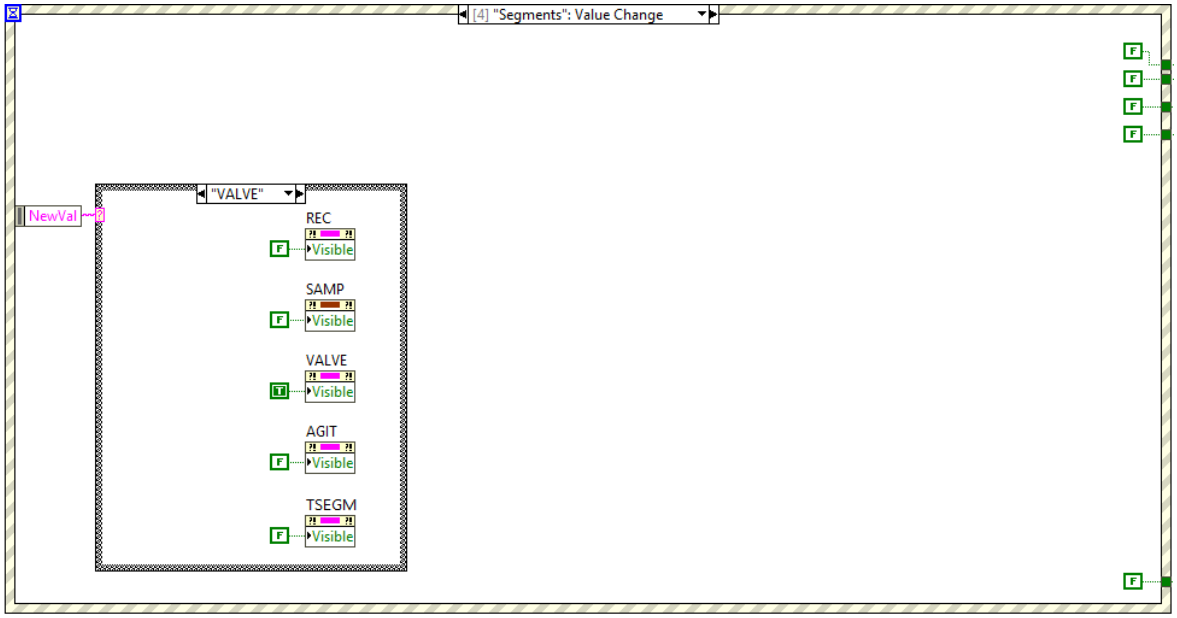

Figure B.9-Zone 4, Change Visible Items option.

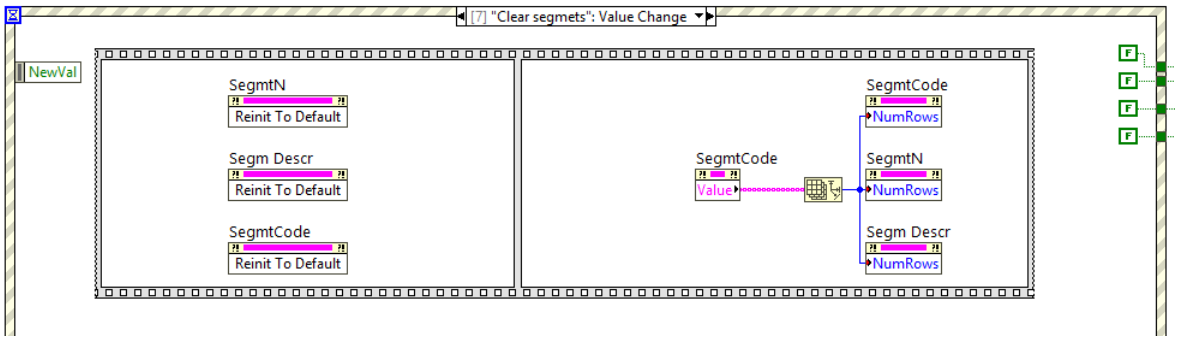

Figure B.10-Zone 4, Clear Program option.

In zone 5 of the diagram the options introduced by the user and transformed into an easily recognized system of instructions to be read later, this comes in a form of a string in which all information is separated by a predetermined separator and the first string segment defines the type of segment being referred to, this zone works when called upon

by zone 4 in the creation of a new segment, an example of the creation of a timed temperature controlled segment is represented in Figure B.11.

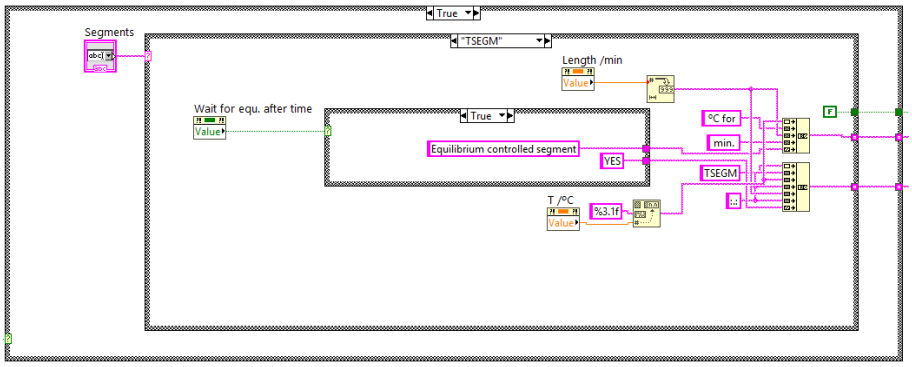

Figure B.11-Zone 5, Temperature Segment creation.

In zone 6 of this diagram, the segments are renumbered whenever a new segment is created or removed, **Figure B.12**

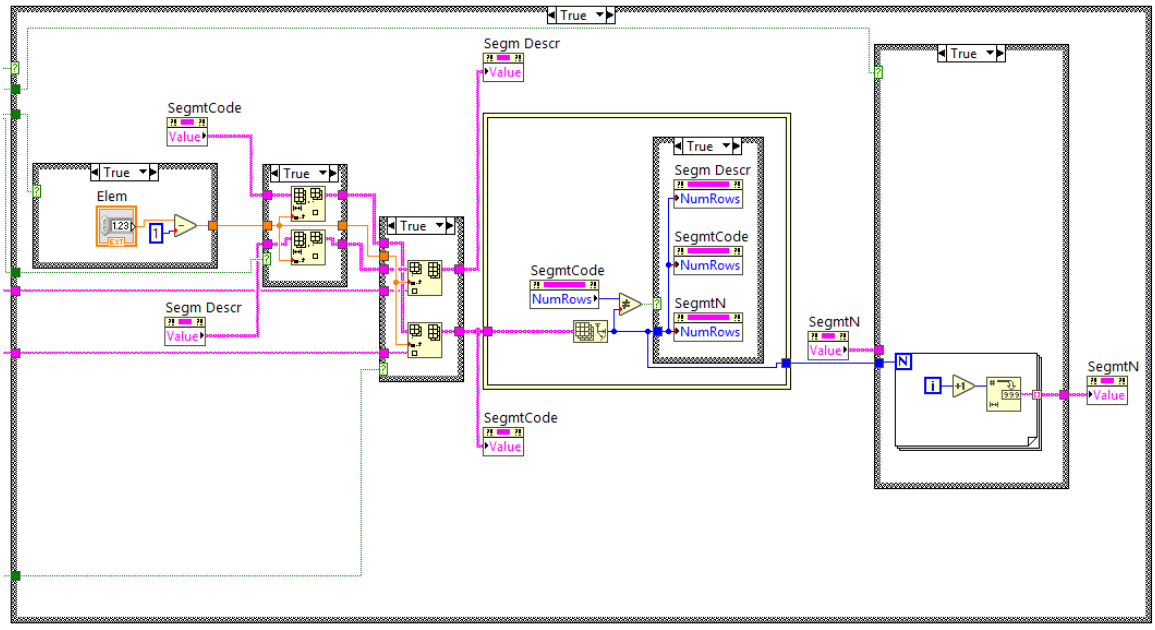

Figure B.12-Zone 6.

Zone 8 of this diagram is the part responsible for reading the segment instructions and enforcing them onto the system when the program is running, each segment has its own set of instructions being the temperature control segment being represented in **Figure B.13**. This zone is also responsible for the change of segment when the conditions have been met, time for temperature segment and for the other segments it is simply performing its action.

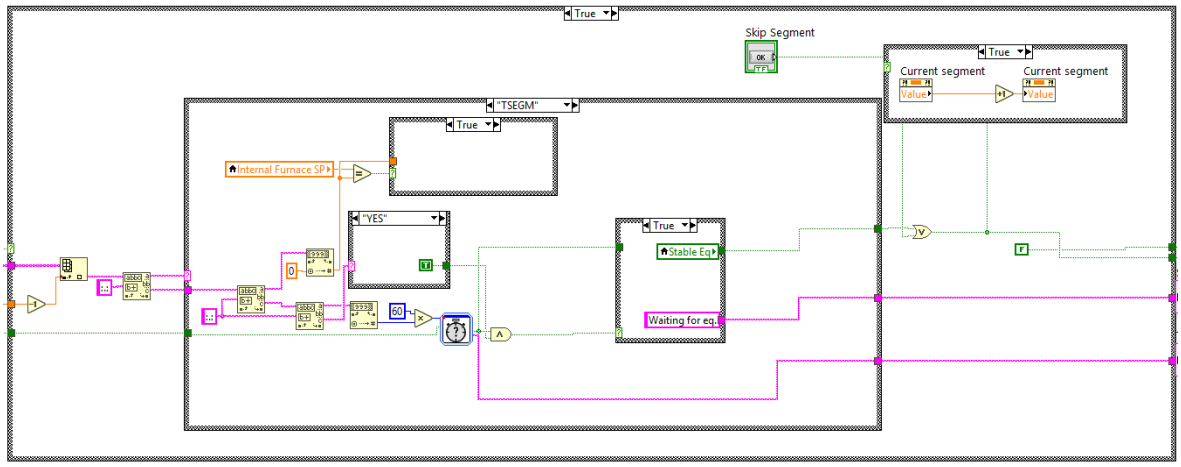

Figure B.13-Zone 8, Temperature Segment reading.

Zone 9 is responsible for the communication with the equipment, it is here that commands are sent to the equipment in their respective communication protocol and the answers are interpreted to be converted into readable data, **Figure B.14**.

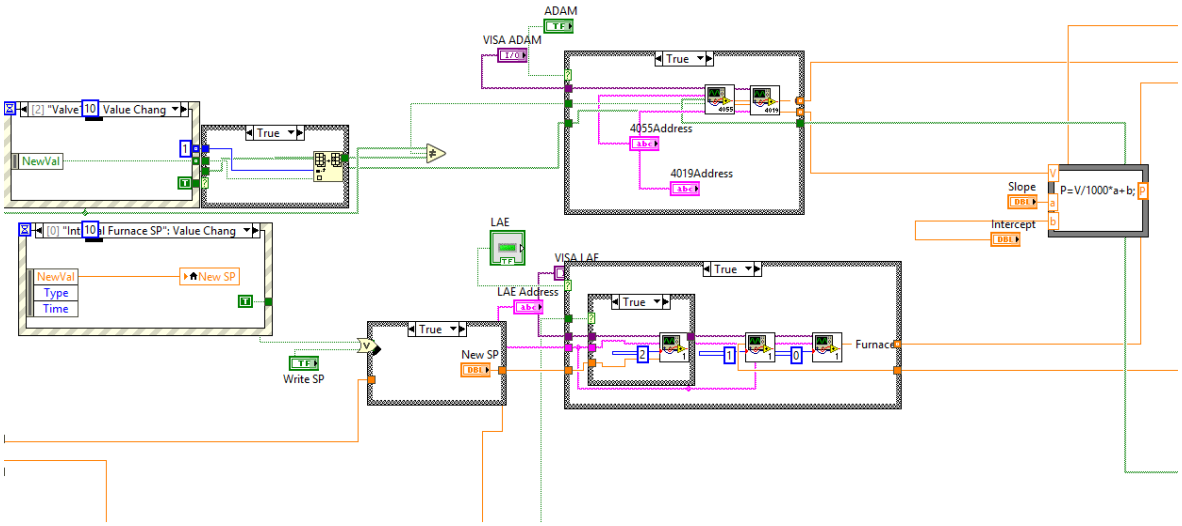

Figure B.14-Zone 9.

In this zone sub-VI's are used to simplify the diagram, there is one for the reading or writing of the valves, Figure B.15, one for the lecture of data, **Figure B.16**, and one for the setpoint reading, temperature reading and set point writing of the oven, .**Figure B.17**.

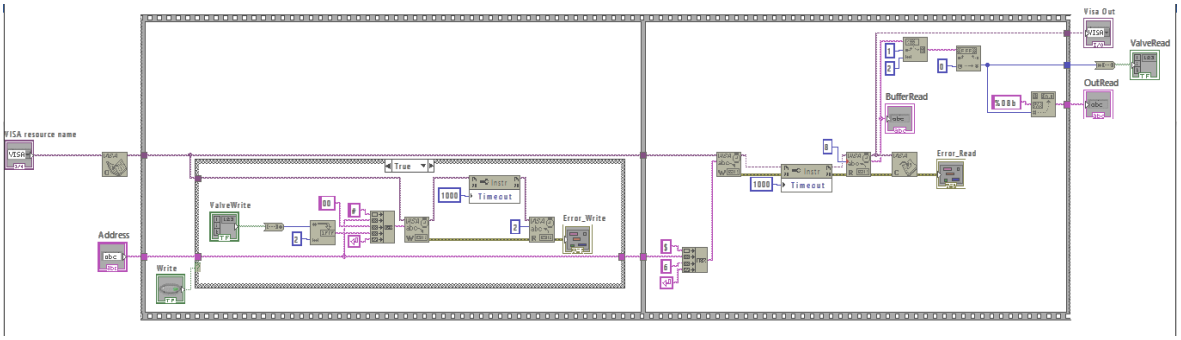

Figure B.15-Sub-VI responsible for valve checks and valve state changes.

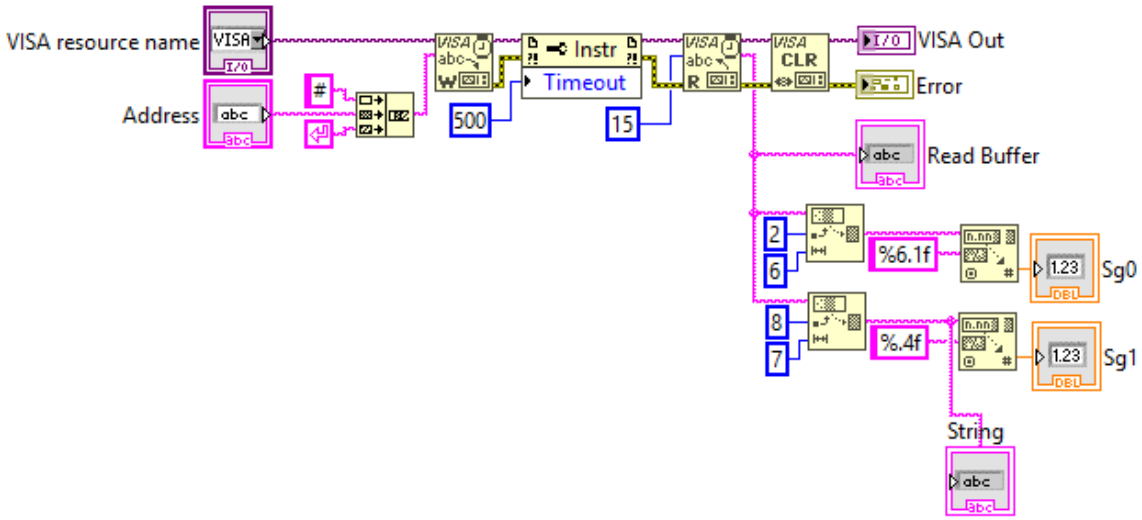

Figure B.16-Sub-VI responsible for data reading (Temperature and Pressure Transducer).

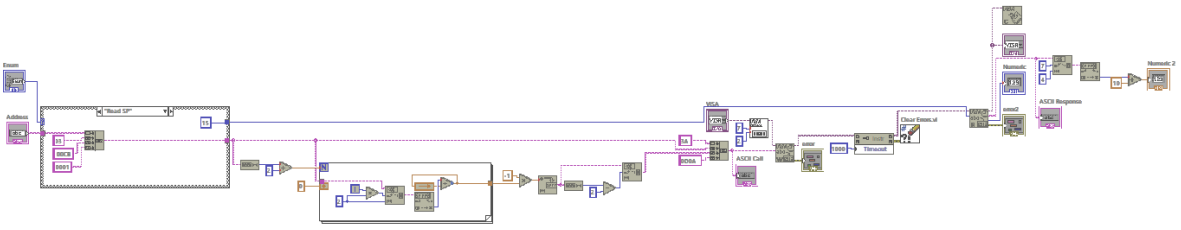

Figure B.17-Sub-VI responsible for oven communication.

In zone 10 the data is treated and analyzed, the gaseous quantity is determined, **Figure B.18**, using a Peng-Robison equation of sate sub-VI, **Figure B.19**, and a sub-VI's that determine if the system equilibrium has been reached or not, **Figure B.20**.

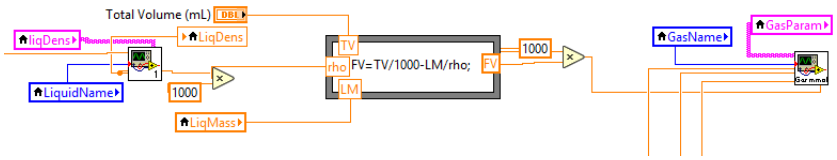

Figure B.18-Zone 10, Gaseous Moles determination.

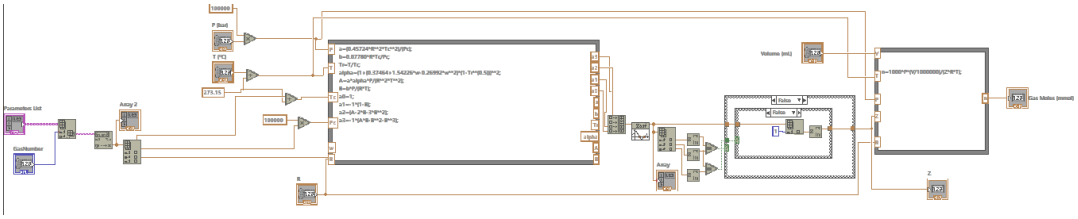

Figure B.19-Peng-Robison EoS sub-VI.

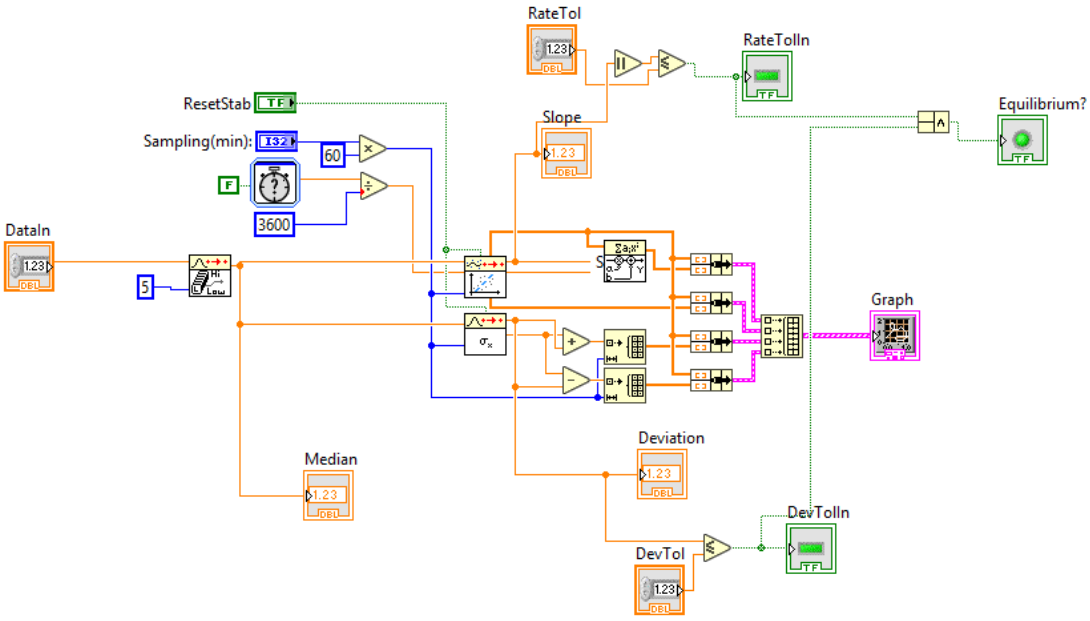

Figure B.20-Example of a equilibrium check sub-VI (pressure).

Finally, in zone 11, all relevant data is saved into a .txt save file in specific time intervals defined by the user whenever the option to save is on,

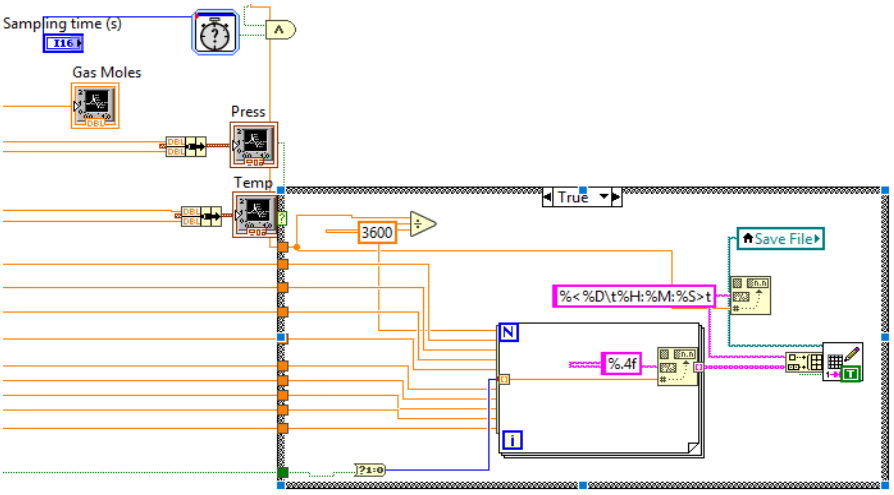

Figure B.21-Zone 11.

Appendix C

C.1. ASCII command communication protocol

The communication between the ADAM's was done using this communication protocol, in which the basic command has the form:

Table C.3-ASCII communication protocol structure.

#	**AA**	**00**	**(Data)**	**[CS]**	**(CR)**
Delimiter	Address	Command	Data[1]	Checksum[2]	Carriage Return

1- Only applicable for some commands; 2- Optional (not used)

The delimiter can only be one of five characters, they cannot be used interchangeably and are particular to the command given. The five characters possible are: # (ASCII value hex 0x23), % (ASCII value hex 0x25), $ (ASCII value hex 0x24), @ (ASCII value hex 0x40) and ~ (ASCII value hex 0x7E). The commands used in the software developed and its respective responses and interpretation are presented in **Table C.4**.

Table C.4-Commands used in ASCII communication protocol and responses.

Command	**Description and Response**
#AA(CR)	Used for ADAM-4019; Reads all analog input data of module with address AA; Response: Used to get the cell thermocouple and pressure transducer output.
#AABBSS(CR)	Used for ADAM-4055 and ADAM-4068; Writes one channel (BB=1X, X is the channel number in hexadecimal) or all (BB=00); SS indicates the state of the change, in one channel change, 00 to close, 01 to open. Only one channel change was used; No response.
$AA6(CR)	Used for ADAM-4055 and ADAM-4068; Indicates the state of all channels;

	Response: !OOII00(CR); OO is a hexadecimal number that after changing to binary every bit corresponds to an output digital channel or relay position in decreasing order, e.g. hex 11 is bin 00010001 which says that only channels 0 and 4 are ON. II is a hexadecimal number that after changing to binary every bit corresponds to an input digital channel in decreasing order. Only used for ADAM 4055.

The address is a numeric value that identifies the module to which the command is referring to, this value can be accessed and changed using the official *Advantech*'s official desktop application.

C.2. Modified Modbus ASCII communication protocol

The temperature controller of the oven only recognized a modified version of the Modbus ASCII communication protocol. In this communication protocol the command has the form:

Table C.5-Modified Modbus ASCII communication protocol.

:	**AA**	**00**	**XXXX**	**YYYY**	**LRC**	**(CR/LF)**
Start	Address	Function	Data identifier	Number of registers/new value	Checksum	Carriage Return/Line Feed

In this protocol the only delimiter accepted is the colon character (**:**), and since this is a modified version only two functions are able to be used: the 03 function, used to read values and the 06 function used to write values. All values are used in hexadecimal.

The data identifier is a numeric value that identifies which data to read or write, for example, to access the oven set point the 00CB identifier is used and to obtain the current oven temperature the identifier is 0000.

This method does not accept decimal point, as such the setpoint must be multiplied by 10 before being turned into its hexadecimal correspondent.

To read the setpoint the command used would be :01 03 00 CB 00 01 30 CR LF. The response of this command would result in a similar string that starts with the same 7 characters and returns the value asked multiplied by 10 and in hexadecimal, the LRC returned could also be used to determine if any error occurred during the communication.

However, to change the setpoint to 50.0 ºC the command would be :01 06 00 CB 01 F4 39 CR LF

The Longitudinal Redundancy Check (LRC) is used to detect when an error occurred, this part is always calculated and depends on the previous terms, to calculate the LRC:

1-Add the address with the function with the first half of data identifier with the second half of the same, the first half of the number of registers and finally the second half of the same

2-Make the result negative;

3-Ignore all but the last two characters.

Appendix D

D.1. Magnetic Agitator Source Code

```
/*
 Created 30 Nov. 2009
 Modified 28 Oct 2010
 by Tom Igoe

 */

#include <Stepper.h>

const int stepsPerRevolution = 200
// initialize the stepper library on pins 8 through 11:
Stepper myStepper(stepsPerRevolution, 8, 9, 10, 11);
int stepCount = 0;  // number of steps the motor has taken

void setup() {
  // nothing to do inside the setup
}

void loop() {
  // read the sensor value:
  int sensorReading = analogRead(A0);
  // map it to a range from 0 to 100:
  int motorSpeed = map(sensorReading, 0, 1023, 0, 100);
  // set the motor speed:
  if (motorSpeed > 0) {
    myStepper.setSpeed(motorSpeed);
    // step 1/100 of a revolution:
    myStepper.step(stepsPerRevolution / 100);
  }
}
```

D.2. Micropump Information Display Source Code

```
#include <SPI.h>
#include <Wire.h>
#include <Adafruit_GFX.h>
#include <Adafruit_SSD1306.h>

#define SCREEN_WIDTH 128 // OLED display width, in pixels
```

```
#define SCREEN_HEIGHT 32 // OLED display height, in pixels

// Declaration for an SSD1306 display connected to I2C (SDA, SCL
pins)
#define OLED_RESET     4 // Reset pin # (or -1 if sharing Arduino
reset pin)
Adafruit_SSD1306 display(SCREEN_WIDTH, SCREEN_HEIGHT, &Wire,
OLED_RESET);

const int pin = 2;

volatile float rev;
float Rpm;
float Flow;
float Voltage;
unsigned long oldtime;
unsigned long t;
void isr() {
rev++;
}

void setup() {
  Serial.begin(9600);

  // SSD1306_SWITCHCAPVCC = generate display voltage from 3.3V
// internally

  if(!display.begin(SSD1306_SWITCHCAPVCC, 0x3C)) { // Address 0x3C
// for 128x32
    Serial.println(F("SSD1306 allocation failed"));
    for(;;); // Don't proceed, loop forever
    }
  // Clear the buffer
  display.clearDisplay();

  // Show the display buffer on the screen. You MUST call
  // display() after drawing commands to make them visible on
  //screen!
  display.display();
  delay(2000);

pinMode(pin, INPUT_PULLUP);
attachInterrupt(digitalPinToInterrupt(pin), isr, RISING);

}

void loop() {
```

```
delay(1000);

detachInterrupt(digitalPinToInterrupt(pin));
  //detaches the interrupt

Voltage = analogRead(A0);
Voltage = Voltage/1023*5;
t = millis()-oldtime;         //finds the time
Rpm=rev/2/t*60000;          //calculates rpm
Flow=0.017*Rpm;             //calculates volumetric flow (cc/min)
  display.clearDisplay();
  display.setTextSize(1);             // Normal 1:1 pixel scale
  display.setTextColor(WHITE);        // Draw white text
  display.setCursor(0,0);             // Start at top-left corner
  display.print(Voltage,2);
  display.print(F(" V     "));
  display.print(Rpm,0);
  display.println(F(" rpm"));
  display.setTextSize(2);
  display.setCursor(0,16);
  display.print(Flow,1);
  display.setTextSize(1);
  display.print(F(" mL/min"));
  display.display();
oldtime = millis();    //saves the current time
rev=0;
attachInterrupt(digitalPinToInterrupt(pin),isr,RISING);
//reattaches the interrupt

}
```

Appendix E

E.1. [C_4C_1im][DCA] Solubility Experiment Raw Data

The data for each experiment is represented as a variation of both temperature and pressure during a period, the experiments where leaks were noticed and the pressure transducer was overflowing are not present.

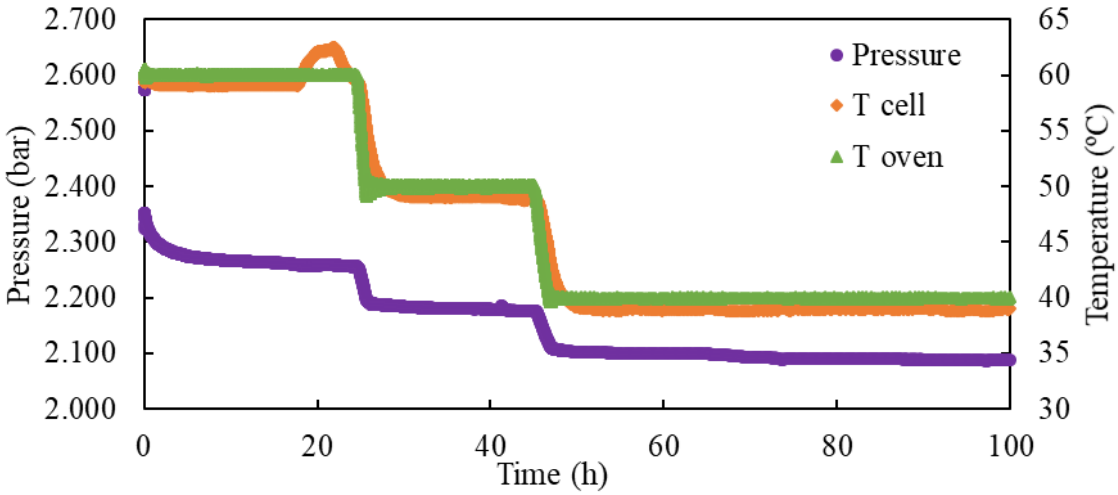

Figure E.1-*pVT* diagram of [C_4C_1im][DCA] with CO_2, m_{IL}=9.753 g, 19/03/2019, V=340 mL.

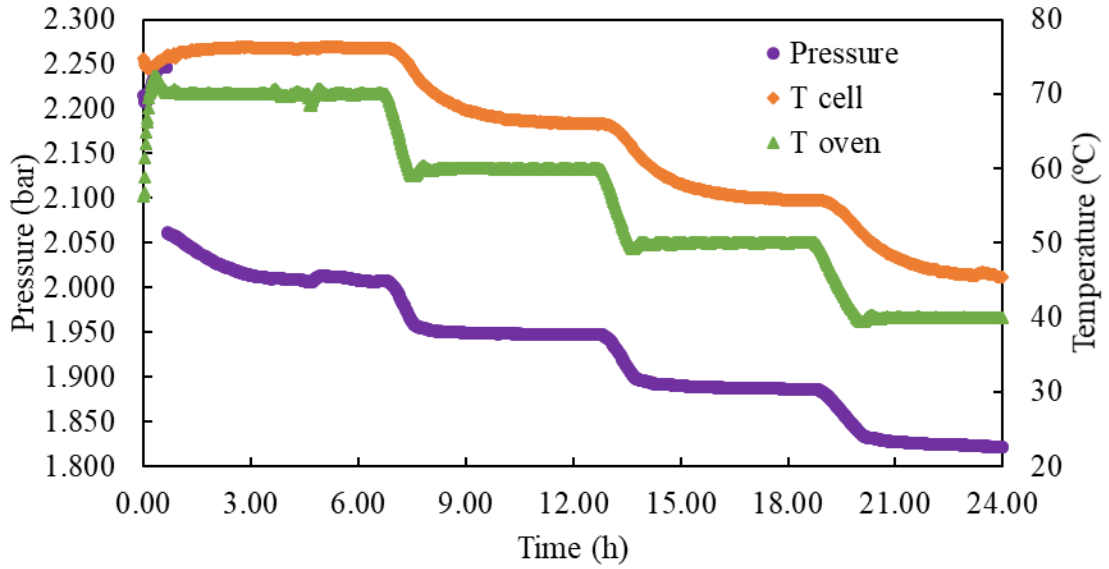

Figure E.2- *pVT* diagram of [C_4C_1im][DCA] with CO_2, m_{IL}=10.571 g, 14/02/2019, V=340 mL.

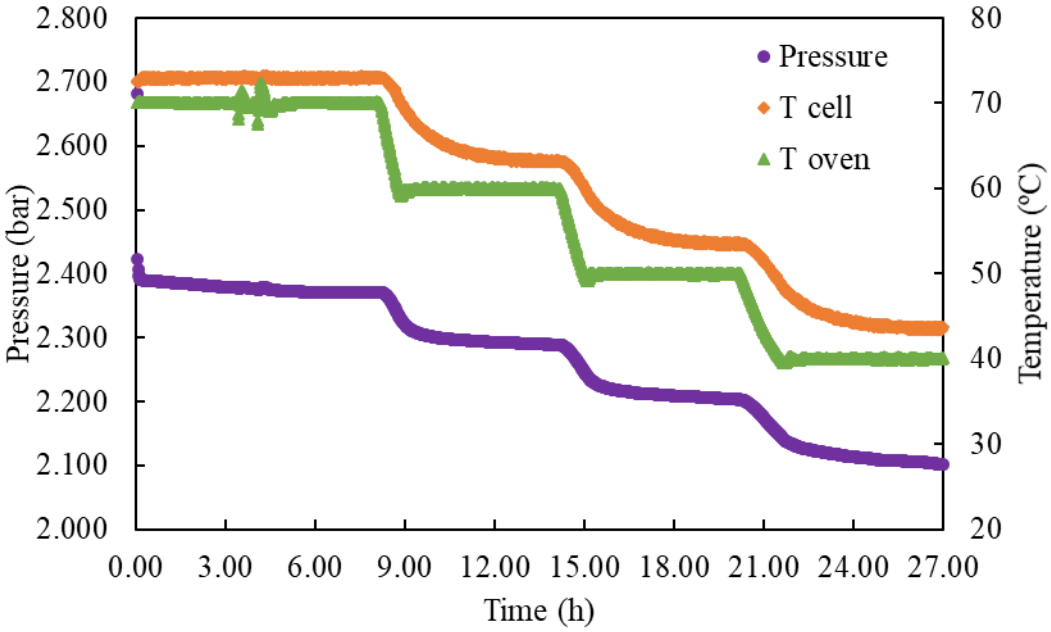

Figure E.3- *pVT* diagram of [C_4C_1im][DCA] with CO_2, m_{IL}=10.571 g, 19/02/2019, V=340 mL.

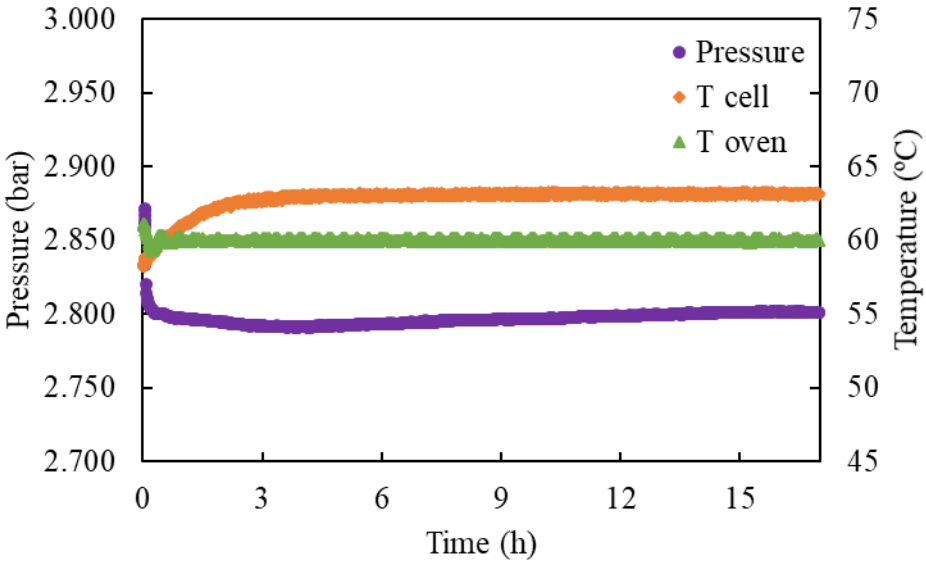

Figure E.4- *pVT* diagram of [C_4C_1im][DCA] with CO_2, m_{IL}=8.477 g, 27/02/2019, V=340 mL.

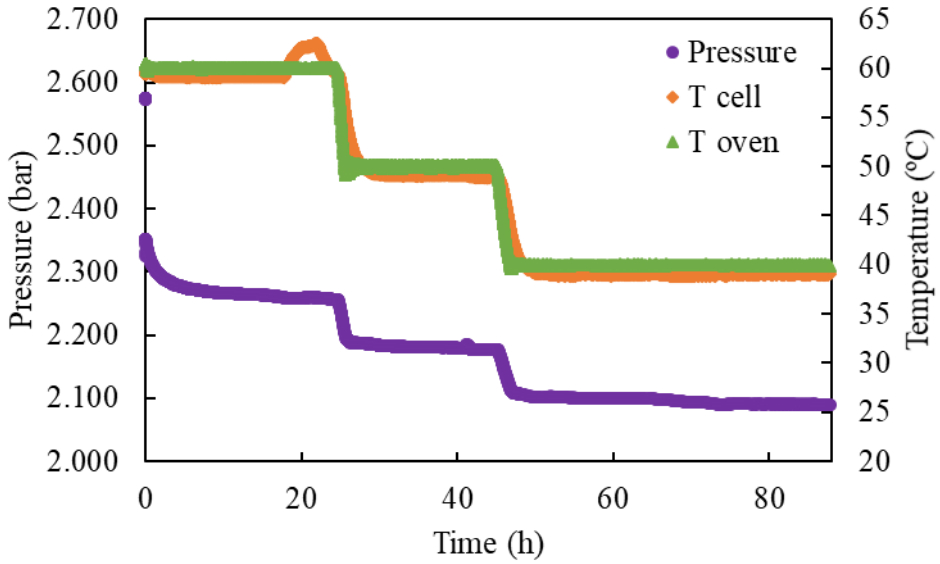

Figure E.5- *pVT* diagram of [C_4C_1im][DCA] with CO_2, m_{IL}=9.753 g, 06/03/2019, V=340 mL.

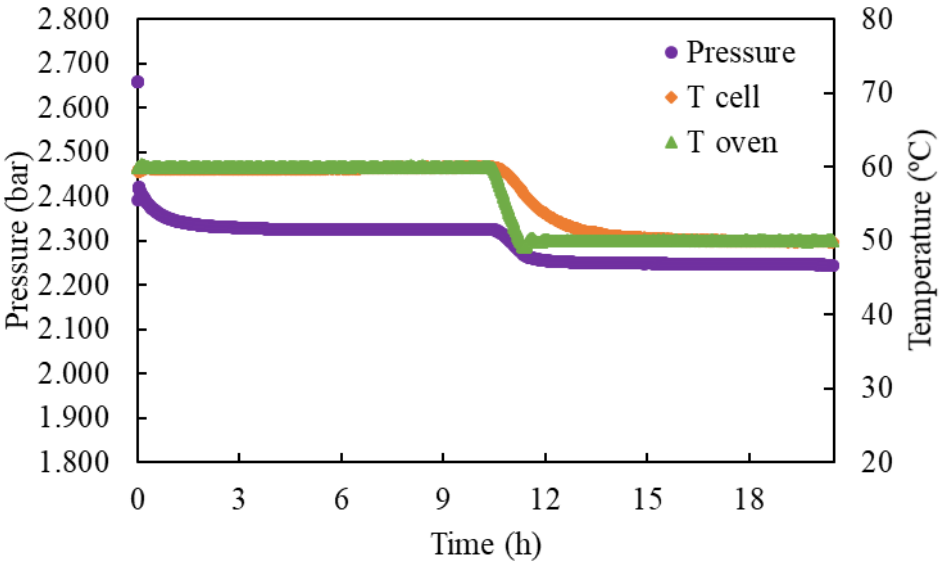

Figure E.6- *pVT* diagram of [C_4C_1im][DCA] with CO_2, m_{IL}=8.656 g, 13/03/2019, V=340 mL.

E.2. [DEEA][Ac] Solubility Experiment Raw Data

The evolution of the system pressure cell temperature and the oven temperature can be seen for every experiment in the following Figures.

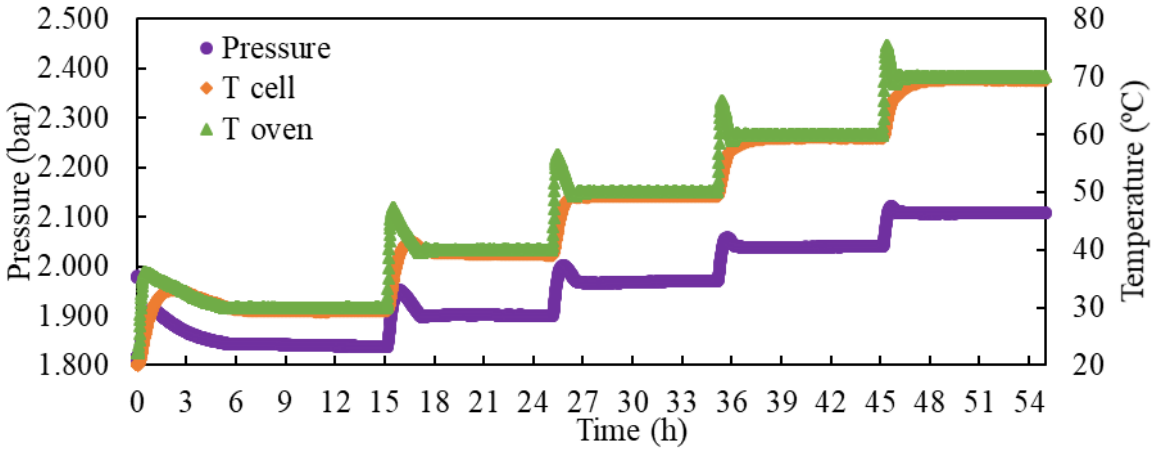

Figure E.7- *pVT* diagram of [DEEA][Ac] with CO_2, m_{IL}=4.922 g, 29/04/2019, V=340 mL.

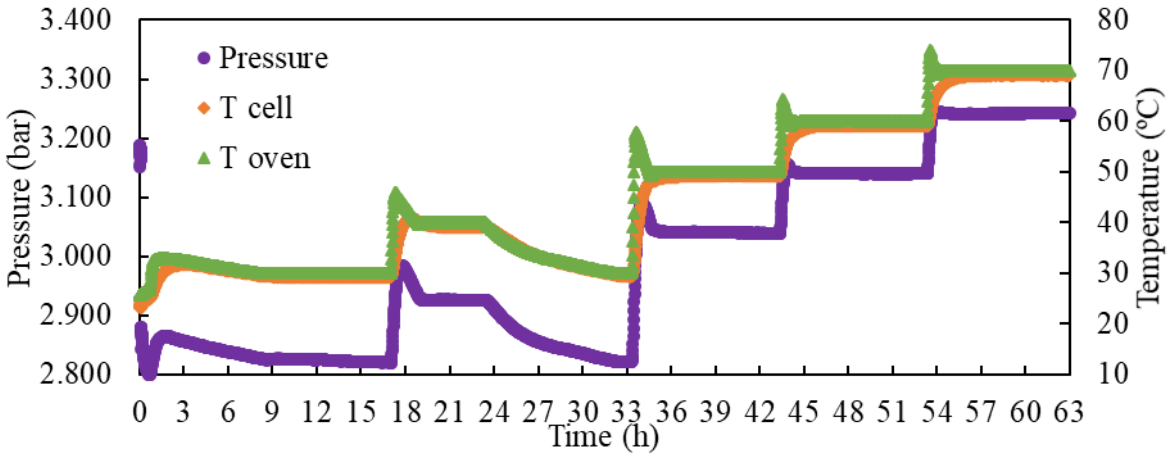

Figure E.8- *pVT* diagram of [DEEA][Ac] with CO_2, m_{IL}=4.922 g, 23/04/2019, V=340 mL.

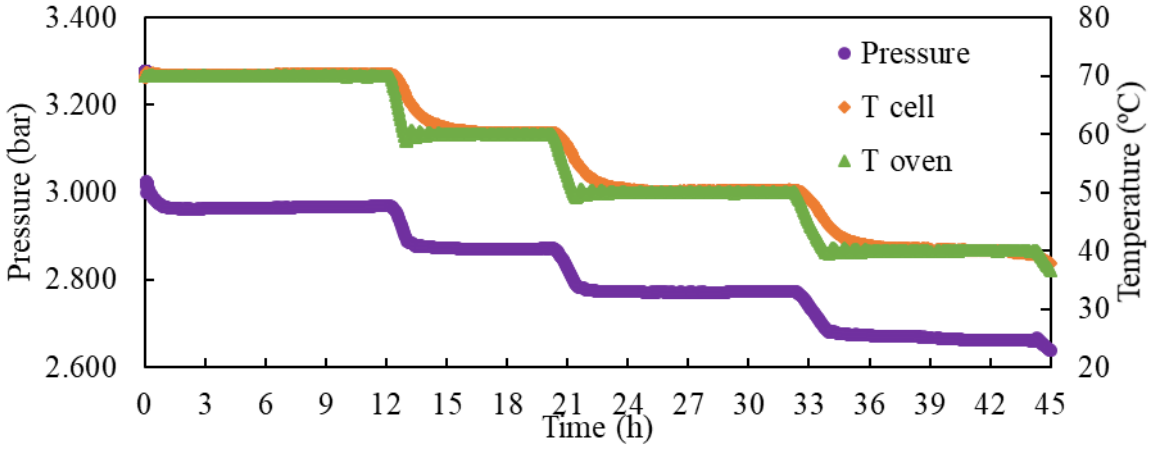

Figure E.9- *pVT* diagram of [DEEA][Ac] with CO_2, m_{IL}=7.339 g, 15/04/2019, V=340 mL.

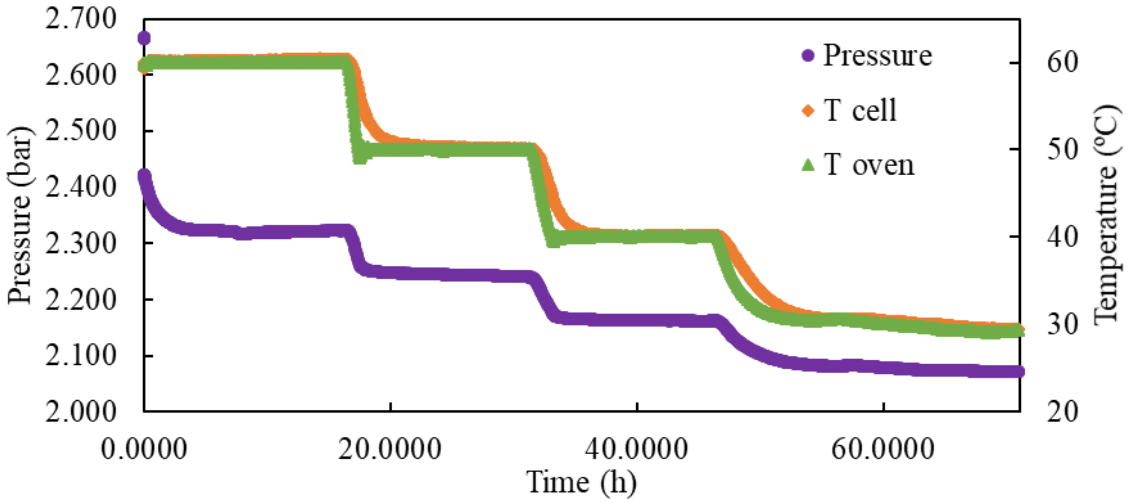

Figure E.10- *pVT* diagram of [DEEA][Ac] with CO_2, m_{IL}=8.440 g, 22/03/2019, V=340 mL.

E.3. [P_{4444}][Ac] Solubility Experiment Raw Data

The evolution of the system pressure cell temperature and the oven temperature can be seen for every experiment in the following Figures.

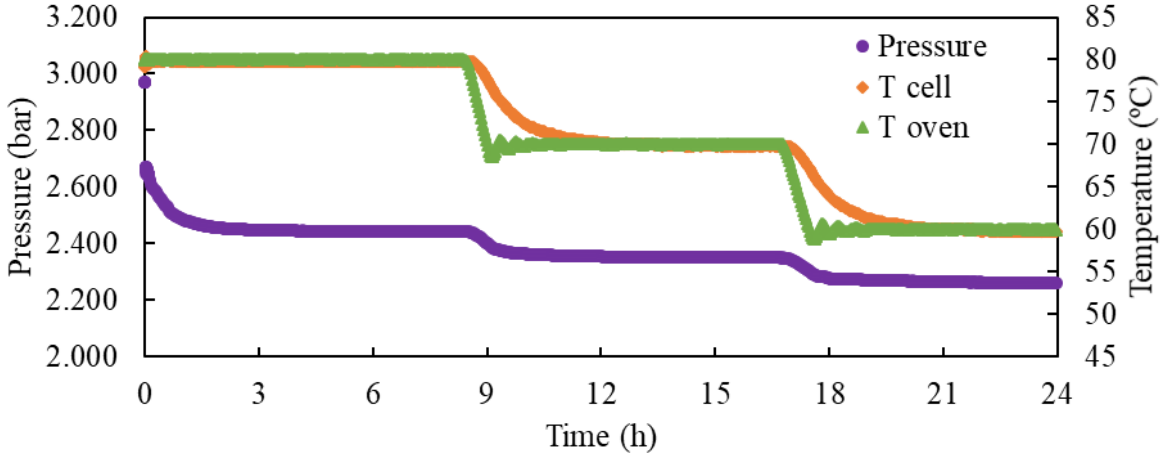

Figure E.11- *pVT* diagram of [P_{4444}][Ac] with CO_2, m_{IL}=3.600 g, 03/05/2019, V=340 mL.

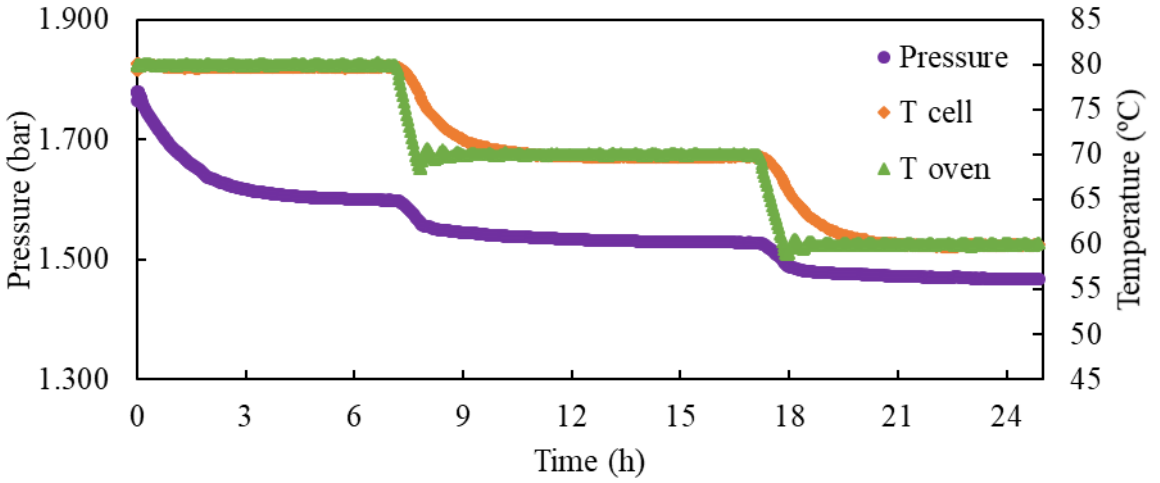

Figure E.12- *pVT* diagram of $[P_{4444}][Ac]$ with CO_2, m_{IL}=3.600 g, 07/05/2019, V=340 mL.

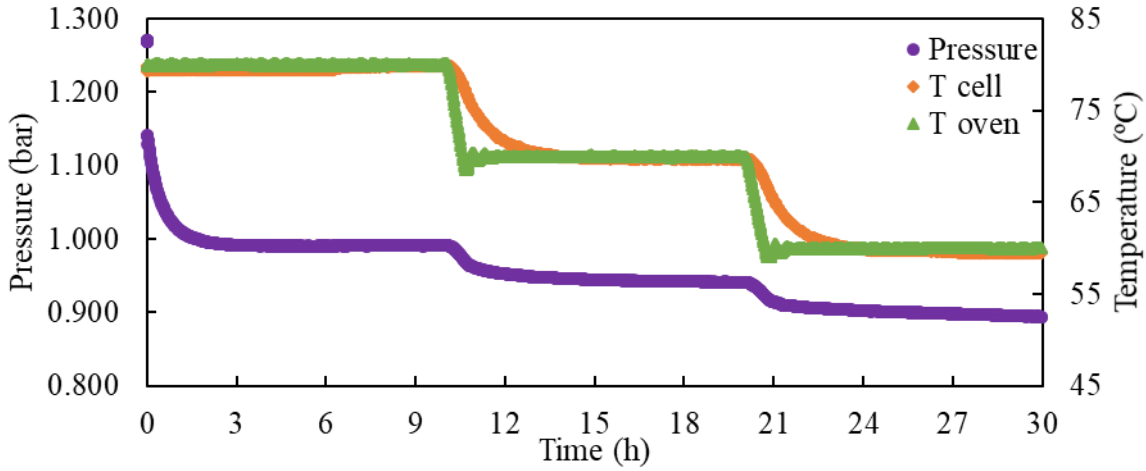

Figure E.13- *pVT* diagram of $[P_{4444}][Ac]$ with CO_2, m_{IL}=3.600 g, 10/05/2019, V=340 mL.

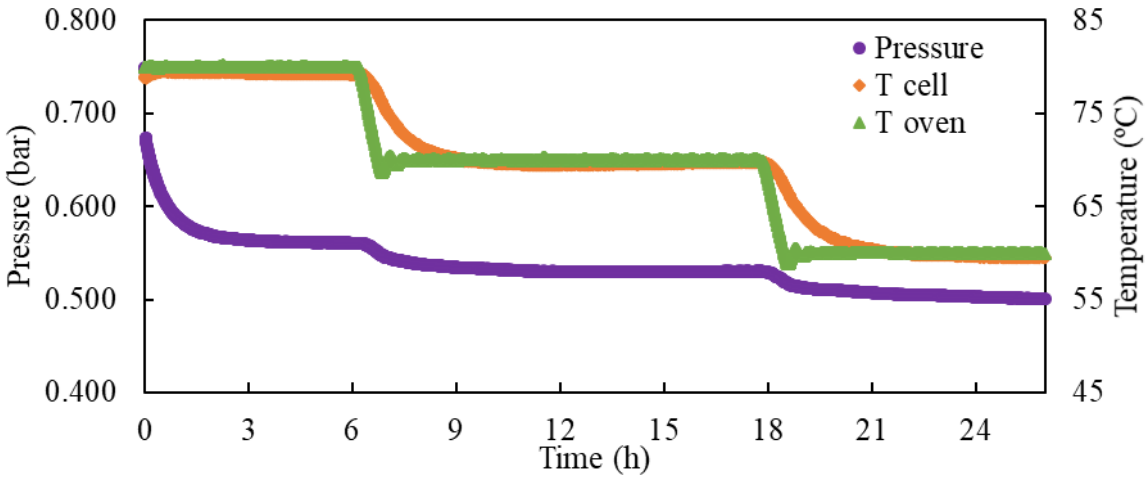

Figure E.14- *pVT* diagram of $[P_{4444}][Ac]$ with CO_2, m_{IL}=3.600 g, 14/05/2019, V=340 mL.

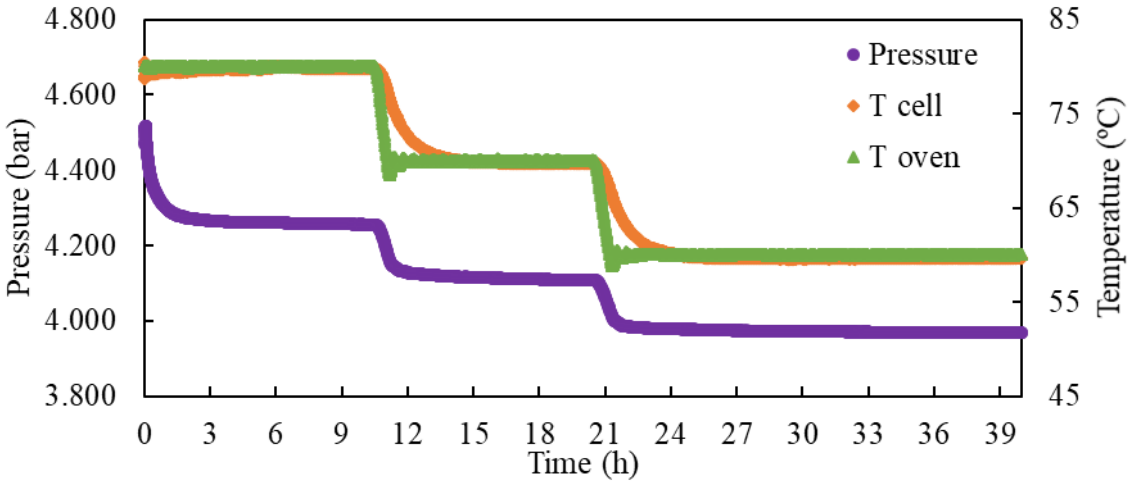

Figure E.15- *pVT* diagram of [P_{4444}][Ac] with CO_2, m_{IL}=3.600 g, 17/05/2019, V=340 mL.

E.4. [$N_{1112(OH)}$][L-Phe] Solubility Experiment Raw Data

The evolution of the system pressure cell temperature and the oven temperature can be seen for every experiment in the following Figures.

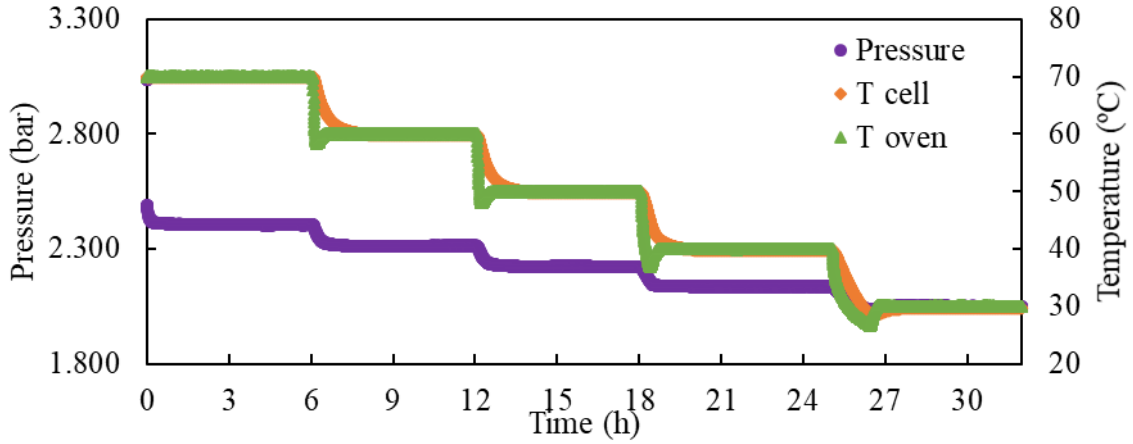

Figure E.16- *pVT* diagram of encapsulated [$N_{1112(OH)}$][L-Phe] with CO_2, mIL=3.288 g, 10/05/2019, V=340 mL.

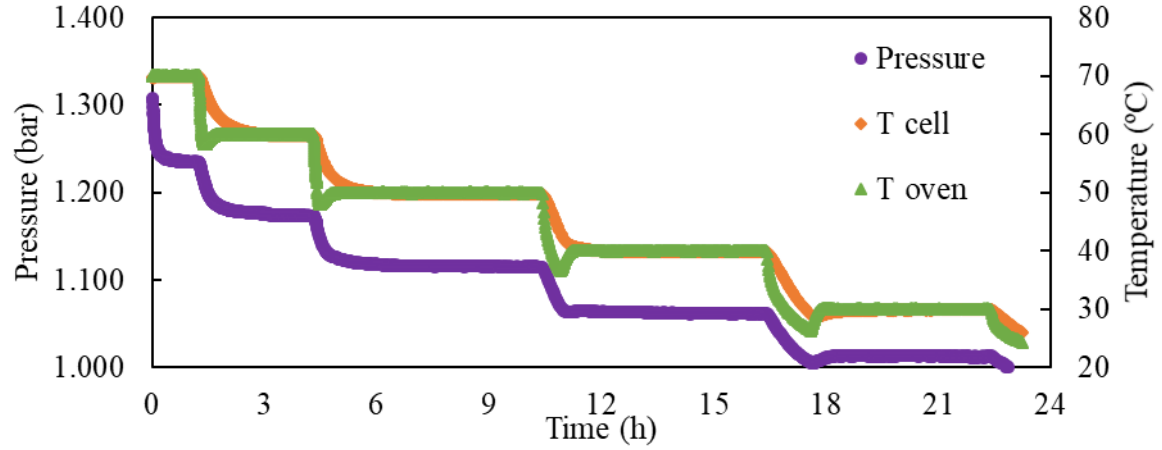

Figure E.17- *pVT* diagram of encapsulated [$N_{1112(OH)}$][L-Phe] with CO_2, mIL=3.288 g, 14/05/2019, V=340 mL.

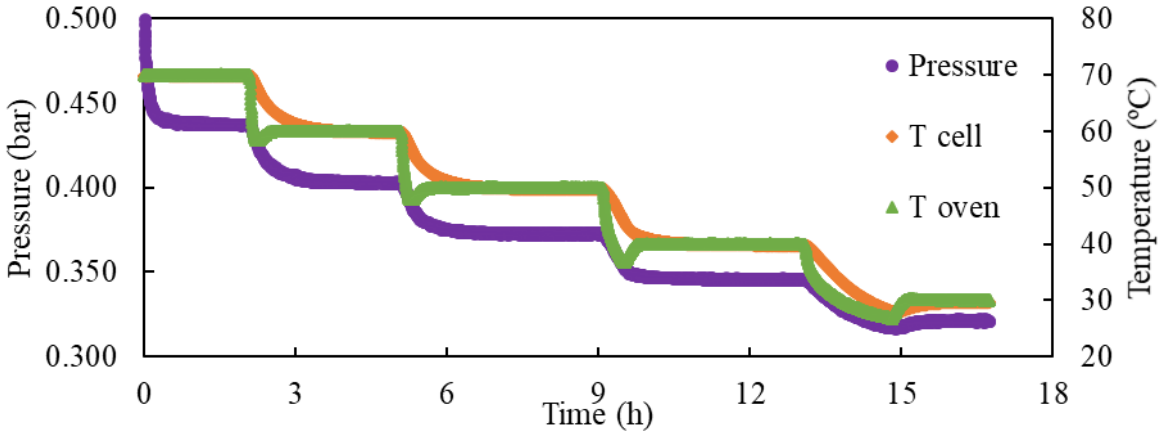

Figure E.18- *pVT* diagram of encapsulated [$N_{1112(OH)}$][L-Phe] with CO_2, mIL=3.288 g, 15/05/2019, V=340 mL.

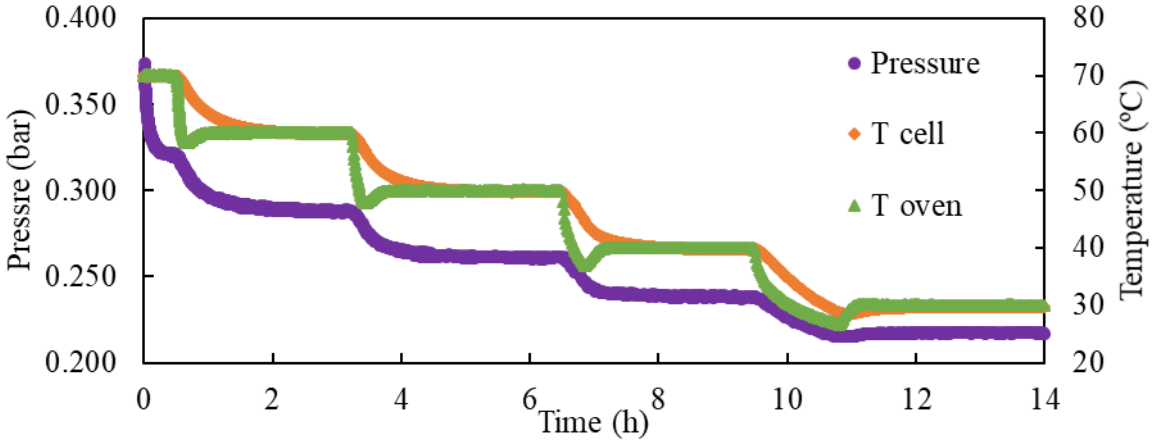

Figure E.19- *pVT* diagram of encapsulated [$N_{1112(OH)}$][L-Phe] with CO_2, mIL=3.288 g, 17/05/2019, V=340 mL.

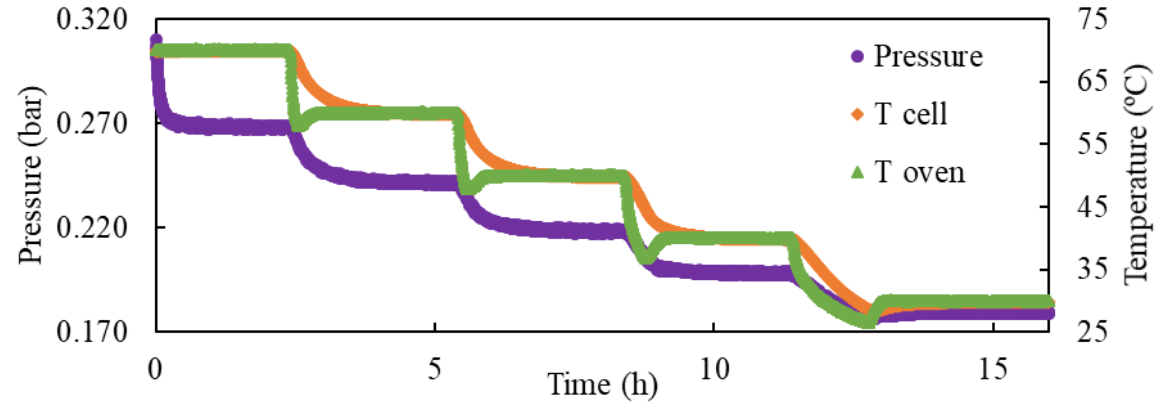

Figure E.20- *pVT* diagram of encapsulated [$N_{1112(OH)}$][L-Phe] with CO_2, mIL=3.288 g, 20/05/2019, V=340 mL.

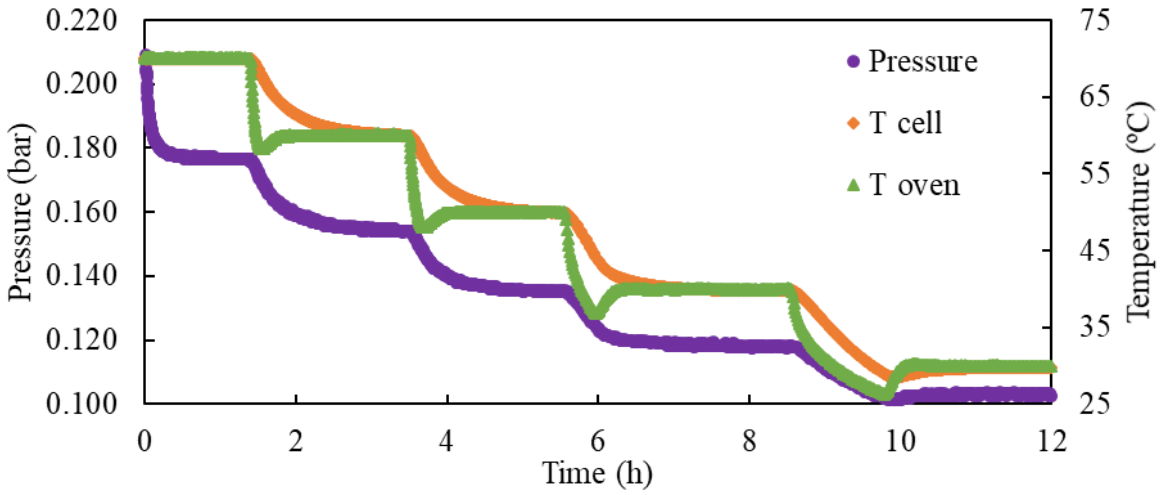

Figure E.21- *pVT* diagram of encapsulated [$N_{1112(OH)}$][L-Phe] with CO_2, mIL=3.288 g, 20/05/2019, V=340 mL.

E.5. [$N_{1112(OH)}$][L-Pro] Solubility Experiment Raw Data

The evolution of the system pressure cell temperature and the oven temperature can be seen for every experiment in the following Figures.

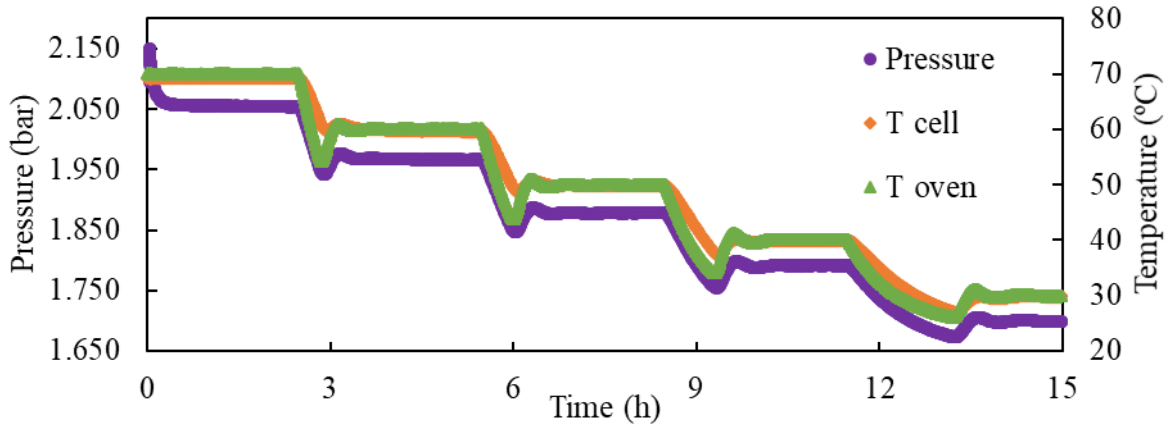

Figure E.22- *pVT* diagram of encapsulated [$N_{1112(OH)}$][L-Pro] with CO_2, mIL=4.210 g, 17/06/2019, V=340 mL.

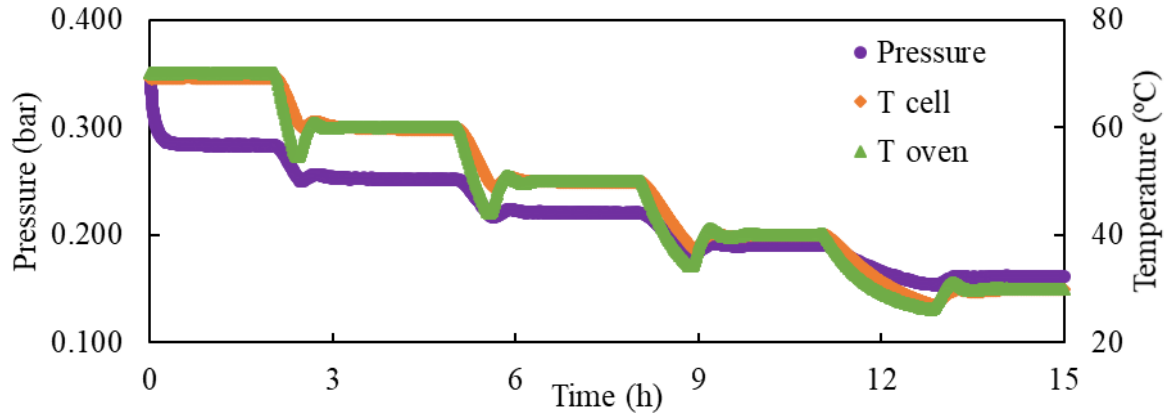

Figure E.23- *pVT* diagram of encapsulated [$N_{1112(OH)}$][L-Pro] with CO_2, mIL=4.210 g, 18/06/2019, V=340 mL.

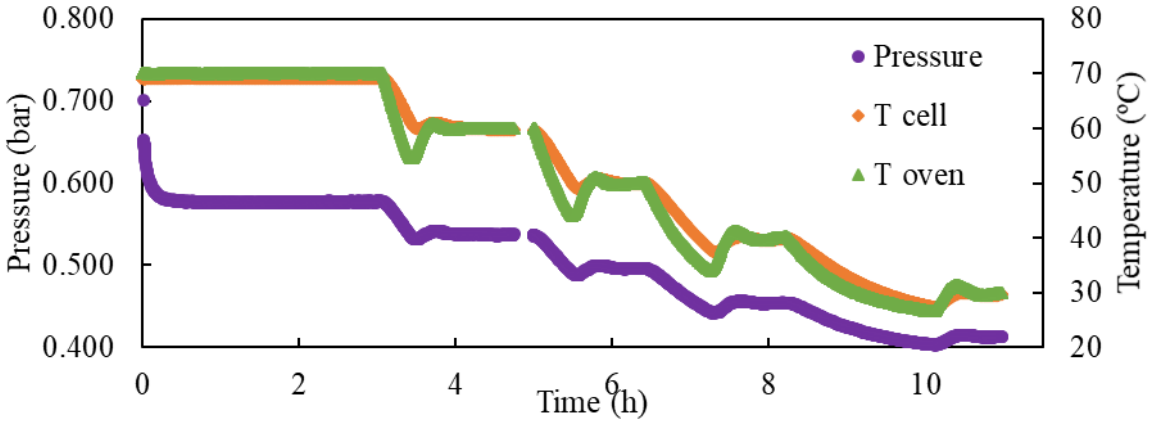

Figure E.24- *pVT* diagram of encapsulated [$N_{1112(OH)}$][L-Pro] with CO_2, mIL=4.210 g, 19/06/2019, V=340 mL.

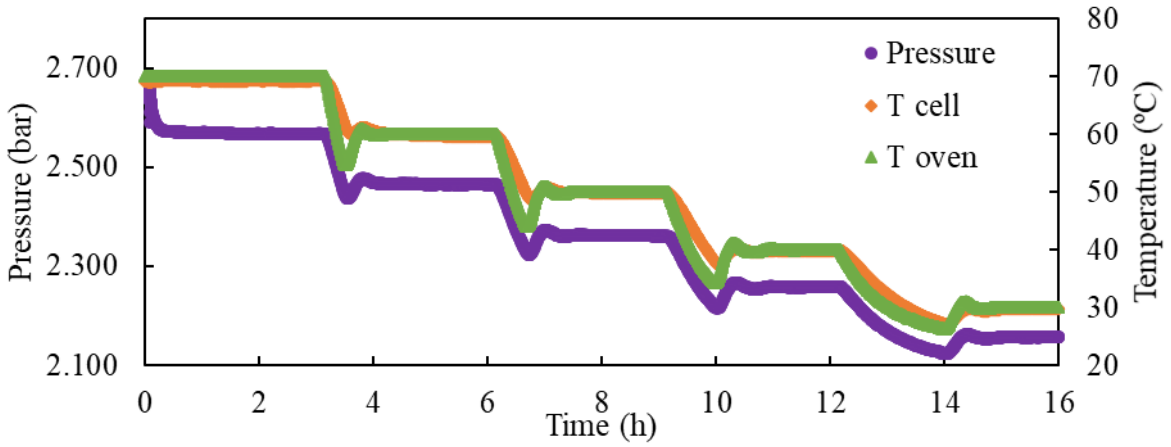

Figure E.25- *pVT* diagram of encapsulated [$N_{1112(OH)}$][L-Pro] with CO_2, mIL=3.918 g, 24/06/2019, V=340 mL.